Light induced assembly of disulfide forming peptides

Masterarbeit zur Erlangung des akademischen Grades Master of Science

im Fachbereich 9 Chemie

der Johannes Gutenberg-Universität Mainz

von

Laura Julia Rosenberger

The presented thesis was prepared from April 2022 to October 2022 in the group of Prof. Dr. Tanja Weil (subgroup of Dr. David Ng) at the Max Planck Institute for Polymer Research in Mainz.

Submission date: 31st October 2022

1. Reviewer: Prof. Dr. Tanja Weil

2. Reviewer: Prof. Dr. Andreas Walther

Eidesstattliche Erklärung

Ich, Laura Julia Rosenberger, Matrikelnummer 2740967 versichere, dass ich meine Masterarbeit selbstständig verfasst und keine anderen als die angegebenen schriftlichen und elektronischen Quellen sowie andere Hilfsmittel benutzt habe. Alle Ausführungen, die anderen Schriften wörtlich oder sinngemäß entnommen wurden, habe ich kenntlich gemacht.

Mainz, 31.10.2022
(Ort, Datum)


(Unterschrift)

Table of content

List of Figures

List of Tables

Abstract

Supramolecular assemblies are known to be instrumental in the existence of living organisms by directing biological processes such as energy metabolism or molecular transport. Mimicking such processes has become a large field in research during the last decades in which many different synthetic self-assembling nanomaterials have been developed to create non-natural superstructures in mammalian cells. A common approach that focuses on controllability is to design stimulus-responsive precursor molecules with the ability to rearrange into self-assembling monomers after activation. The dynamic properties of the cellular environment can be exploited by using intracellular components and metabolites such as enzymes or hydrogen peroxide as triggers. In this thesis, the approach for a photosensitive precursor molecule was pursued to obtain spatiotemporal control over the initiation of fibrillation. In order to achieve this, an isopeptide with an attached 2-nitrosobenzyl-based protecting group was designed to develop a photoinduced self-assembling system suitable for intracellular application. Irradiation of this precursor leads first to cleavage of the photolabile group with a following rearrangement resulting in the self-assembling peptide monomer. Depending on the design of the peptide sequence, properties of the monomer can be adjusted or tuned regarding dynamics and fibrillation characteristics. Combination of the photolabile protecting group with a cysteine-containing peptide allows the development of a dynamic system in which cysteine residues can be oxidized to disulfides. Within this work, the self-assembly of this photosensitive peptide was investigated to test its suitability for intracellular applications. Therefore, kinetics of the light-induced reaction cascade and supramolecular structures of the resulting self-assembling monomers were analyzed.

Zusammenfassung

Es ist bekannt, dass supramolekulare Assemblierungen für die Existenz lebender Organismen entscheidend sind, da sie biologische Prozesse wie den Energiestoffwechsel oder den Transport von Molekülen steuern. Die Nachahmung solcher Prozesse ist in den letzten Jahrzehnten zu einem großen Forschungsgebiet geworden, in dem viele verschiedene synthetische, selbstorganisierende Nanomaterialien entwickelt wurden, die in Säugetierzellen nicht natürliche Überstrukturen bilden. Ein gängiger Ansatz, bei dem die Kontrollierbarkeit im Fokus steht, besteht darin, auf Reize reagierende Vorläufermoleküle zu entwickeln, die sich nach der Aktivierung in selbstorganisierende Monomere umlagern können. Die dynamischen Eigenschaften der zellulären Umgebung werden ausgenutzt, indem intrazelluläre Komponenten und Stoffwechselprodukte wie Enzyme oder Wasserstoffperoxid als Auslöser verwendet werden. In dieser Arbeit wurde der Ansatz für ein lichtempfindliches Vorläufermolekül verfolgt, um eine räumlich-zeitliche Kontrolle über die Fibrillierungsinitiation zu erhalten. Zu diesem Zweck wurde ein Isopeptid mit einer angehängten 2-Nitrosobenzyl-Schutzgruppe entwickelt, um ein photoinduziertes selbstorganisierendes System für die intrazelluläre Anwendung zu schaffen. Die Bestrahlung dieses Vorläufermoleküls führt zunächst zur Abspaltung der photolabilen Gruppe mit anschließender Umlagerung zum selbstorganisierenden Peptidmonomer. Je nach Gestaltung der Peptidsequenz können die Eigenschaften des Monomers in Bezug auf Dynamik und Fibrillierungscharakteristika angepasst oder abgestimmt werden. Die Kombination der photolabilen Schutzgruppe mit einem cysteinhaltigen Peptid ermöglicht die Entwicklung eines dynamischen Systems, in dem Cysteinreste zu Disulfiden oxidiert werden können. Im Rahmen dieser Arbeit wurde die Selbstorganisation dieses lichtempfindlichen Peptids im Hinblick auf dessen Eignung für intrazelluläre Anwendungen zu testen. Dazu wurden die Kinetik der lichtinduzierten Reaktionskaskade und die supramolekularen Strukturen der entstehenden selbstassemblierenden Monomere analysiert.

1 Introduction

1.1 Peptides and supramolecular structures

Amino acids (AA) are small molecules acting as building blocks for biomacromolecules in living organisms. Other small molecules, for example lipids, nucleic acids and carbohydrates, are responsible for membrane formation, storing of genetic information and energy, whereas AAs play a huge role in protein biosynthesis. The general structure of an AA is characterized by the residues at its α-carbon atom. Every AA consists of an α-carboxylic acid (pink), an α-amino group (blue), an α-hydrogen atom (white) and a side chain (green) that is unique for each AA.[1] As the α-carbon atom represents a chiral center (except for glycine with R = H), there are L- and D-isomers possible which are shown in Figure 1. However, most eukaryotic and prokaryotic species use L-isomers in their cells for biosynthesis of peptides and proteins.[1,2]

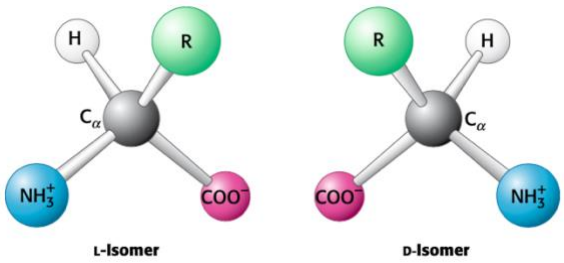

Figure 1: General three-dimensional structure of L- and D-amino acids.[1]

In nature, ribosomes take care of protein biosynthesis and are responsible for the coupling of 20 proteinogenic AAs to a peptide. The AAs are connected via an amide bond, the so-called peptide bond. This peptide bond arises from a reaction between an α-carboxylic acid of an AA and an α-amino group of another AA. The resulting chain is the primary structure of the peptide. Further, there are the secondary, tertiary, and quaternary structure of peptides. The flexibility of a peptide chain limited by the partial double-bond character of the peptide bonds.[1] Secondary structures are formed when primary structures fold into regular, repeating structures stabilized by hydrogen bonds and Van-der-Waals-forces. The main and often occurring conformations are β-sheets and α-helices, β-turns and random coil. Random coils are defined as structures with no discernible secondary structure.[3] β-Turns are structural principles creating directional changes of peptide chains. This occurs through hydrogen bonding of the carbonyl group of an AA with the amide group of an AA which is three residues away.[1]

β-sheets are formed as zigzag structures of peptide backbones, the alternating sequences of peptide bonds and α-carbons. Parallel and antiparallel β-sheets can be formed depending on the emerging interactions (Figure 2, right). In the antiparallel arrangement, amide and carbonyl groups of an AA in one strand are each connected to the carbonyl and amide groups of a partner in the adjacent strand via hydrogen bonds. In the parallel alignment, the amide group of an AA is hydrogen bonded to the carbonyl group in the adjacent strand, whereas the carbonyl group of the same AA forms a hydrogen bond with an amid group two residues away in the adjacent strand.[1] An α-helix is characterized by a twisted peptide backbone with outward facing side chains (Figure 2, left).[1,2]

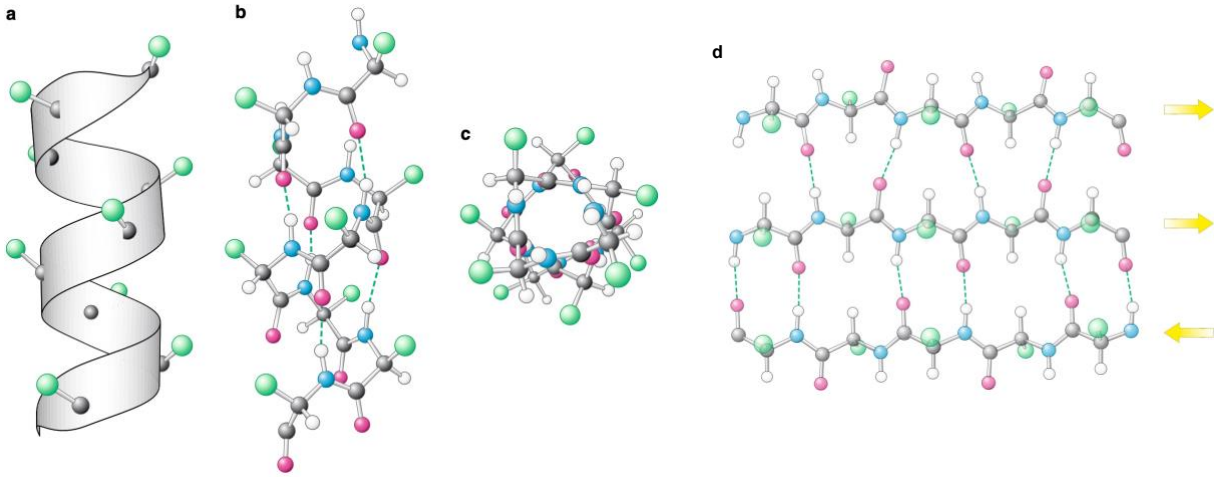

Figure 2: Schematic illustrations of an α-helix with a side (a and b) and a top (c) view and parallel (upper two) and antiparallel (lower two) peptide chains, forming β-sheets (d). Hydrogen bonds are represented as dashed lines. Carbon-atoms: grey, amino groups: blue, hydrogen-atoms: white, carbonyl oxygen: pink, side chains: green.[1]

Regularly, an α-helix contains 3.6 AAs in each completed 360 degree turn.[1] However, α-helices with 3.5 AAs each turn are found in coiled coil superstructures. They typically consists of two to five α-helices wrapped around each other resulting in a left-handed helix forming a supercoil.[4] Under aqueous conditions, helices interact with each other through hydrophobic and ionic interactions. Hydrophilic side chains point to the outside of the coiled coil and interact with the solvent. [4]

As the sequence is often designated *abcdefg*, hydrophobic residues can be found in positions *a* and *d* whereas ionic AAs in positions *e* and *g* (Figure 3).[5]

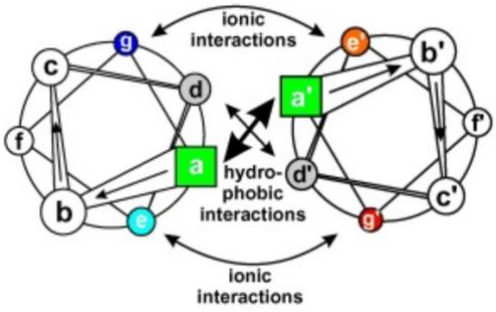

Figure 3: Interacting AAs *a-f* (representing two complete turns) in a coiled coil structure of two α-helices.[4]

Coiled coil structures are a class of the tertiary structures which are formed through the interaction between AAs that are located far away from each other in the linear sequence of a completed peptide chain. These include interactions between defined secondary structures via hydrogen bonds, Coulomb-interactions, and Van-der-Waals-forces but also disulfide bridges. Proteins consist of at least one completely folded AA-chain. Assembly of more than one of these tertiary superstructures to a quaternary structure enables a great variety of different proteins. An overview over the different peptide superstructures is shown in Figure 4.

Again, hydrogen bonds, Coulomb-interactions, Van-der-Waals-forces and disulfide bridges are responsible for structure stability.[1,2] Disulfide bridges are the most common cross-bridges in tertiary and quaternary structures resulting from a reaction of two cysteine residues. Cysteine contains a thiol group in the side chain which can form a disulfide bridge by oxidation with another thiol group. Biochemistry takes advantage of the reversibility of this oxidation by using dithiothreitol (DTT) to reduce disulfide bridges in protein analysis.[1,6,7]

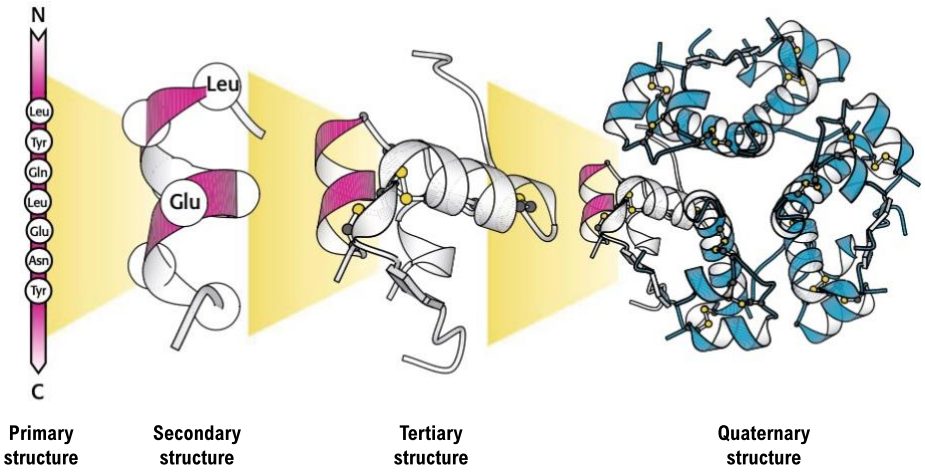

Figure 4: Schematic illustration of peptide superstructures including primary, secondary, tertiary, and quaternary structure.[adapted from 1]

As already mentioned, peptide production in living cells is executed by ribosomes. In synthetic chemistry, there is a long history of peptide synthesis and method optimization.[8] One of the first famous approaches for synthetic peptide synthesis was the preparation of a dipeptide by Fischer and Fourneau in 1901.[9] Limitations of their work included the absence of easily removable *N*-terminal protecting groups (PGs). About 30 years later the carbobenzoxy group was introduced as a temporary PG by Bergmann and Zervas.[8] Several small peptide sequences such as glutathione or carnosine could be synthesized using these advantages.[10,11] New PGs were developed, starting with the discovery of the tert-butyloxycarbonyl group (Boc) in 1957. These groups are stable towards hydrogenation, Birch reduction and strong alkali but also acid-labile and therefore easily to remove.[8,12] Multiple coupling reagents were discovered throughout the next decades to optimize peptide synthesis.[8] Until Merrifield published a method for solid phase peptide synthesis in 1963, all approaches in this scientific field have been performed in solution.[13] From this point, solid phase peptide synthesis (SPSS) became one of the most used methods in peptide synthesis. Cross-linked polystyrene or polyethylene glycol-based polymers are used as solid supports until today. Introduction of the base-labile *N*-terminal PG 9-fluorenylmethyloxycarbonyl (Fmoc) in 1970, lead to development of the recent method of choice: Fmoc-solid phase peptide synthesis (Fmoc-SPPS).[14] Fmoc-SPPS consists of four repetitive steps (Figure 5): (1) N-terminal deprotection, (2) washing, (3) coupling of a Fmoc-protected AA and (4) another washing step.[15] The growing peptide is C-terminal linked to the solid support and cleaved off using trifluoracetic acid (TFA), that also cleaves all acid-labile PGs from side chains, after completed synthesis (5).[16] Nowadays, a variety of PGs is known for α-amino groups and side chain functional groups (see Chapter 1.4).

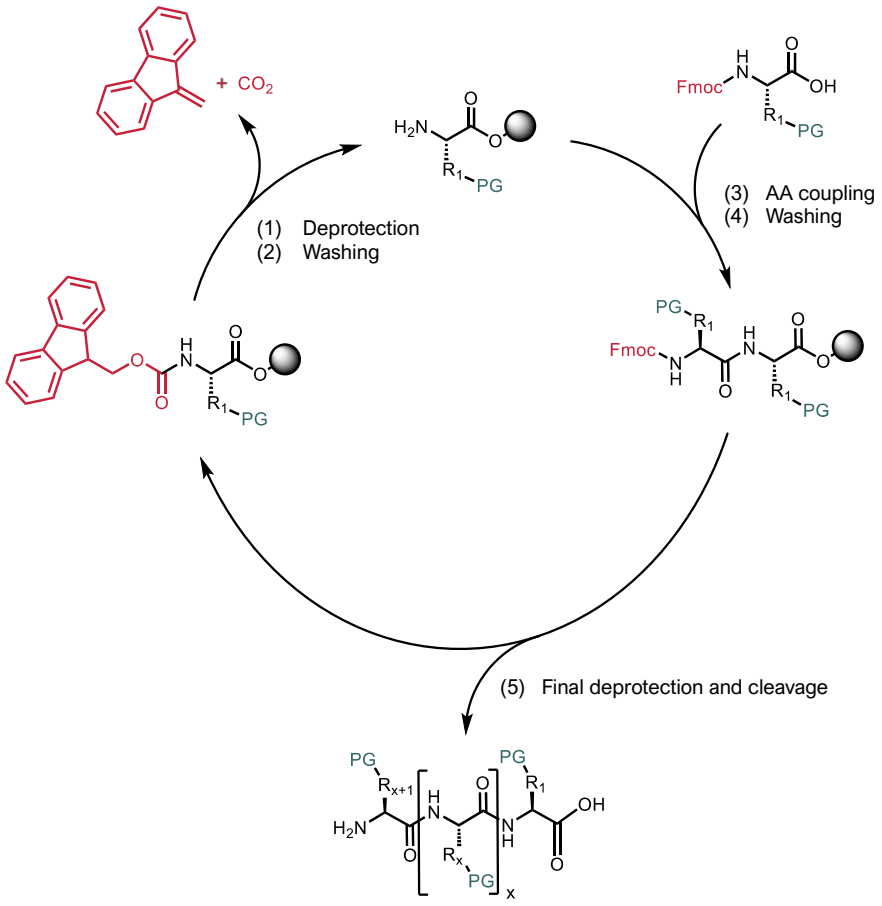

Figure 5: Scheme of a standard Fmoc-SPPS cycle with Fmoc (red) as N-terminal PG and acid-labile PGs (grey) at side chain residues.

1.2 Self-assembly inside living cells

The idea of self-assembling building blocks has been adapted from biology. Proteins and their different superstructures are only one example for biological self-assembly. Other intracellular examples are the cytoskeleton or DNA, the double-helical structure that also contains the genetic information coding for functional peptides in living organisms. Building blocks of DNA are nucleotides consisting of a pentose sugar (desoxyribose), a nitrogenous base and a phosphate group. An alternating sequence of sugar and phosphate builds the DNA backbone polymer where bases extend away from the chain. The four nucleotides adenine, guanine, thymine and cytosine differ only in the nitrogenous base and are responsible for the formation of the double-helix. Non-covalent interactions lead to complementary stacking of bases (A-T and G-C) including hydrogen bonding and π-π stacking.[1,2,17]

Since self-organization is driven by non-covalent interactions, their nature is of great importance when it comes to design of new self-assembling building blocks. One group of these interactions are long-range coulomb interactions (ion-ion, ion-dipole and dipole-dipole) resulting in attractive or repulsive effects. Ionic forces have been employed as a straightforward chance for self-assembly regarding designed building blocks.[1,17,18] Van-der-Waals forces are defined as short ranging and weak interactions between hydrophobic parts of molecules. Additionally, the hydrophobic effect leads to repulsion of solutes in polar solvents, causing self-assembly that can also be seen in the formation of micelles.[1,17] Hydrogen bonds form between an electronegative atom and a hydrogen atom that is bound to another electronegative atom. Usually, nitrogen, oxygen or fluorine are found as electronegative parts and called hydrogen acceptor while the hydrogen is referred to as hydrogen donor. Hydrogen bonds are highly directional, long- or short-range forces occurring inter- and intramolecular. Superstructures containing multiple hydrogen bonds are stabilized and spatial arranged with enhanced specificity.[1,17,19] Lastly, interactions of aromatic rings (π-π stacking) can also lead to self-assembly or intramolecular stability. π-π stacking occurs between aromatic rings when oriented face-to-face or edge-to-face. All noncovalent interactions are illustrated in Figure 6.[1,17]

Functional self-assembly inside living cells is a highly flexible and dynamic process not least because of their noncovalent binding character. In the complexity of cell metabolism, these mechanisms are mostly controlled by proteins and triggered by messengers or other molecules.[19] In terms of synthetic life-like systems, such complexity is not realizable or wanted. Therefore, it was and is a task of science to discover new triggers and inducing methods for synthetic self-assembling molecules.

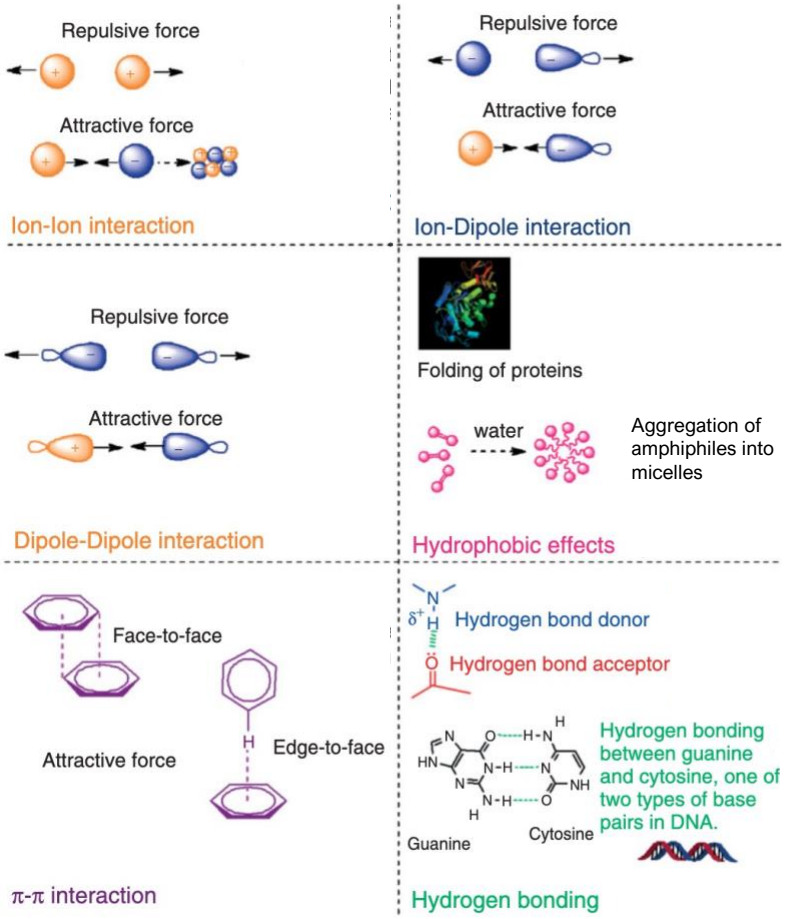

Figure 6: Noncovalent interactions responsible for self-assembly and building of superstructures.[adapted from 17]

1.3 Designed short self-assembling amphiphiles

In the field of synthetic small self-assembling building blocks, a huge research progress has been achieved during the last decades. Many different nanoparticles have been developed for use in technological areas and in medicine.[20,21] When it comes to medical applications, self-assembling peptides play a great role regarding drug delivery and direct disease treatment.[22] Assembled peptide structures were shown to increase fibroblast migration, drug stabilization and even regeneration of neurons.[23–25] Despite great difficulties in the use of peptides as pharmaceuticals due to poor oral availability, short half-lives or rapid metabolism, this approach is gaining more and more importance. One reason for this is that peptide applications include protein targeting that is more selectively than of small molecules, thereby reducing potential off-target side effects.[26]

Science is constantly searching for new design strategies for self-assembling peptides with predefined supramolecular structures in view of function and therapeutics. Besides the work with fiber or hydrogel forming β-strand peptide strategies, another subfield concentrates on high-ordered and discrete structures with α-helical peptides.[27] Coiled coils, consisting of several α-helices, are an example for those systems highly supported by bioinformatics and experimental studies allowing predictive structural designs.[28] However, β-strand forming amphiphiles are still in focus of research and can form a lot of different kinds of superstructures depending on their molecular design. Many short peptide building blocks require hydrophobic residues to facilitate self-assembly. They are constructed by a repeated scheme of an aromatic compound (for example Fmoc), a linker and an AA chain with an unprotected *C*-terminal carboxylic acid (Figure 7).[29]

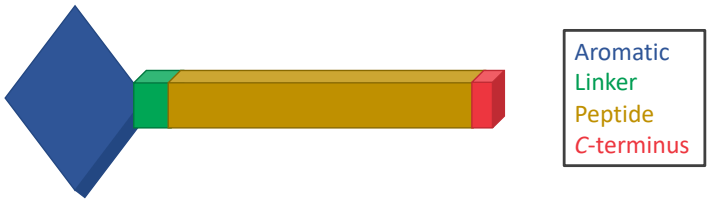

Figure 7: Scheme of an aromatic peptide amphiphilic building block for self-assembly divided in four segments: aromatic moiety (blue), linker (green), peptide (yellow) and *C*-terminus (red).[adapted from 29]

Generally, aromatic self-assembling amphiphiles lead to structures that assemble due to aromatic stacking and hydrogen bonding. These structures can be divided into definite assemblies (micelles and vesicles) with a discrete dimension and indefinite assemblies (tubes, fibers, sheets and tapes) (Figure 8).[30]

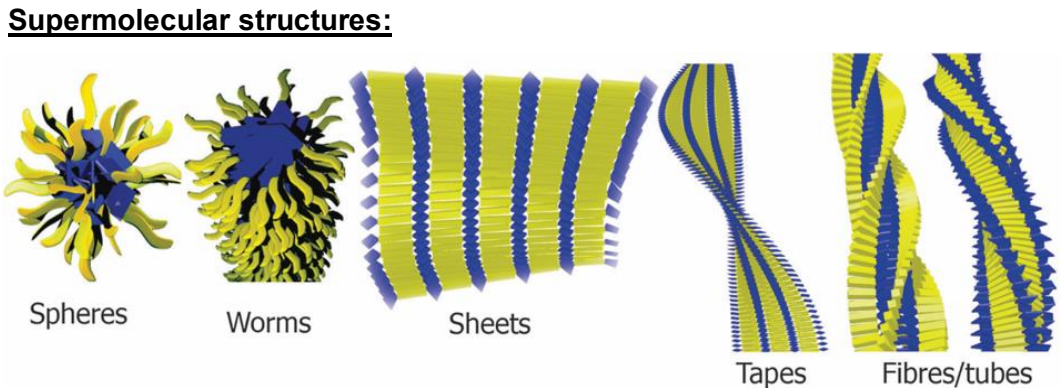

Figure 8: Simplified illustration of aromatic peptide amphiphile assemblies showing possible supramolecular structures due to hydrogen bonding and aromatic interactions.[adapted from 29]

The design of an aromatic peptide amphiphile can vary in all four segments shown in Figure 7. For example, Fmoc, pyrene and naphthalene derivates can be used as aromatic moieties to facilitate self-assembly. Ring substitutions have an impact on hydrophobicity with consequences for assembling conditions. Some aromatic parts, for example azobenzene and dithienylethene, also have an additional functional role causing switchable morphological or spectroscopic changes.[31,32] Co-assembling fluorophores can be used for stabilizing, responsiveness or imaging purposes, contributing new application methods.[29]

The choice of linker also seems to influence the formation of superstructures. An increase of molecular curvature was found to be detrimental to effective assembly. Therefore, linear geometries appear to be more useful in allowing effective intermolecular interactions in both the aromatic and peptide self-assembly domains. Additionally, the linear methoxy linker is a potential hydrogen bond acceptor with implications for self-assembly.[29]

Regarding the variety in AA structural side chain differences, it isn't surprising that the peptide sequence is an important design aspect. Amino acids can be classified as hydrophobic or hydrophilic with respect to their side chain properties. For example, aromatic amino acids such as phenylalanine or tyrosine and aliphatic ones such as valine or leucine are classified as hydrophobic. In addition, there are five hydrophilic amino acids that occur loaded at physiological pH and contain either an acidic (glutamic acid and aspartic acid) or basic (histidine, arginine and lysine) functional group. In addition, there are three amino acids with special properties: glycine is very flexible and is the only non-chiral amino acid; proline is rigid and, in combination with glycine, important for the formation of beta-turns in proteins; and cysteine, whose thiol group can be easily oxidized to form disulfide bonds.[33–36] Accordingly, flexibility, conformation, and mechanical properties of the resulting superstructures can be determined by the AA choice in the designed peptide sequence.[37]

For small AA sequences of aromatic amphiphiles, the free acid is often left at the C-terminus because this allows self-assembly to be easily triggered by pH adjustments. In contrast, with a functionalized C-terminus, for example, one has a broader pH range stability.[29,37]

Since the cellular environment is very complex, crowded and has a neutral pH value, self-assembling amphiphiles must also be able to organize themselves under these circumstances. Wang developed an enzyme responsive peptide-conjugate that could have an application in cancer therapy. Precursors are enzymatically cleaved releasing functional building blocks and forming fibrous assemblies.[38] Another research group concentrated on intramolecular

condensation reactions leading to a biorthogonal cyclization of a thiol and a cyanobenzothiazole. Their monomers were released by enzymatic cleavage or the cells´ redox environment.[39,40] Recently, the Weil group investigated self-assembling nonfunctional building blocks forming fibred superstructures inside living cells and therefore inducing cell death through apoptosis.[41–43] One approach were kinked bioinspired tripeptides (ISA) with an ester bond between serine and isoleucine, so called isopeptides, which were used as precursors. A ROS-sensitive phenylboronic acid trigger group capps the *N*-terminus of serine and contained an attached cell-penetrating peptide. Cytosolic ROS causes the degradation of the phenylboronic acid group and reveals the free reactive amine. Under neutral conditions, the amino group can perform an intramolecular nucleophilic attack on the ester bond between serine and isoleucine (*O,N*-acyl shift), yielding linearized peptides (Figure 9).[41]

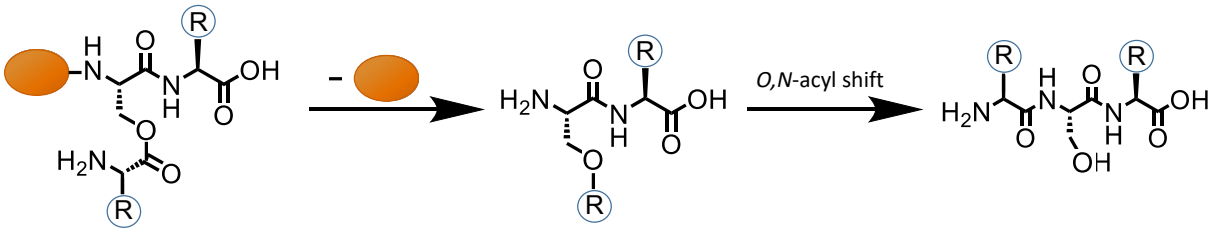

Figure 9: Cleavage of a *N*-terminal trigger group and following rearrangement of the molecule via nucleophilic attack of the freed amino group forming an amide bond (*O,N*-acyl shift).

Isoleucine was either Fmoc or Coumarine343 protected, leading to co-assembly into cytotoxic peptide fibres inside ROS-overproducing cancer cells (reaction scheme is shown in Figure 10). Such a multistep approach offers more opportunities to direct the transformation of a precursor into the self-assembling monomer.[41]

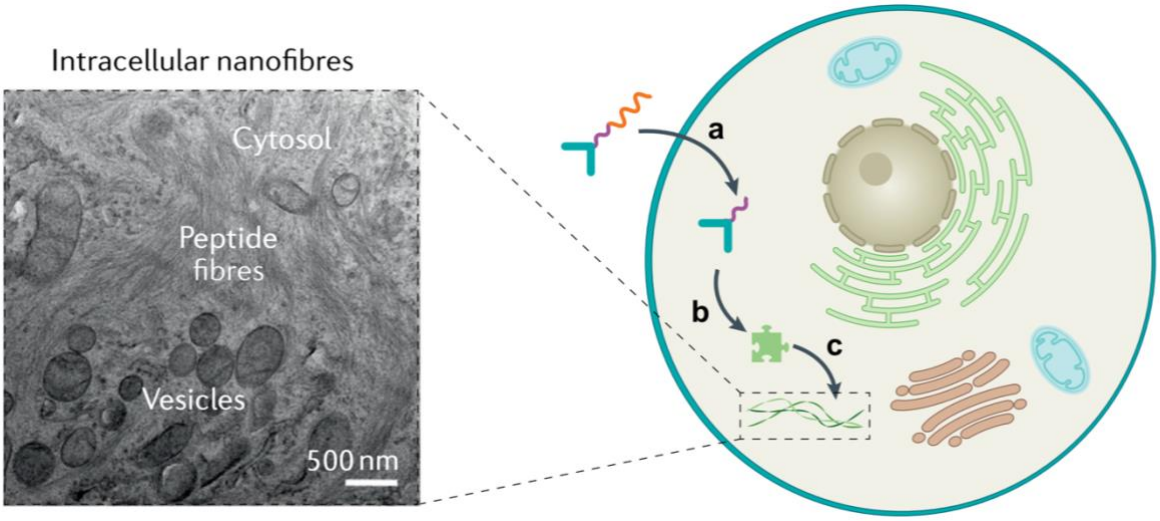

Figure 10: Multistep reaction of kinked isopeptides forming intracellular superstructures. After self-assembly precursors are uptaken due to the attached cell-penetrating peptide (orange), it is cleaved by hydrolysis (a). Intracellular ROS-species cleave the caging group (purple) followed by an *O,N*-acyl shift releasing the self-assembling building blocks (green) (b). Monomer assembly forms a fibrillar network inside the cell (c) leading to apoptosis.[adapted from 44]

1.4 Protecting groups

For a protecting group (PG) to be widely used in syntheses, it must possess several properties: It should be introduced selectively and in high yields without influencing other functional groups. The PG should be stable under all conditions during synthesis, including purification steps, until the protecting group is cleaved selectively. It should prevent racemization or epimerization and, in the best case, have a stabilizing effect on the molecule. In addition, PGs may offer other advantages such as better solubility or more suitable physical properties. This makes some intermediates easier to isolate, for example by crystallization. PGs should be able to be introduced and cleaved using readily available reagents, which also facilitates purification. Only a handful of PGs meet these requirements. Often a compromise has to be found, taking into account the most important criteria in terms of synthesis. In most cases, high stability of the PG with simultaneous easy cleavage is the decisive problem.[45]

So far, many easily usable and stable PGs have been discovered and explored. Depending on the reaction conditions, acid-labile, base-labile, redox-labile, enzyme-labile or photolabile PGs can be used. The choice of the appropriate PG depends, of course, also on the functional group to be protected.[45] In case of peptide synthesis, side chains of AAs can contain different kinds

of functional groups that interfere with reagents and reactants. Therefore, these groups must be capped with PGs preventing side reactions and resulting in better yields. Due to the great variety of functional groups, for example hydroxy, amino, carboxylic and thiol groups, many different PGs are used and must be matched.[14,46] SPPS strategies with various protection methods for the α-amino group have been developed and constantly optimized over the years. Most common are strategies with 9-fluorenylmethoxycarbonyl (Fmoc), used in combination with ^{t}Bu-type side-chain protection, or the *tert*-butyloxycarbonyl (Boc) group in combination with Bn-type side-chain protection. Whereas the Boc group is stable against bases, nucleophiles and catalytic hydrogenation, it can be removed with 25-50% trifluoroacetic acid (TFA) in DCM. On the other hand, Fmoc is a base-labile PG which is cleaved by solutions of 20% piperidine in DMF.[46,47] ^{t}Bu-type side-chain PGs are acid labil, which allows side chain cleavage without Fmoc removal in SPPS. Further, Trityl (Trt), Monomethoxytrityl (MMT), Boc, 2,2,4,6,7-Pentamethyl-2,3-dihydrobenzofuran-5-sulfonyl (Pbf) are acid-labile PGs. Due to the differences in stability, it is possible to selectively deprotect side chains to perform functionalizations without affecting other PGs that require more acidic cleavage conditions.[46,48,49]

1.4.1 Photo-labile protecting groups – light as a trigger

A functional PG is often selected on the basis of its cleavage conditions and is sometimes also used to form precursors of chemically or biologically active molecules. In research, many approaches follow strategies with enzyme-labile PGs, which are then cleaved within cells. Precursors that only acquire their properties after PG cleavage can thus be activated inside the cells.[50] Here it is a question of activation at the destination of the system, but there are other parameters for such an approach. Photo-labile PGs are cleaved by light and therefore no additional reagents are needed. This creates a good opportunity when it comes to work with cells in biochemistry.[45] Spatiotemporal control of the activation of the precursor allows more flexibility in this method. Some known photolabile protecting groups used for bio-applications such as 2-nitrobenzyl, 3-nitrophenyl, benzyloxycarbonyl, phenacyl, benzoinyl and related groups have been used for capping peptides, polysaccharides and nucleotides.[51] 2-Nitrobenzyl derivatives are commonly used photolabile PGs and were originally developed for organic synthesis. Biochemical application of 2-nitrobenzyl related groups was pioneered 1978 by Kaplan with the synthesis of caged ATP.[52]

In principle, a photolytic cleavage of a chemical bond is the result of the absorption of a photon by the molecule. Cleavage mechanisms can follow several numbers of pathways. For example, excitation of an organic chromophore can lead to the formation of a highly reactive diradical species. Considering all possible reaction pathways, hydrogen abstraction in the γ-position is quite common, and was identified by Norrish.[53] He described a mechanism for carbonyl compounds that is now known as a Norrish-type II reaction.[54] Cleavage of 2-nitrobenzyl derivatives also follow the Norrish-type II reaction where in the first step the double bond of the nitro-group is split homolytically forming a diradical species (Figure 11; A). After that, γ-hydrogen is abstracted creating a 1,4-diradical intermediate (Figure 11; B) followed by an intramolecular migration (Figure 11; C). The negatively charged oxygen of the nitro-group then attacks the γ-carbon atom leading to a five-membered cyclic intermediate (Figure 11; D). Photolytic cleavage of the PG and the capped molecule occur under release of carbon dioxide (Figure 11; E).[54]

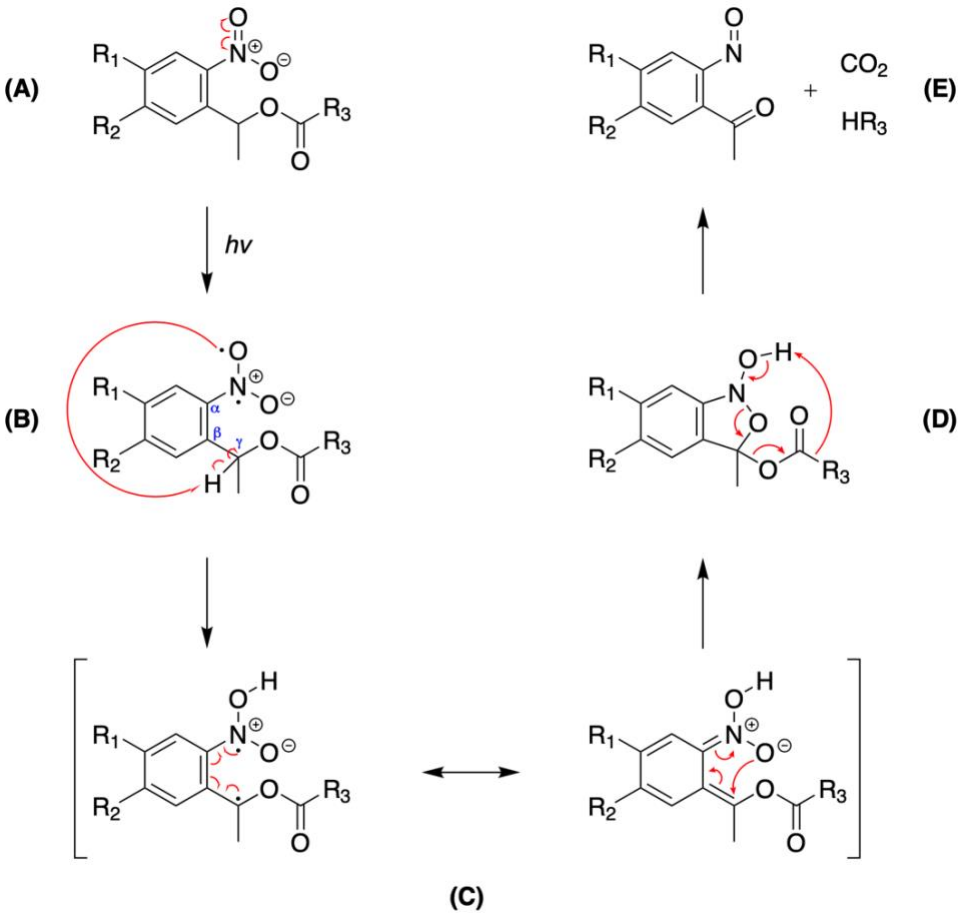

Figure 11: Photolytic cleavage of 2-Nitrobenzyl-based PGs through Norrish-type II reaction.[55]

1.5 Click chemistry

Advances in the understanding of molecular biology and other disciplines have led to an increasing demand for materials with clear and defined structures. The production of such multifunctional molecules presents significant synthetic challenges to the scientific community. Many synthetic strategies allow only rough control over the resulting product structure. For an organic synthetic approach to be widely used for material production, the reaction must have several properties. It must form stable bonds and have low cross-reactivity with other functional groups. Further, the reactants should be fully converted, and thus the reaction should be free of large amounts of byproducts. Additionally, the synthesis must proceed under mild reaction conditions and should be performed with readily available reagents.[56,57]

This year, in 2022, the Nobel Prize in Chemistry was awarded to Bertozzi, Meldal and Sharpless for the development of the reaction framework often referred to as click chemistry.[58] This synthetic framework meets all of the criteria mentioned above and can offer great potential for the synthesis of any type of material. Click reactions are driven by a high thermodynamic gain, resulting in stereospecific, fast reactions with high yields. Thus, it is not a specific reaction type, but rather defines a concept that encompasses multiple reactions with different mechanisms but share the same reaction processes and conditions. Sharpless described click chemistry early on as the formation of complex substances by bringing together smaller units via heteroatoms.[59] Bertozzi began using click chemistry in living organisms to study biological processes and target anticancer drugs. To do this, she developed bioorthogonal reactions that can occur in living organisms while not disrupting the normal chemistry of the cell. The application of click chemistry is a major advance for research at the cellular level in living organisms.[58,60]

Examples for click reactions include the Cu(I)-catalyzed Huisgen-1,3-dipolar cycloaddition and which is ideal for the controlled preparation of multifunctional materials (Figure 12).[56]

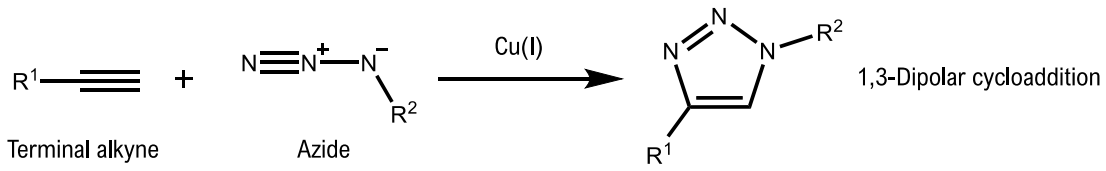

Figure 12: Cu(I)-catalyzed Huisgen-1,3-dipolar cycloaddition as example for click chemistry.[56]

The Huisgen-1,3-dipolar cycloaddition is a reaction between azides and terminal alkynes, the so called copper-catalyzed azide-alkyne cycloaddition (CuAAC), resulting in 1,4-disubstituted 1,2,3-

triazoles in very high yields under mild conditions.[61] This regioselective reaction has already been used as a powerful ligation tool for the most disparate molecular fragments. With the triazole ring as a non-toxic, robust keystone in complex molecular architectures, this click reaction has already been used for the selective modification of enzymes, viruses, and cells.[62–65] Besides organic synthesis, another area of application is in drug discovery, even though 1,2,3-triazoles have rarely been found in marketed drugs, demonstrating that there are still some limitations in the molecules of drug candidates.[66] Click reactions have been used for nucleotide labelling, peptide ligation and functionalization of solid surfaces for protein binding.[67–69] The potential applications of click chemistry in organic chemistry and biology are far from exhausted and will be further expanded and explored in the future.

2 Motivation

The aim of this work is the synthesis of a new photosensitive pro-self-assembling peptide amphiphile, and the analysis of its kinetics and structural characteristics. This molecule should be functionalizable with a linker for the introduction of a cell penetrating peptide, so that the system could be developed into a new modulated cancer therapy.

In recent years, the Weil group has conducted research on the synthesis of short self-assembling peptide amphiphile precursors for the use in cancer therapy.[41,43] They developed systems in which caged isopeptides were introduced into A549 breast cancer cells using the endocytotic pathway. Due to the characteristic environment in cancer cells, the pH and hydrogen peroxide labile groups were cleaved off, forming self-assembling monomers.[44] Fibre formation of these monomers led to a disruption of cell metabolism and thereby to apoptosis of the cancer cells. Pieszka and Zhou both used ISA-isopeptides with a boronic acid as the caging group, TAT for cell penetration and aromatic (with or without platinum) systems for self-assembly.[41,43] A new approach is to use photolabile protecting groups for such a system to have spatiotemporal control over the fibrillation initiation. A major advantage of the work with photolabile protection groups is that no chemical treatment is required for cleavage instead light of a specific wavelength.[45] In yet unpublished work, the Weil group used a 2-nitrosobenzyl-based protecting group for the synthesis of a self-assembling peptide precursor. A change in the isopeptide sequence to ICA resulted in an even more dynamic system with several chemical steps. Fmoc was selected as aromatic group for the self-assembly, which was initiated by irradiation for a short period of time with approximately complete cleavage. With its oxidizing potential, the 2-nitrosobenzyl group could be recycled for thiol oxidation, forming disulfides with other fibrillation properties. As disulfides are easily reducable (for example with DTT), this dynamic system was found to be, even in the fibrillation state, highly reversible.

Based on this work, a new pro-self-assembling peptide amphiphile should be developed with the possibility to attach a cell penetrating species to address cancer cells. This amphiphile should have the same properties and characteristics in fibrillation, reversibility and dynamics as the one mentioned before. Therefore, an ICA-isopeptide (Figure 13, black) will be synthesized using the Fmoc-SPPS-strategy and a manual esterification method. Attached Fmoc (Figure 13, green) should drive self-assembly via π-π-stacking and nvoc3 (Figure 13, orange) should act as the precursor protecting group and oxidizing reagent that can be cleaved off at 365 nm. Another

advantage of nvoc3 is the terminal alkyne group that can be used for functionalization via Huisgen-1,3-dipolar click reaction. Additionally, a coumarin343 (Figure 13, blue) varaint of the described amphiphile will be synthesized for coincubation which could be an imaging possibility in later cell experiments as shown in the publication of Pieszka.[41] The aimed system and expected reaction cascade after irradiation of Iso(Fmoc-I)nvoc3CA and Iso(C343-I)nvoc3CA is shown in Figure 13.

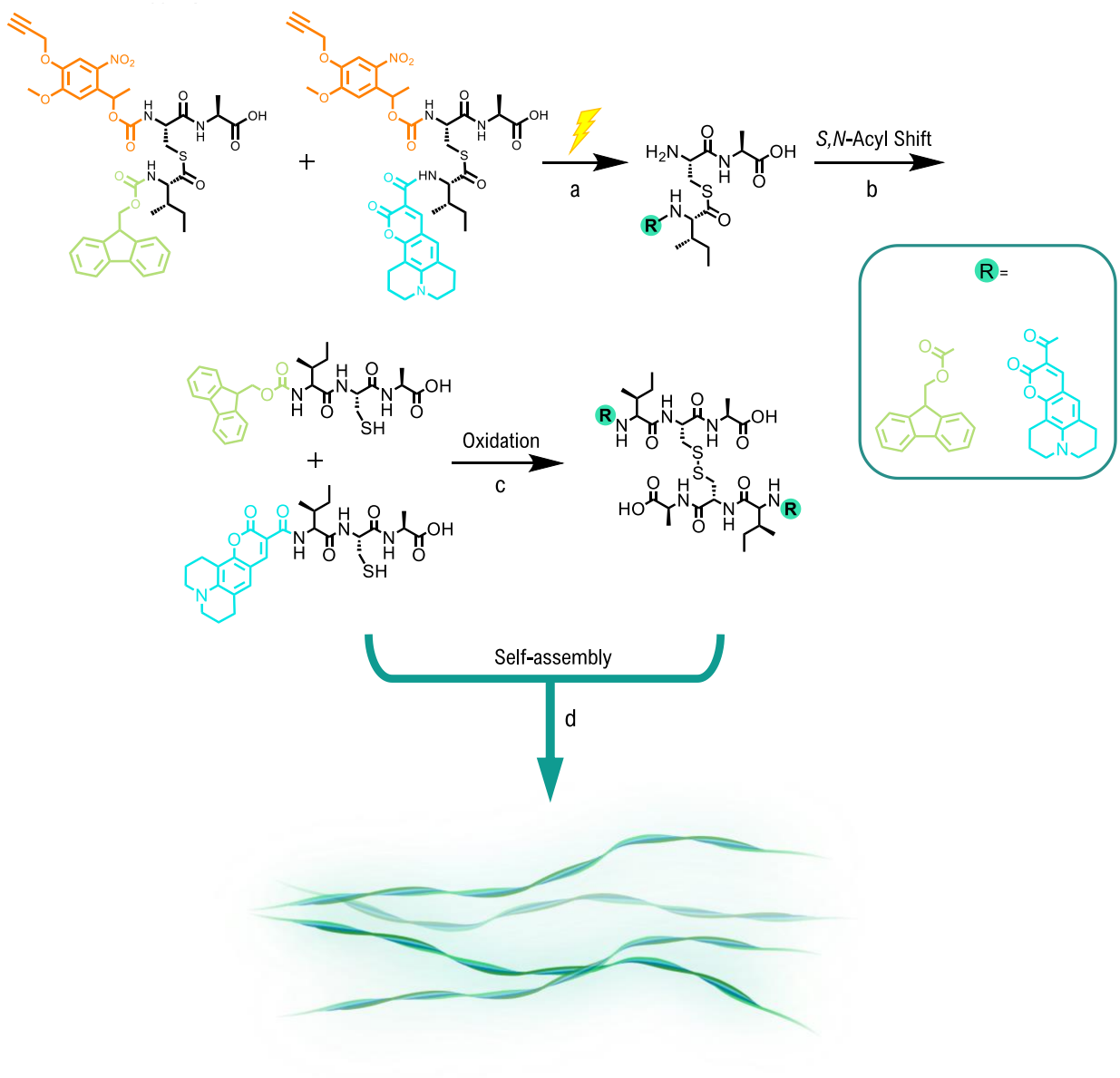

Figure 13: Expected reaction cascade for Iso(Fmoc-I)nvoc3CA and Iso(C343-I)nvoc3CA (top left). First step is the controlled irradiation and cleavage of nvoc3 at 365 nm (a), followed by the *S,N*-acyl shift (b) that results in the linear peptide amphiphiles Fmoc-ICA and C343-ICA. Oxidation of the monomers leads to disulfides (c) and both structures can self-assemble and form fibres through π- π-stacking (d).

The synthesized products will be purified by high performance liquid chromatography (HPLC) and following lyophilization. Further, nuclear magnetic resonance (NMR), liquid chromatography (LC) and mass spectrometry (MS) will be used for characterization measurements. Photolysis kinetics will be used to develop an irradiation protocol for this new class of pro-self-assembling peptide amphiphiles. Afterwards, *S,N*-acyl shift kinetics will be investigated through multiple time point measurements with an analytical HPLC setup after irradiation. Circular dichroism (CD) and transmission electron microscopy (TEM) measurements will be performed for analysis of secondary structure and fibrillation properties.

This work was carried out under the supervision of *Patrick Roth* and the synthetic protocols and experimental procedures were partly based on his work. Therefore, the following results will be included in his dissertation.

3 Results and Discussion

In the following chapter, results collected during this work are described and discussed regarding synthesis, characterization and structure analysis.

3.1 Synthesis

Synthesis of isopeptides and the control peptide

Synthesis of isopeptides and the control peptides was performed using the Fmoc solid-phase peptide synthesis strategy (SPPS) with a Liberty Blue Automated Microwave Peptide Synthesizer by CEM Corporation or a Merrifield apparatus (esterification).

A Wang-resin with an attached Fmoc-protected alanine was deprotected with 20% piperidine in DMF and either Fmoc-protected cysteine or serine coupled to the growing peptide. After another Fmoc-deprotection step, *N*-terminal protection with nvoc3 and esterification with Fmoc- or C343-proteced isoleucine were performed outside of the SPPS-device in a Merrifield apparatus. Cysteine containing peptides were treated with a mixture of DCM/TIPS/TFA (6x 10 mL; 95%/5%/1%) to cleave the side chain protecting MMT group. Protection with nvoc3 was needed to enable the coupling of isoleucine to the hydroxy or thiol group (ester) in the side chain of serine or cysteine, resulting in a so-called isopeptide. Synthesized isopeptides were cleaved from the resin with a mixture of TFA/TIPS/MilliQ water (95%/2.5%/2.5%) and purified by HPLC. Since nvoc3 is a photolabile protecting group, every working step with nvoc3 was performed under exclusion of light. Figure 14 and Figure 15 show the reaction schemes of all synthesized isopeptides: Iso(Fmoc-I)nvoc3CA (**1**) (70 mg, 17.4%) , Iso(C343-I)nvoc3CA (**2**) (20 mg, 5.0%), Iso(Fmoc-I)nvoc3SA (**3**) (10 mg, 12.7%) and Iso(C343-I)nvoc3SA (**4**) (4 mg, 4.8%). Decreased yields can be explained due to the many reaction steps and loss through purification.

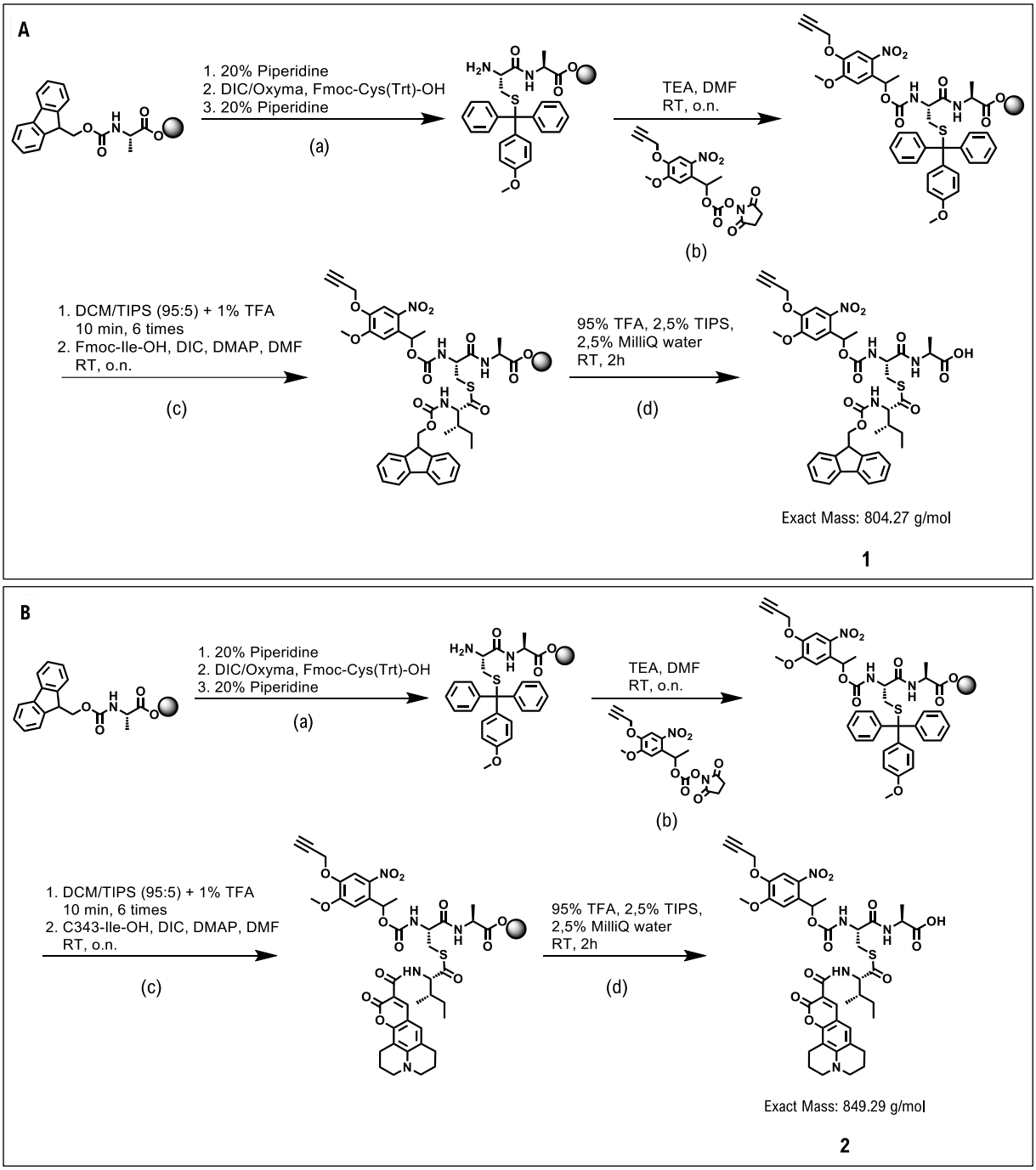

Figure 14: Reaction schemes of cysteine containing isopeptides Iso(Fmoc-I)nvoc3CA (**A**, **1**) and Iso(C343-I)nvoc3CA (**B**, **2**): SPPS-cycle of deprotection with 20% piperidine and AA coupling with DIC/Oxyma (a), protection with nvoc3 using TEA (b), cleavage of MMT group with DCM/TIPS/TFA (95:5 +1%) and esterification with Fmoc-Ile (**A**) or C343-Ile (**B**) (c), cleavage from the resin (d).

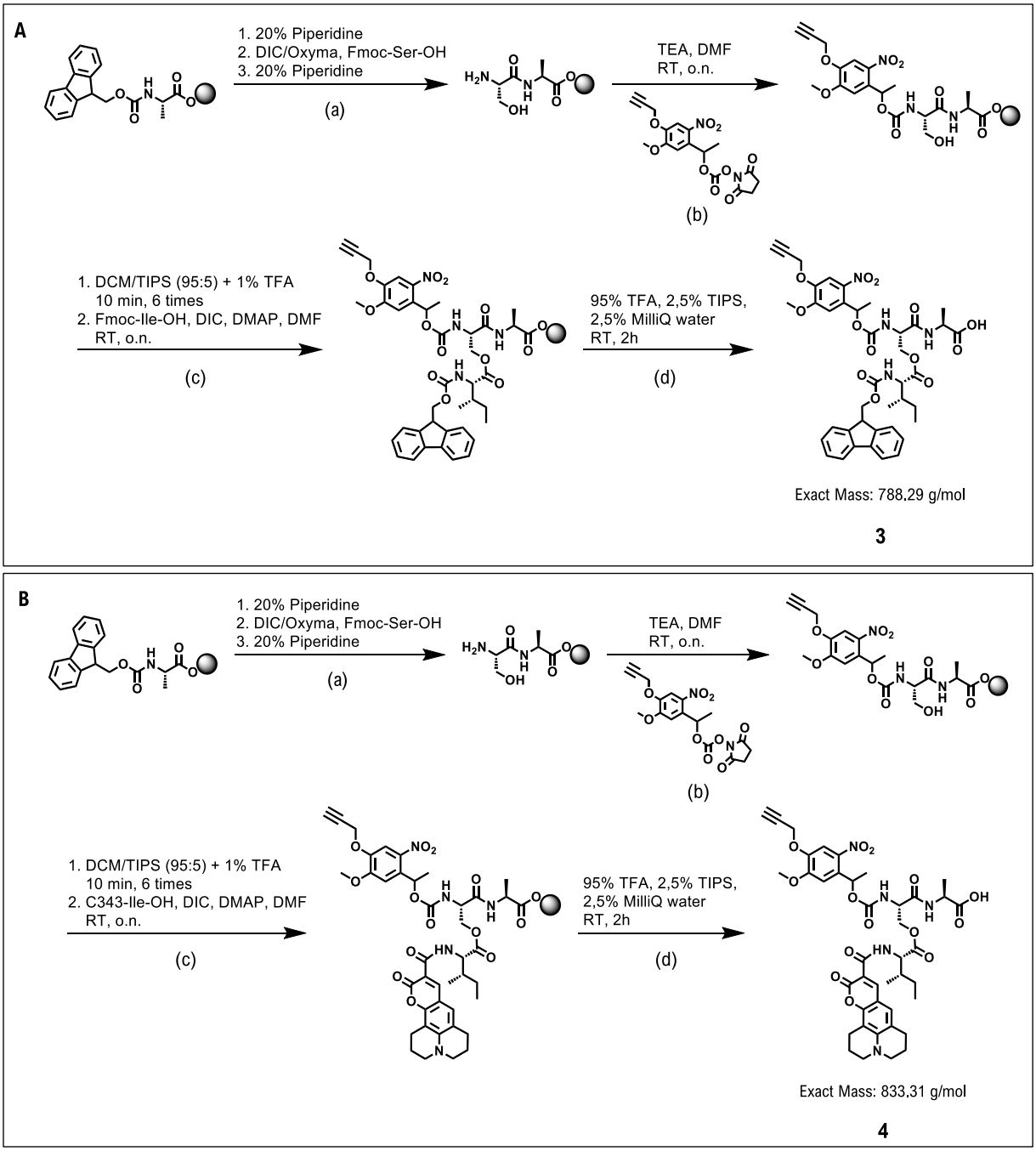

Figure 15: Reaction schemes of serine containing isopeptides Iso(Fmoc-I)nvoc3SA (**A**, **3**) and Iso(C343-I)nvoc3SA (**B**, **4**): SPPS-cycle of deprotection with 20% piperidine and AA coupling with DIC/Oxyma (a), protection with nvoc3 using TEA (b), esterification with Fmoc-Ile (**A**) or C343-Ile (**B**) (c), cleavage from the resin (d).

At first, synthesis of **2** was performed by attaching Fmoc-isoleucine and following deprotection with 20% piperidine. Later purification showed that the thiol ester was piperidine labile and hydrolyzed. Therefore, another approach was developed including the linkage of C343 to isoleucine before used for esterification.

Synthesis of C343-ile was realized by coupling of H-Ile-OtBu · HCl and Coumarin343 using PyBOP as a coupling reagent and DIPEA as a base. After purification through flash column chromatography (2:1 CH/EA, R_f=0.41), the ^{t}Bu protecting group was cleaved under acidic conditions. The yellow-orange product was analyzed by NMR-spectroscopy and could then be used for the isopeptide synthesis.

Yield: 541.6 mg (90.7%)

Later during this work, difficulties were encountered in the analysis of the model compounds **1** and **2** , which will be explained in more detail in later chapters. The reason for difficulties could be due to the alkyne group, as it represents one of the few differences to the already known and analyzed nvoc. After irradiation with UV-light, the alkyne group could undergo unwanted side reactions due to its high electron density, which could prevent self-assembly and therefore show other characteristics. To exclude this possible interfering factor, the alkyne group of **1** was linked to 6-azidohexanoic acid via a Cu(I)-catalyzed Huisgen-1,3-dipolar cycloaddition. TBTA was used as ligand and $CuSO_4$ as the copper source which was reduced by sodium ascorbate to generate Cu(I)-ions freshly in solution. This reaction could be performed in a DMSO/MilliQ water mixture at room temperature and be purified via HPLC yielding a white powder. Purification could be verified by analytical HPLC and LC-MS (Figure 16). The HPLC trace shows two peaks at 18.9 min and 19.7 min, representing both isomers, due to the chiral center of the molecule being located in the nvoc3 protecting group.

Yield: 3 mg (52.0%)

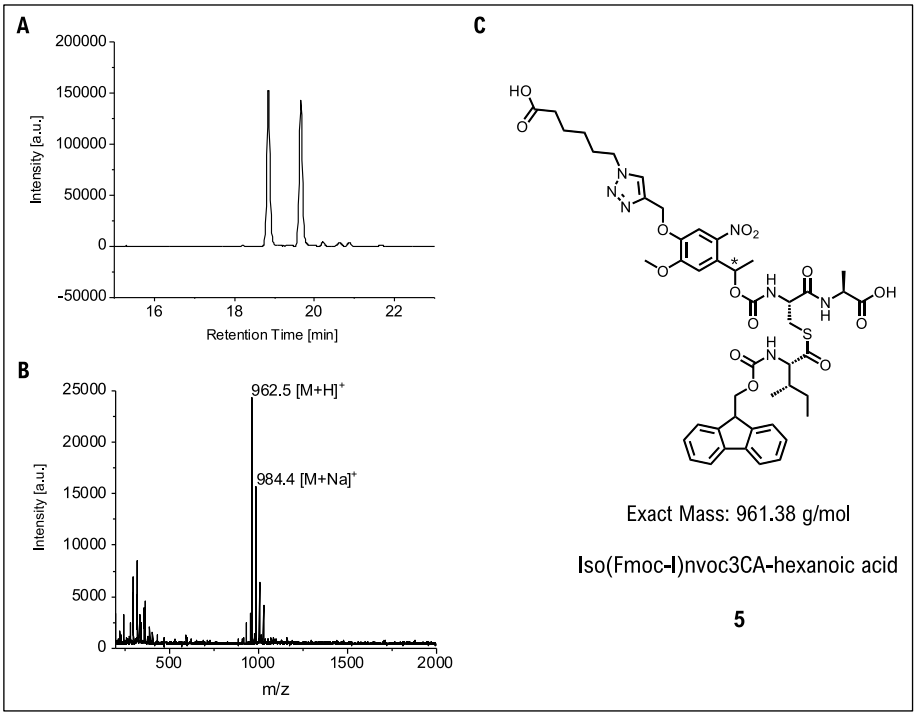

Figure 16: HPLC-chromatogram (A), MS-spectrum (B) and molecular structure with marked chiral center (*, C) of Iso(Fmoc-I)nvoc3CA-hexanoic acid **5**. Calculated: M = 961.38 g/mol. Found: $[M+H]^+$ = 926.5 g/mol, $[M+Na]^+$ = 984.4 g/mol.

C343-ICA

The control peptide C343-ICA **6** was synthesized on a Chlorotrityl-resin with an attached unprotected alanine. Fmoc-protected cysteine and isoleucine were coupled to the peptide and then Fmoc-deprotected with 20% piperidine in DMF. For *N*-terminal protection with C343, the coupling reagents PyBOP and DIPEA were used and added to the resin in a reaction vail. C343-ICA was cleaved from the resin and side chain deprotected before purification by HPLC (Figure 17). A yellow-orange product was obtained and analyzed through LC-MS and NMR. The control peptide was synthesized for use in structure analysis and characterization experiments as a reference compound and for system validation experiments.

Yield: 80 mg (27.9%)

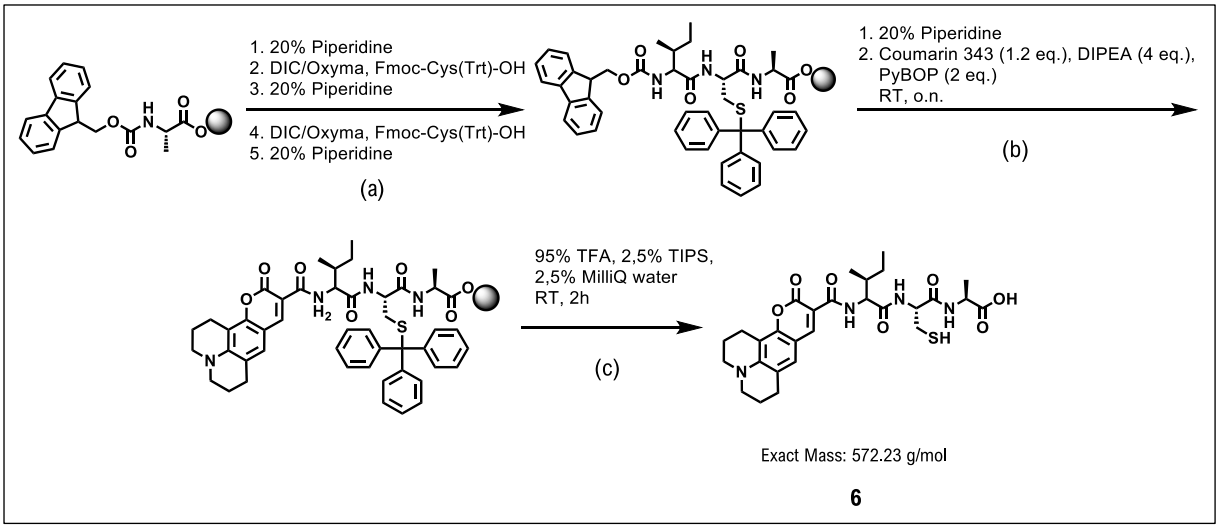

Figure 17: Reaction scheme for the synthesis of C343-ICA using the Fmoc-SPPS strategy: SPPS-cycle of Fmoc-deprotection with 20% piperidine and AA coupling with DIC/Oxyma (a), Fmoc-deprotection and C343-coupling with PyBOP and DIPEA (b), cleavage of side chain protecting groups and from the resin (c).

Since the thiol groups are to be oxidized to disulfide bridges in the system, DiC343-ICA **7** was also prepared as a control compound. Therefore, C343-ICA was dissolved in DMSO in MeOH (v/v) and stirred at room temperature for 72 h. Purification by HPLC yielded in an orange powder that was analyzed by LC-MS.

Yield: 3 mg (44.8%)

ESI-MS spectra and HPLC-chromatograms of synthesized isopeptides, control peptides and provided control peptides that were only used as references in HPLC-analyses are shown in Figure 18 and Figure 19.

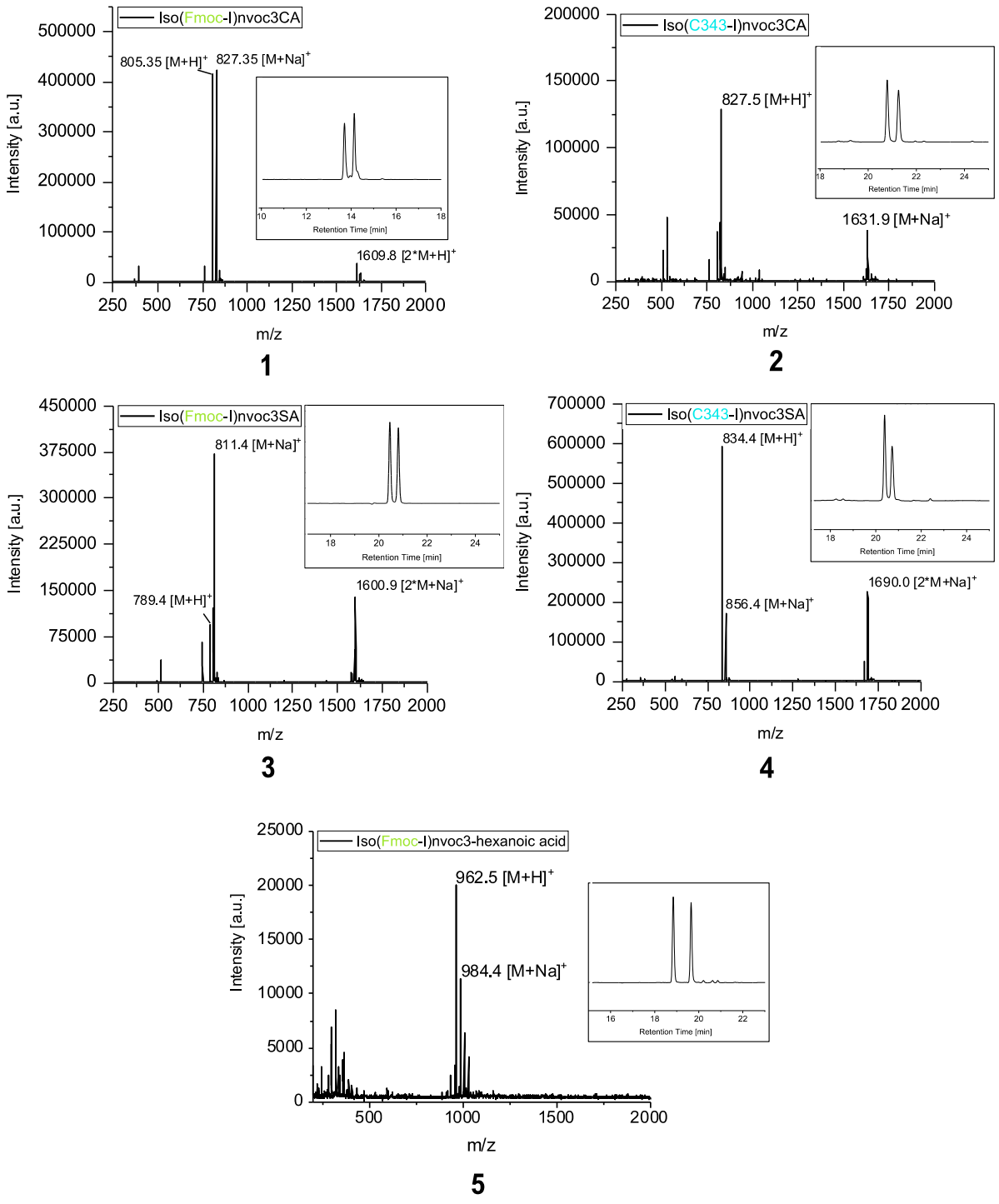

Figure 18: ESI-MS spectra and HPLC chromatograms of the synthesized isopeptides **1**, **2**, **3**, **4**, and **5**.

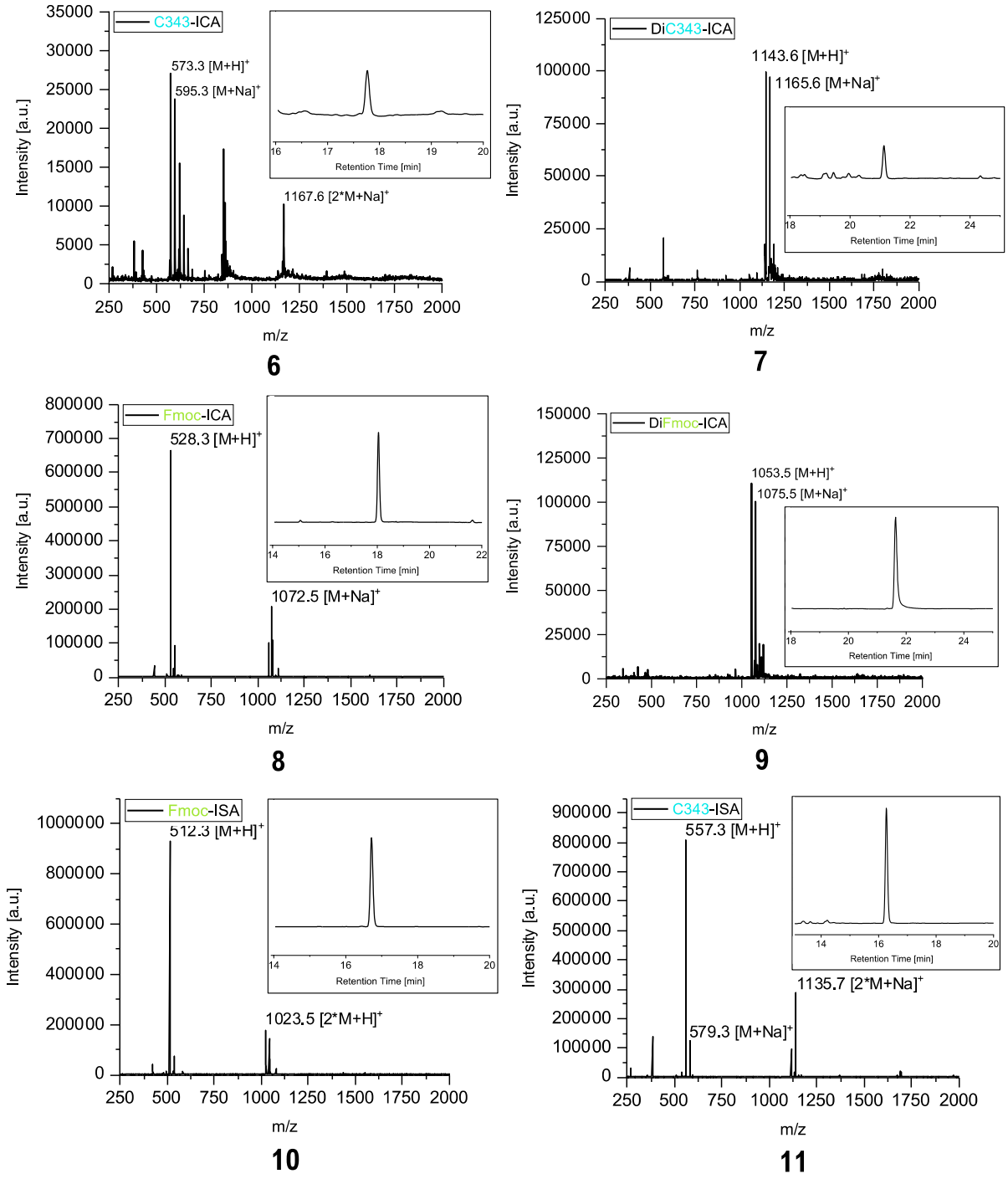

Figure 19: ESI-MS spectra and HPLC chromatograms of the control peptides **6**, **7**, Fmoc-ICA **8**, DiFmoc-ICA **9**, Fmoc-ISA **10** and C343-ISA **11**.

3.2 Characterization and Analysis

The following chapter shows the results of characterization and analysis of synthesized isopeptides and control peptides in terms of self-assembly and the reaction cascade. Fmoc-ICA and DiFmoc-ICA were provided by Patrick Roth of the Max-Plank-Institute for Polymer Research. C343-ISA was provided by Sarah Chagri and nvoc-glycine was provided by Raphael Meyer of the Max-Plank-Institute for Polymer Research.

3.2.1 Photolysis rate of isopeptides

During this work, isopeptides were irradiated to investigate the rate of cleavage of the photolabile PG. This was realized by irradiation of 100 µM isopeptide solutions (MeOH/NH_4HCO_3-buffer; pH=7.4, 5 mM; 1:1) at 365 nm for 0 s, 30 s, 60 s, 90 s, 120 s, and 600 s (n=3) and analyzed via HPLC. The photolysis rate results from the quotient of the calculated areas under the peaks that occur at the retention times of the non-irradiated (0 s) reference samples. It describes the percentual rate of nvoc3 cleavage after different irradiation times.

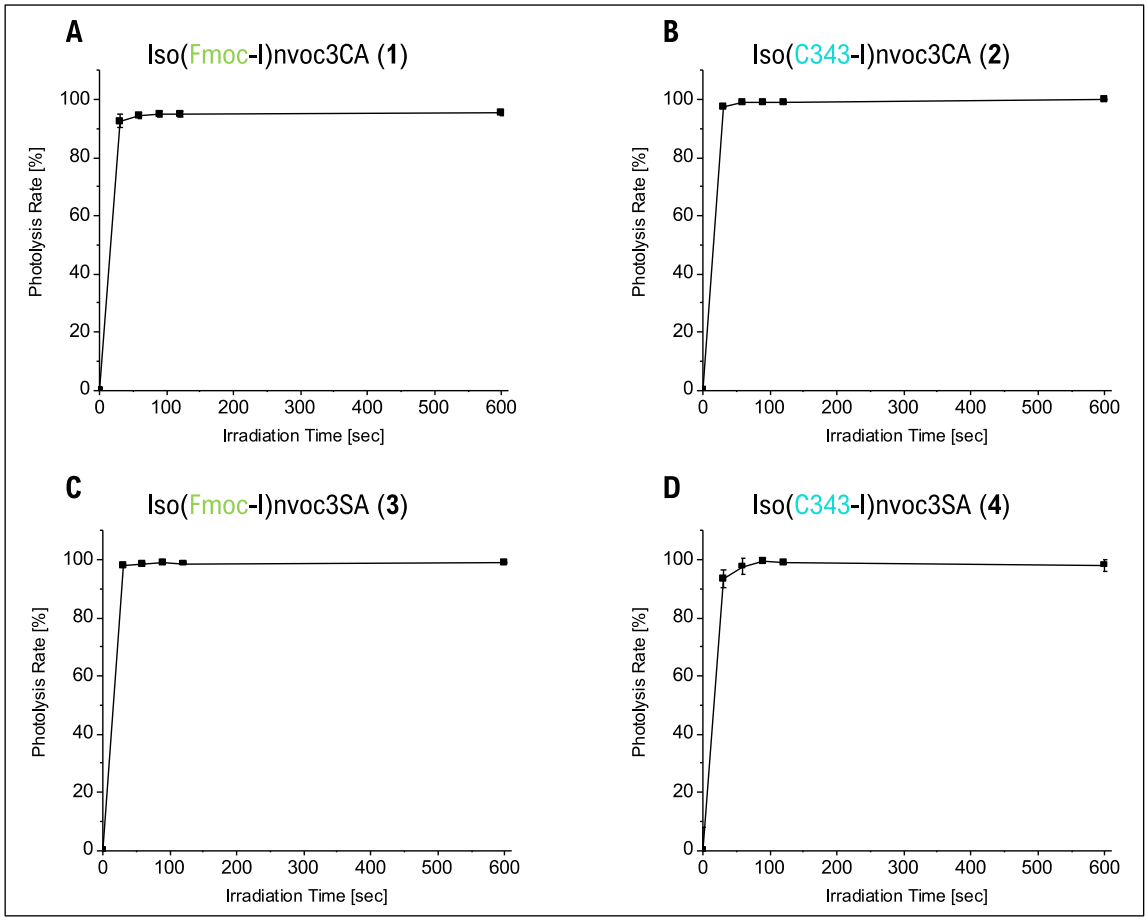

Figure 20: Photolysis rates of **1**, **2**, **3** and **4** are shown in percent plotted against irradiation times in seconds. Samples were irradiated at 365 nm for 0 s, 30 s, 60 s, 90 s, 120 s, and 600 s (n=3).

Figure 20 shows the photolysis rates of **1**, **2**, **3** and **4** plotted against irradiation times resulting in comparable curves. An initial sharp increase is followed by a slow approach to 100%, showing an increase in the photolysis rate with increasing irradiation times. After 30 s of irradiation, photolysis rates of more than 90% are found for **1** and **4**, whereas for **2** and **3** these rates are even higher than 95%. From this it can be concluded that more than 90% of each isopeptide can be deprotected, in comparison to the non-irradiated protected samples, with an irradiation time of 30 s. Irradiation times of 60 s and higher did not lead to further significant increases of the photolysis rates and therefore, 30 s was set as the irradiation time for further experiments.

During analyzation of C343-containing isopeptides, decreasing yellow coloring with simultaneously increasing irradiation times was observed. To further investigate the impact of irradiation on C343, absorbance measurements were performed with irradiated samples of C343-ICA (100 µM in PBS). Obtained data showed a decrease in absorption with longer irradiation times (see Figure 55, appendix), which can be explained by photobleaching. Photobleaching or chemical quenching is the permanent loss of fluorescence of a fluorophore as a result of irradiation. The fluorophore molecules are photochemically destroyed by the excitation light and lose their fluoresce ability.[] However, C343 still shows a high absorption after irradiation of 30 s, which indicates suitability of C343 as a fluorophore for the system.

Based on these results, the successful UV-induced cleavage of nvoc3 could be confirmed. Thus, the conditions for the further analyses of isopeptides for this work are fulfilled. In addition, future cell experiments with this system could be carried out due to the relatively short irradiation times despite the use of UV light.

3.2.2 *S,N*-acyl and *O,N*-acyl shift-kinetics

For the analysis of *S,N* and *O,N*-acyl shifts of **1**, **2**, **3** and **4**, 100 µM peptide solutions ($MeOH/NH_4HCO_3$-buffer; pH=7.4, 5 mM; 1:1) were irradiated for 30 s at 365 nm and injected into a HPLC setup. Data was collected at different time points after irradiation and plotted in comparison to chromatograms of non-irradiated isopeptide, the corresponding linear- and disulfide-peptides. After successful nvoc3 cleavage (a, Figure 21), the unprotected isopeptide should rearrange by *S,N*- or *O,N*-acyl shift to form the linear peptide amphiphile (b, Figure 21). In the case of the cysteine containing peptides, the thiols can further oxidize into disulfides (c, Figure 21).

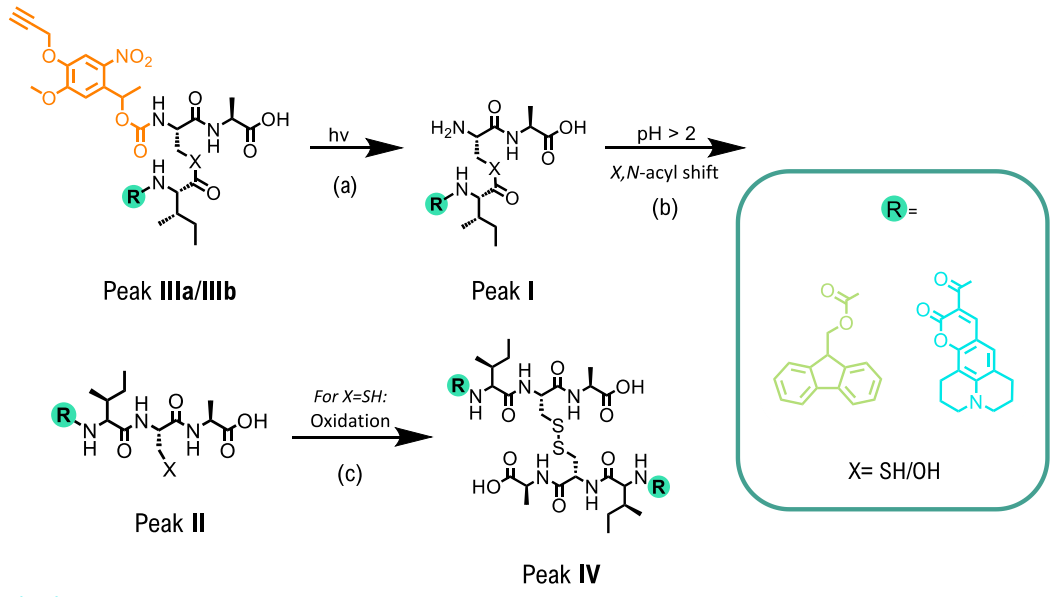

Figure 21: Reaction cascade of nvoc3 cleavage through isopeptide irradiation (a), *S,N*- or *O,N*-acyl shift at a pH > 2 (b) and oxidation of two thiol groups of cysteine containing peptides to a disulfide peptide (c).

For the analysis of Iso(Fmoc-I)nvoc3CA **1**, HPLC-measurements were performed 0 min, 20 min, 40 min, 60 min, 120 min, 240 min, 360 min and 24 h after irradiation. The obtained data are shown in Figure 22 along with Fmoc-ICA, DiFmoc-ICA and non-irradiated isopeptide **1** as controls.

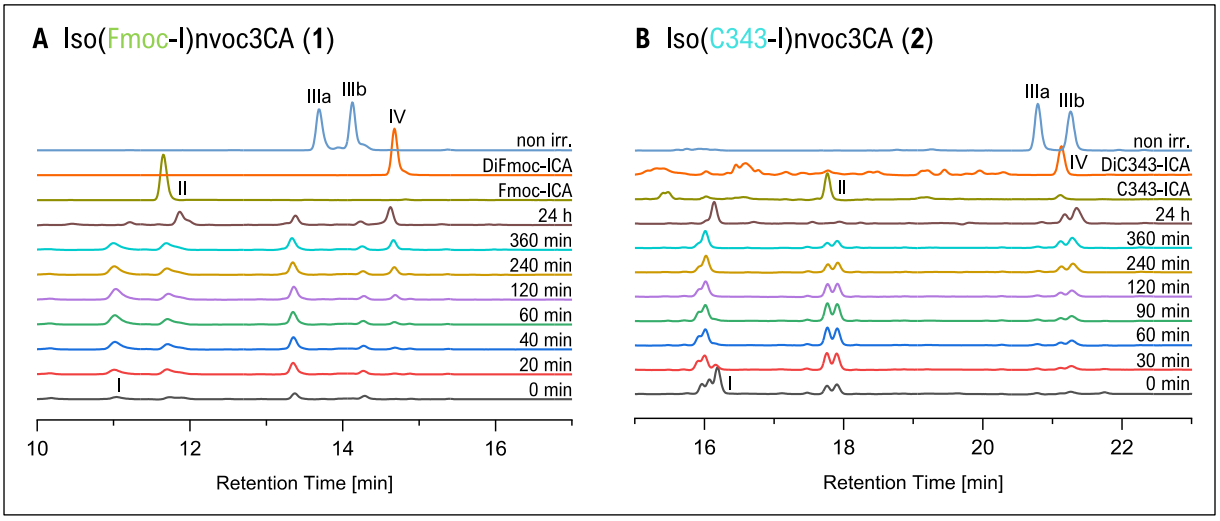

Figure 22: HPLC-chromatograms or irradiated (30 s) Iso-(Fmoc-I)nvoc3CA **1** (**A**) and Iso(C343-I)nvoc3CA **2** (**B**) measured after different periods of time compared to non-irradiated isopeptide (light blue) and corresponding linear (khaki) and disulfide (orange) peptides.

The analyzed isopeptide shows two peaks (peaks IIIa and IIIb) which represent the R- and S-isomer due to the chiral center in the PG. Already at 0 min the chromatogram shows, besides the complete isopeptide cleavage, two small peaks with retention times of 11 min (peak I) and 11.8 min (peak II). Peak I decreases after 240 min, indicating the unprotected isopeptide formed during irradiation gradually rearranges to the linear peptide. Contrary to expectation that the amount of unprotected isopeptide should be highest directly after irradiation, peak I initially increases. Since the used HPLC setup cools samples down to 15 °C, different injection concentrations may have occurred because the peptide solution was still at room temperature during the first injection.

The peak of Fmoc-ICA (peak II) continues to rise, whereas peak I is no longer present after 24 h, demonstrating a complete successful rearrangement within 24 h. After 40 min, a new peak at 14.7 min (peak IV) arises and increases over time, representing the disulfide species formed through oxidation of the linear peptide. Since no other reagents were added to the sample solution, it can be assumed that the cleaved PG acts as an oxidizing agent showing a functional recycling for the formation of the disulfide peptide.

In addition to this reaction cascade, another peak at 13.4 min occurs immediately after irradiation and shows no change in intensity over time. Since this peak does not belong to any molecule of the cascade, it can be assumed that another species was formed after the nvoc3 cleavage. The work with thiols involves relatively dynamic systems, therefore, in addition to the model compounds Iso(Fmoc-I)nvoc3CA **1** and Iso(C343-I)nvoc3CA **2,** serine containing isopeptides were synthesized and analyzed to determine possible differences. The following figure shows *S,N*- and *O,N*-acyl shift kinetics of Iso(C343-I)nvoc3CA **2,** Iso(Fmoc-I)nvoc3SA **3** and Iso(C343-I)nvoc3SA **4**.

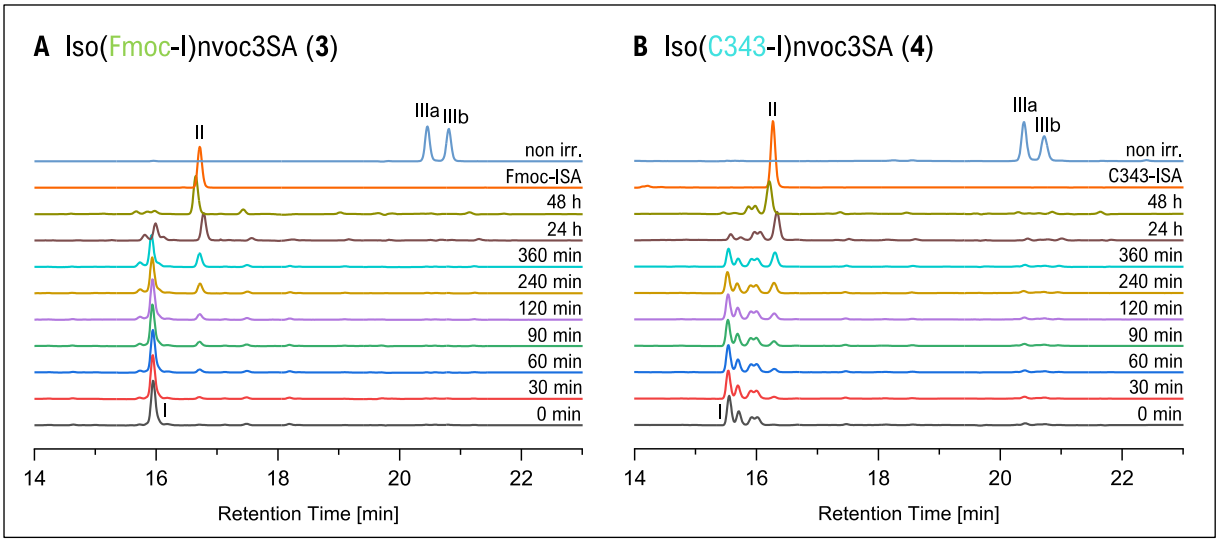

Figure 23: HPLC-chromatograms of irradiated (30 s) Iso(Fmoc-I)nvoc3SA **3** (**A**) and Iso(C343-I)nvoc3SA **4** (**B**) measured after different periods of time compared to non-irradiated isopeptide and corresponding linear and disulfide peptides.

HPLC-measurements of the isopeptides **2**, **3** and **4** were conducted 0 min, 30 min, 60 min, 90 min, 120 min, 240 min, 360 min, 24 h and 48 h after irradiation (Figure 22, Figure 23). Obtained HPLC traces are shown in comparison to the non-irradiated peptide and the corresponding linear and disulfide peptides as controls. Each kinetic shows the same scheme with an arising and decreasing peak I (Figure 22 **A**: R_T =16 min; Figure 23 **A**: R_T =15.9 min; **B**: R_T =15.5 min) and an increasing peak II with comparable retention times as the linear control peptides (Figure 22 **A**: R_T =17.8 min, Figure 23 **A**: R_T =16.6 min, **B**: R_T =16.3 min). In case of Iso(C343-I)nvoc3CA, peak II decreases whereas peak IV starts to arise. This can be explained due to the disulfide formation out of two linear peptide monomers.

Peak I in Figure 22 **B** can still be seen after 24 h, whereas peak II disappears after 24 hours. This leads to the suggestion that part of peak I could arise due to the formation of a by-product during the irradiation process, which was also suspected in Figure 22 **A**. Formation of a peak at 16 min in Figure 23 **A** supports this assumption and shows that the by-product is also obtained in serine systems. Structural properties of these peptides (**3** and **4**) were not further investigated.

LC-MS analysis showed a peak (R_T=6.6 min) with a mass to charge ratio of m/z=451.2 (Figure 24) in every irradiated kinetic solution measured after 24 h.

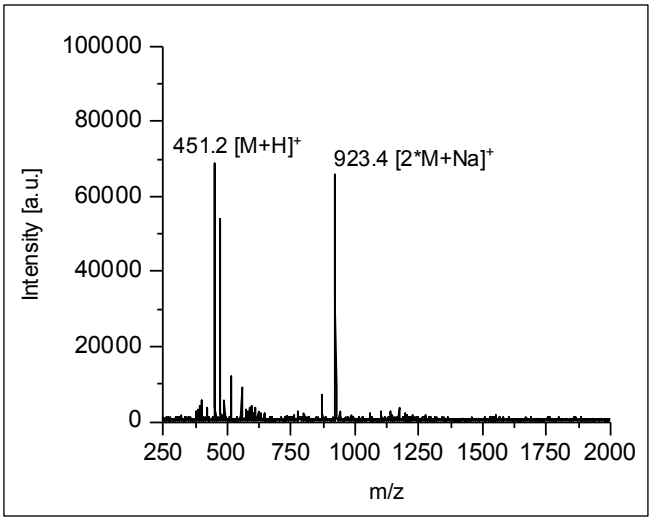

Figure 24: ESI-MS of the arising peaks in shift kinetics measured after 24 h.

Future experiments could include the analysis of the by-product, which could be realized through isolation, enrichment and structure clarification via NMR-spectroscopy.

To test whether the formation of the by-product occurs due to the free alkyne group, the *S,N*-acyl shift kinetic was performed with iso(Fmoc-I)nvoc3CA-hexanoic acid **5** (Figure 25).

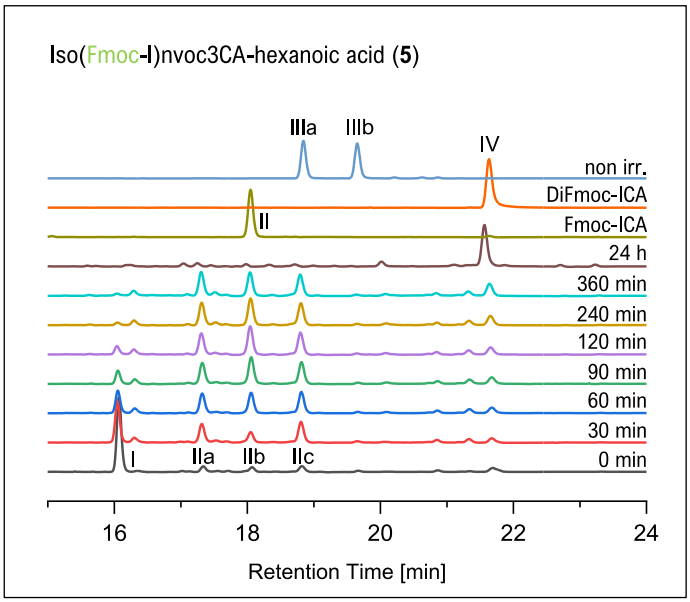

Figure 25: HPLC-chromatograms of irradiated (30 s) Iso-(Fmoc-I)nvoc3CA-hexanoic acid **5** measured after different periods of time compared to non-irradiated isopeptide and corresponding linear and disulfide peptides.

Immediately after irradiation, peak I (R_T=16.1 min) and peaks IIa, IIb and IIc (IIa: R_T=17.3 min, IIb: R_T=18.1 min, IIc: R_T=18.9 min) appear, with peak I decreasing steadily and the other three peaks increasing up to 360 min and then disappearing after 24 hours. The middle peak IIb has

the same retention time as the control peptide Fmoc-ICA (peak II) and all three peaks disappear within 24 which suggests that they represent the rearranged linear peptide. To analyze the distribution of peaks IIa/b/c, the kinetics should be repeated under different conditions in future experiments. Another possibility would be the use of a LC-MS for the kinetic analysis to directly analyze the masses of occurring peaks.

From the disappearance of peaks I and IIb, it can be concluded that both the rearrangement of isopeptides and the oxidation of linear peptides to disulfides have taken place completely after 24 h. Peak IV occurs immediately after irradiation and increases over time. By comparison with the control, this peak can be assigned to the DiFmoc-ICA. Furthermore, there is no peak to be seen at a retention time of 16 min that would be comparable to the peaks of the other kinetics that occurred after irradiation but did not disappear over time (see Figure 23). This allows the conclusion that these peaks are actually caused by the free alkyne group during or after irradiation.

Through the analysis of kinetics, it was shown that the rearrangement of isopeptides **1-5**, deprotected by UV-light, takes place within 24 h (*S,N*-acyl shift) or 48 h (*O,N*-acyl shift), respectively. The expected reaction cascade could be confirmed by the time-delayed occurrence, increase and decrease of the individual peaks. In this context, the formation of linear and disulfide peptides is of particular importance, as these are expected to function as self-assembling monomers. However, it has also been shown that a by-product is arising during cleavage, which is probably formed by a reaction of the free alkyne group.

3.2.3 Structure analysis via Circular Dichroism (CD)

To analyze the secondary structure of the synthesized model compounds Iso(Fmoc-I)nvoc3CA, Iso(C343-I)nvoc3CA and Iso(Fmoc-I)nvoc3CA-hexanoic acid, CD-spectra were conducted for 100 µM in NH_4HCO_3-buffer (pH=7.4, 5 mM). One sample of each compound was irradiated in MeOH for 30 s at 365 nm before evaporation and incubation in buffer for 24 h. The linear peptides Fmoc-ICA and C343-ICA and the disulfide peptides DiFmoc-ICA and DiC343-ICA were measured as controls. Samples were measured from 180 nm to 300 nm via 3 times data accumulation at 20 °C. Figure 26 shows the processed data of the isopeptides compared to the CD-spectra of the control peptides.

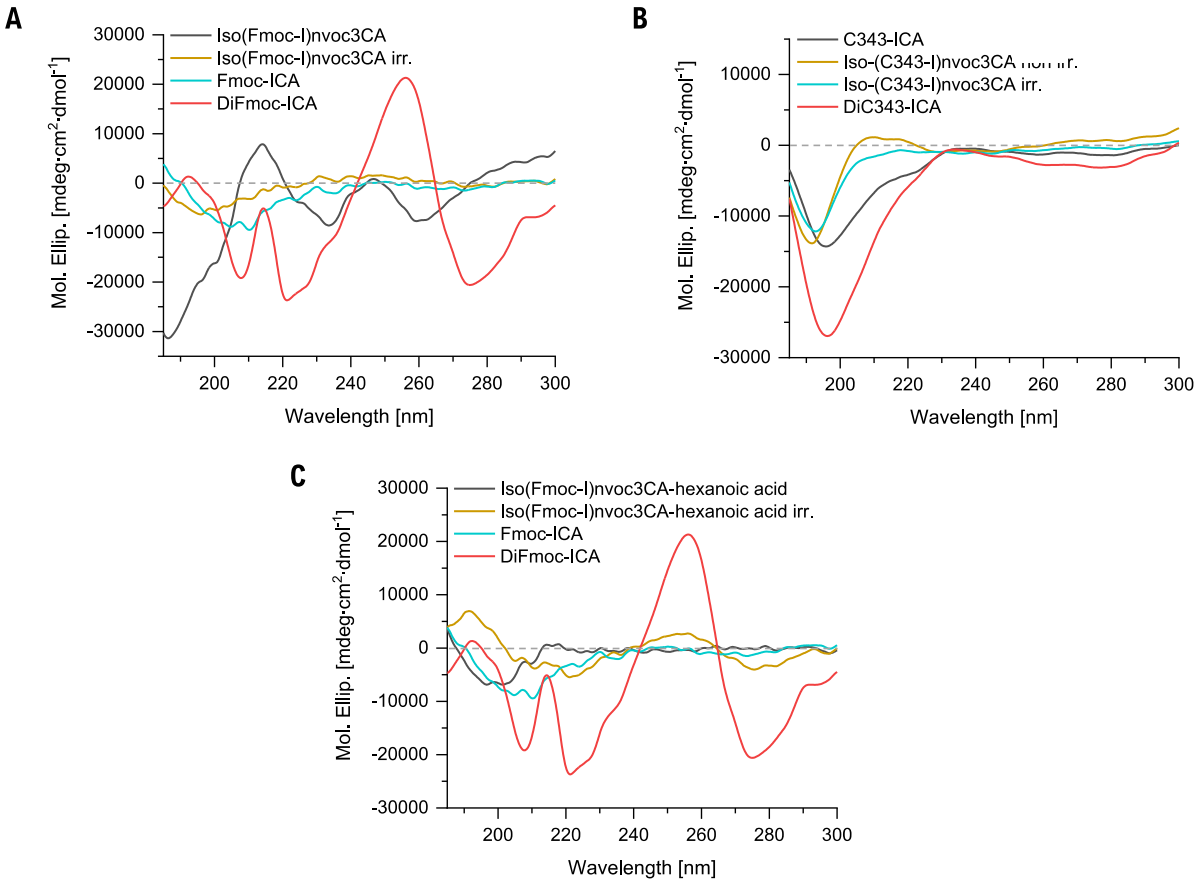

Figure 26: CD-spectra of Iso(Fmoc-I)nvoc3CA **1** (**A**), Iso(C343-I)nvoc3CA **2** (**B**) and Iso(Fmoc-I)nvoc3CA-hexanoic acid **5** (**C**), each with an irradiated sample and corresponding linear and disulfide peptide. Samples were measured in 100 µM in NH_4HCO_3-buffer (pH=7.4, 5 mM).

CD-spectra of C343 containing peptides shows similar curves with minima between 190 nm and 200 nm that are typical for no defined secondary structure.[70] Peptides were further analyzed via TEM-measurements, which could confirm these findings (see chapter 3.2.5).

CD-spectra of **8** shows a maxima before 190 nm and a minimum at 210 nm. These findings indicate formation of ordered β-sheet structures.[70]

For the control peptide DiFmoc-ICA **9**, as maximum at 193 nm and a minimum at 208 nm were observed in the CD spectrum. The maximum around 218 nm, which can be attributed to a $n \rightarrow \pi^*$ transition, whereas the maximum at 258 nm is corresponding to the $\pi \rightarrow \pi^*$ transition. Another minimum at 220 nm indicates atypical twisted β-sheet structures.[41,43,71,72] CD-spectra of **5** contains a maximum at 193 nm, followed by a minimum at around 221 nm and a maximum at 258 nm, whereby it shows few similar events when compared to **9**. This could be explained by self-assembly after irradiation driven by aromatic interactions and resulting in atypical twisted β-sheet structures.[72]

However, the curves of irradiated Iso(Fmoc-I)nvoc3CA **1** and non-irradiated Iso(Fmoc-I)nvoc3CA-hexanoic acid **5** show maxima before 190 nm and a minimum around 198 nm, respectively, which indicates a more disordered structure as random coil.[70] Irradiated **1** was expected to show ordered β-sheet structures, as it forms Fmoc-ICA after exposure to UV-light. Since the cleaved PG remains in the sample solution it could interfere with the measurement.

The CD spectrum of non-irradiated Iso(Fmoc-I)nvoc3CA **1** possesses a minimum at 185 nm followed by a maximum at 218 nm, which can be attributed to a $n \rightarrow \pi^*$ transition.[41,43] These findings suggest ordered β-sheet structures, which were not assumed since the sample was not irradiated and should therefore not form self-assembling amphiphiles. Further experiments could investigate structural changes in correlation to used solvents.

Through secondary structure analysis via CD-measurements could be shown that C343-containing peptides form random coil structures, whereas Fmoc-containing peptides can show ordered β-sheet structures. DiFmoc-ICA and irradiated Iso(Fmoc-I)nvoc3CA-hexanoic acid also showed atypical twisted β-sheet structures and aromatic π-π *i*nteractions. Future experiments could vary in the choice of solvent or peptide concentration. Further, coincubation tests of Fmoc-ICA and C343-ICA could be analyzed via CD to monitor structure formation through co-assembly.

3.2.4 Reduction of disulfides with DTT

Reduction of disulfides with DTT was performed to investigate the possibility of preventing disulfide formation after irradiation and reversibility of the disulfide formation. Therefore, CD and LC-MS-measurements were conducted and analyzed regarding structural change.

CD-measurements were performed with Iso(Fmoc-I)nvoc3CA **1**, Iso(Fmoc-I)nvoc3CA **2** and DiFmoc-ICA. 100 µM methanolic solutions were mixed with different DTT concentrations (0 equiv., 2 equiv., 5 equiv. or 10 equiv.) before irradiation for 30 s at 365 nm. MeOH was evaporated the samples resolved in NH_4HCO_3 buffer (5 mM, pH=7.4). After 24 h incubation at room temperature samples were measured via CD. Disulfide peptide DiFmoc-ICA **9** was equally prepared and mixed with 0 equiv., 10 equiv. or 100 equiv. DTT. Since the interfering DTT remained in sample solutions during measurements, the range between 185 nm and 240 nm was not taken into account. DiC343-ICA was not analyzed due to low availability and the lack of ordered structure formation as seen in TEM and CD-measurements. Because of this deficit, CD-

spectra of 2 showed no structural changes and will not be discussed further (see Figure 54, appendix).

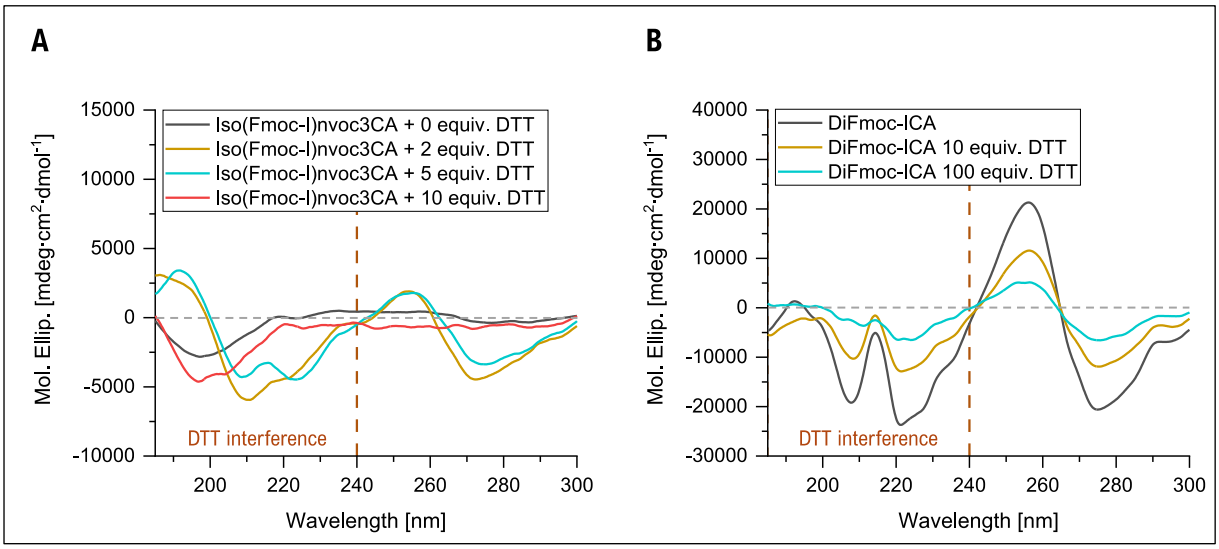

Figure 27: CD-spectra of irradiated Iso(Fmoc-I)nvoc3CA **1** (**A**) and DiFmoc-ICA **9** (**B**) measured in NH_4HCO_3 buffer (5 mM, pH=7.4, DTT). DTT interference marked by the dashed red line (< 240 nm).

Figure 27 shows CD-spectra of Iso(Fmoc-I)nvoc3CA **1** (**A**) and DiFmoc-ICA **9** (**B**). In **A**, similarities between the curves of 0 equiv. and 10 equiv. can be observed as well as comparable curves for 2 equiv. and 5 equiv. DTT. CD-spectra for 0 equiv. and 10 equiv. show no defined local minimum or maximum above 240 nm indicating random coils.[70] In contrast, 2 equiv. and 5 equiv. have maxima at around 255 nm. These curves are typically found for peptides containing atypical twisted β-sheet structures.[72] Self-assembly of the irradiated sample also wasn't observed during previous measurements (see chapter 3.2.3). For the curve of 10 equiv. DTT, disulfide formation could be suppressed to an extent to which it could no longer be detected. The reason why the samples with 2 and 5 equiv. DTT show ordered structures in contrast to the sample with 0 equiv. needs to be investigated further.

DiFmoc-ICA **9** analysis shows similar curves for 0 equiv. DTT as previously described (see chapter 3.2.3). With increasing DTT concentrations, the maximum of the CD-spectrum which is corresponding to the $\pi \rightarrow \pi^*$ transition decreases in intensity indicating reduction to the Fmoc-ICA monomer which forms untwisted β-sheet structures.[41,43,71] Further experiments could investigate at which DTT concentrations no more aromatic interactions occur and therefore structures would be disassembled.

For LC-MS-measurements, isopeptide **1** (100 µM) was combined with an equal amount of NH_4HCO_3 buffer (5 mM, pH=7.4). DTT was added in different concentrations (0 equiv., 2 equiv.,

5 equiv. or 10 equiv.) before irradiation for 30 s at 365 nm. After 24 h incubation at room temperature samples were injected into LC-MS. Disulfide peptides DiFmoc-ICA and Di-C343-ICA were equally prepared and mixed with 0 equiv., 10 equiv. or 100 equiv. DTT. Iso(C343-I)nvoc3CA wasn't included in this experiment due to the lack of structure formation as seen in TEM and CD-measurements.

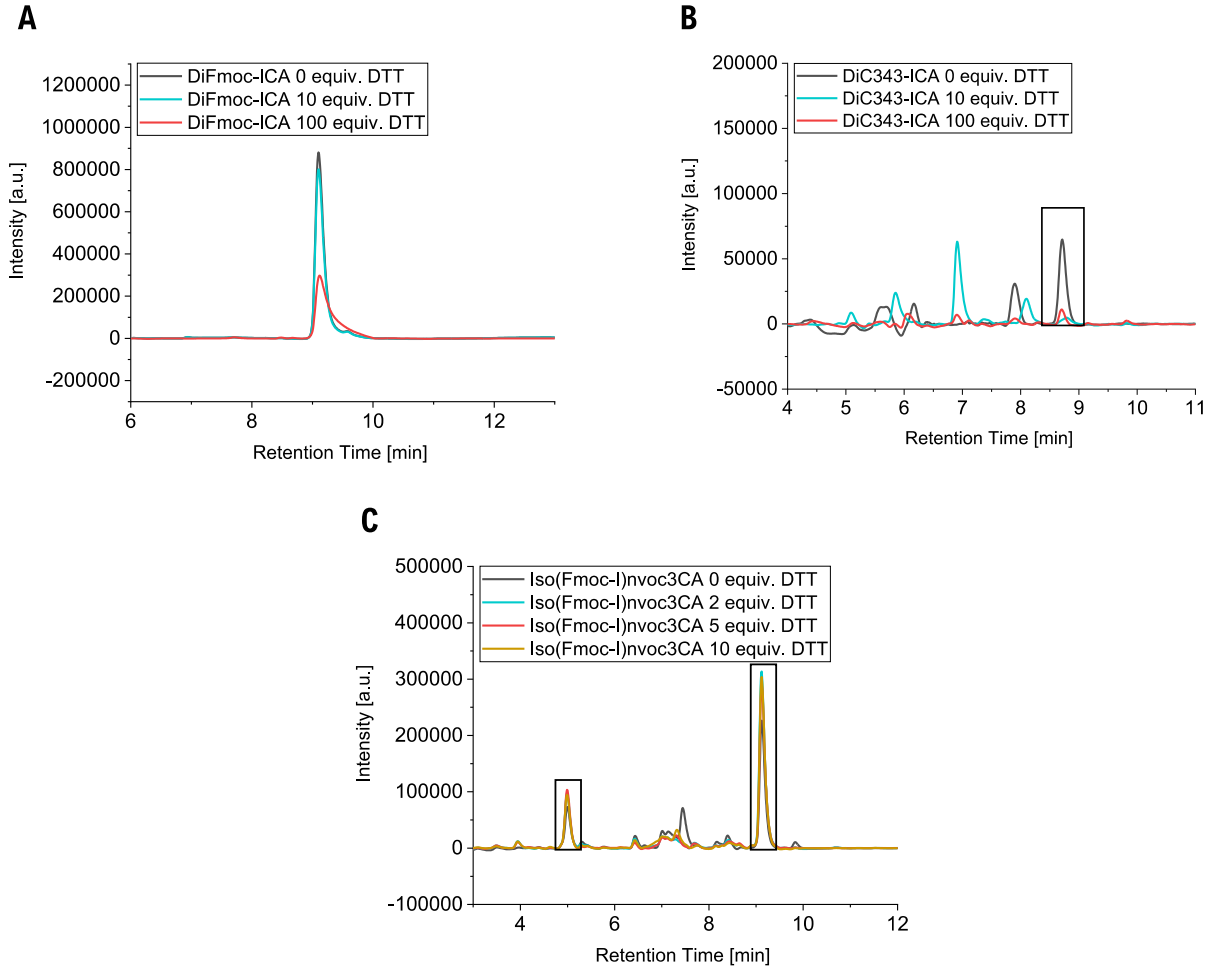

Figure 28: LC-chromatograms of DiFmoc-ICA **9** (**A**), DiC343-ICA **7** (**B**) and Iso(Fmoc-I)nvoc3CA **5** (**C**) with different concentrations of DTT.

LC-chromatogram of **9** (Figure 28, **A**) shows no significant change comparing 0 and 10 equiv. DTT whereas an increased disulfide peak for the sample with 100 equiv, DTT could be detected. This leads to the suggestion that a partly reduction of the compound to the linear peptide Fmoc-ICA **8** took place. The peak of Fmoc-ICA was suggested to be a part of the increasing injection peak. Complete conversion could be achieved with higher concentrations of DTT and could be subject of future experiments.

An decreasing disulfide peak for 10 and 100 equiv, DTT was detected for **7** in Figure 28 **B**, indicating reduction of the disulfide bond. However, since the 100 equiv. sample still shows a small disulfide peak higher concentrations are necessary for complete reduction. DiC343-ICA showed significantly more lability towards the reducing agent compared to DiFmoc-ICA which could be explained by the ordered structure formation that was observed for **9** but not for **7**. This could make it harder for DTT to attack the disulfide bond resulting in a lower conversion rate. Additionally, the linear C343-ICA **6** was observed with a retention time of 6.9 min. The peak increased at 10 equiv. but decreased again with 100 equiv. When looking at the chromatograms, it becomes apparent that the samples are contaminated by other by-products or substances. Due to lack of time, the DTT LC-MS experiments to analyze the reducibility of the disulfides could not be repeated, which should be done in future experiments.

Figure 28 **C** shows that up to 10 equiv. DTT had no effect on the formation of disulfides after irradiation of **1**. The graph shows similar peaks for DiFmoc-ICA (right box) and Fmoc-ICA (left box) in every measured sample. These results differ from those obtained from the CD measurements, which could be due to the different sample preparations and solvents. Another reason could be that the PG, which acts as an oxidizing agent after irradiation, cancels out the reducing effect of DTT which would require significantly higher DTT concentrations for future experiments.

Reducing experiments with DTT resulted in CD spectra of Iso(Fmoc-I)nvoc3CA that showed changes with first an increasing and then a decreasing rate of ordered structures. In contrast, its LC chromatograms showed no change with increasing DTT concentration suggesting that the irradiated PG, which acts as an oxidizing agent, cancels out the reducing effect of DTT. Therefore, higher DTT concentrations could be used for future experiments to investigate the possibility of preventing disulfide formation after irradiation.

The reducing properties of DTT with respect to the disulfides could be shown by CD- and LC-measurements. This showed that disulfide formation of this system is reversible and that the rate of disulfide can be reduced by the addition of DTT. Future experiments could focus on developing methods to image reversibility even further, such as TEM studies.

3.2.5 Imaging of self-assembly through transmission electron microscopy (TEM)

For the analysis of self-assembling behavior, samples of irradiated isopeptides **1**, **2** and **5** were analyzed using TEM-measurements. Additionally, the synthesized linear C343-ICA and DiC343-ICA were investigated using this method.

In a first attempt, all peptides were solved in DMSO and diluted 1:10 (v/v) with filtered PBS. A sample of each isopeptide was irradiated for 30 s at 365 nm. After incubation of 24 h, samples were applied to plasma etched copper grids and imaged with TEM (Figure 29, **A**-**D**).

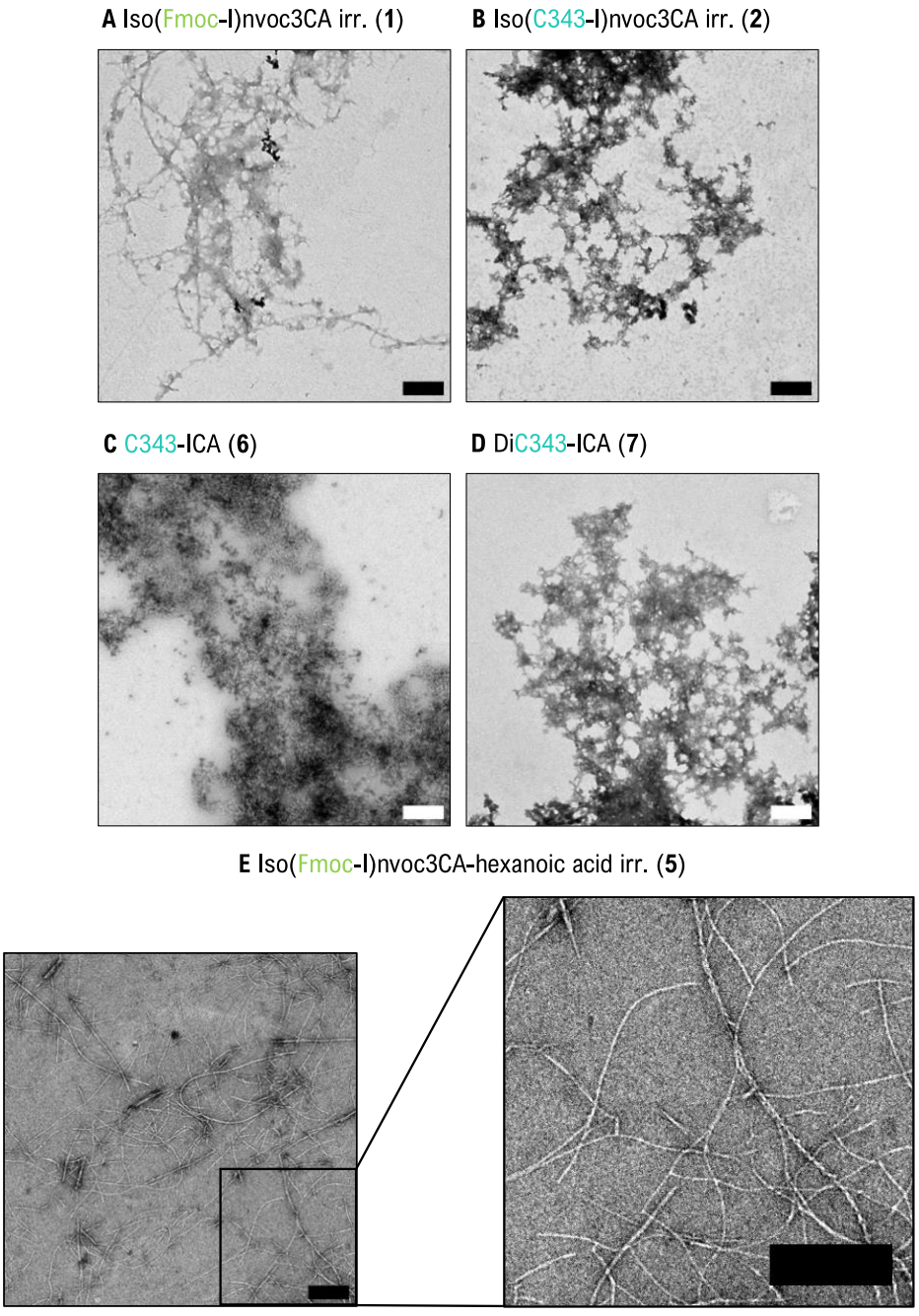

Figure 29: TEM images of 100 µM solutions of isopeptides **1** (**A**) and **2** (**B**), C343-ICA (**C**), DiC343-ICA (**D**) and Iso(Fmoc-I)nvoc3CA-hexanoic acid (**E**). Scale bars 250 nm.

Every image shows a high amount of aggregates, which was suggested for C343-containing controls and isopeptides. For Iso(Fmoc-I)nvoc3CA **1**, fibres, which can only be seen in the rudimentary, should be expected based on previous work of the Weil group. To improve fibrillation conditions, Iso(Fmoc-I)nvoc3CA was dissolved in MeOH (100 µM) irradiated for 30 s at a wavelength of 365 nm before solvent was evaporated and replaced with filtered PBS. However, imaging of these samples showed no difference in self-assembly behavior. Another interfering factor for structure formation could be the resulting by-product, which was discovered in the shift kinetics. Since the by-product could be eliminated by capping the alkyne group with a click reaction of **1** and 6-azidohexanoic acid, TEM analysis were repeated with this isopeptide (Figure 29, **E**). TEM-images of irradiated isopeptide **5** (100 µM) show overall self-assembly of the rearranged linear peptide monomers into long and thin fibres. In addition to the relatively untwisted fibres, there are also strongly twisted structures that can be identified as disulfide-assemblies by comparison with previous work. Therefore, it can be assumed that the oxidation by the protecting group as oxidizing agent has proceeded, as shown in the shift kinetic.

Further experiments could investigate the critical fibrillation concentration of **5** via TEM-imaging. Large concentrations of fibrillation amphiphiles could not be used for cell experiments which makes it important that the critical fibrillation concentration is low enough. Since 100 µM is a sufficient concentration, it could be used for cell experiments in the future. These findings prove that model compound **5** is suitable for the development of the desired system.

As a proof-of-concept experiment, coincubation tests were performed with 1:1 and 5:1 ratios of Fmoc-ICA and C343-ICA and 1:1 and 5:1 ratios of Iso(Fmoc-I)nvoc3CA and Iso(C343-I)nvoc3CA. Therefore, DMSO-stock solutions of the linear control peptides were diluted with filtered PBS (200 µM) and Nvoc-glycine (50 µM) added as an oxidizing agent. Peptide solutions were mixed in 1:1 and 5:1 ratios and irradiated at 365 nm for 30 s. Coincubation of isopeptides was realized by mixing methanolic solutions of Iso(Fmoc-I)nvoc3CA **1** and Iso(C343-I)nvoc3CA **2** (200 µM) in 1:1 and 5:1 ratios. Samples were irradiated at 365 nm for 30 s and MeOH was evaporated before resolving in filtered PBS. TEM-measurements of coincubation tests are shown in Figure 30.

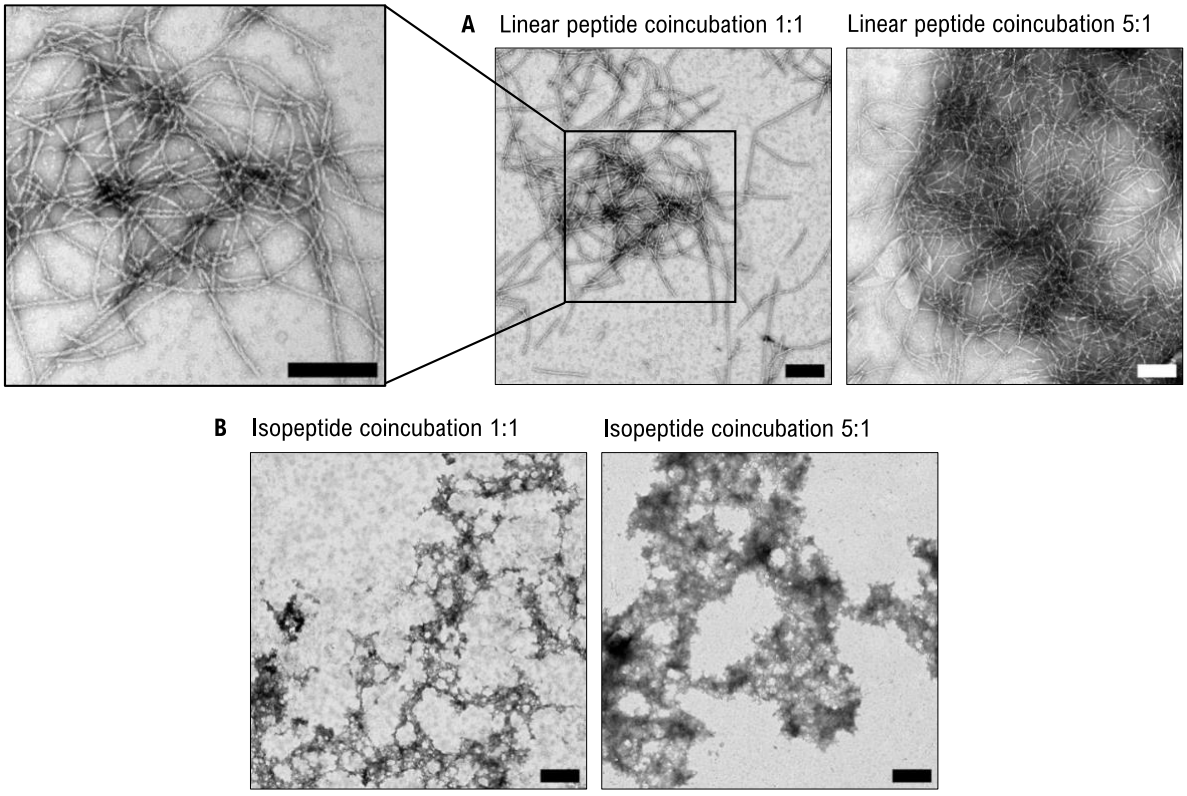

Figure 30: TEM-images of coincubation test in 1:1 and 5:1 ratios of linear control peptides (**A**) and irradiated isopeptides **1** and **2** (**B**).

A shows the coincubation of Fmoc-ICA **8** and C343-ICA **6** in which fibres can be found for both analyzed ratios. Structures are both twisted and untwisted, indicating a mixture of assembling linear peptide as well as assembling disulfide peptide. A stronger formation of fibrils is observed at the 5:1 ratio which can be explained due to the larger proportion of self-assembling Fmoc-ICA. Coincubation of irradiated isopeptides **1** and **2** showed amorphous aggregates (**B**). It can be assumed that the self-assembly of linear and disulfide monomers is disturbed by the formed by-product, as already indicated in TEM-measurements of **1**.

The formation of fibrils during the coincubation of Fmoc-ICA **8** and C343-ICA **6** demonstrated that the concept of the system works and can be further investigated. Isopeptide coincubation could be repeated by using Iso(Fmoc-I)nvoc3CA-hexanoic acid **5** to reduce a disturbance caused by the by-product. Additionally, a click reaction with **2** and 6-azidohexanoic acid could be performed and the resulting product used for further analysis.

4 Summary and Outlook

In previous work, the Weil group developed several systems of short self-assembling peptide amphiphile precursors for use against cancer cells. Different triggers were investigated to activate caged isopeptides to rearrangement of the precursor-molecule into the active monomer capable of self-assembly. Besides pH- and hydrogen-responsive systems[41,43], a new kind of caging group should be investigated in this work which could allow creation of a system with spatiotemporal control about fibrillation independently of cell metabolism and without additional chemical initiators. Therefore, the aim of this work was the synthesis and analysis of a new photolabile pro-self-assembling peptide amphiphile bearing the possibility to attach a cell penetrating species that could address cancer cells in future research.

During this thesis, five photolabile isopeptides were synthesized, including the model compunds Iso(Fmoc-I)nvoc3CA **1** Iso(C343-I)nvoc3CA **2** Iso(Fmoc-I)nvoc3CA-hexanoic acid **5**. Iso(Fmoc-I)nvoc3SA **3** and Iso(C343-I)nvoc3SA **4** were synthesized as test molecules since the serine system was suggested to be less dynamic and reactive. Synthesis of isopeptides and the control peptides C343-ICA **6** and DiC343-ICA **7** was achieved by Fmoc-solid phase peptide synthesis with subsequent esterification (**1-5**), oxidation (**7**) or click reaction (**5**).

Analysis of photolysis rates resulted in successful UV-induced cleavage of over 90% of nvoc3 after 30 s of irradiation (365 nm) which confirms suitability of synthesized isopeptides for the desired photolabile peptide precursor system.

Furthermore, rearrangement of the irradiated isopeptides by *S,N*-acyl shift and *O,N*-acyl shift was successfully shown via HPLC kinetics. In addition, by-product formation was observed after cleavage, which is probably due to a reaction of the free alkyne group. Analyzation of test molecules **3** and **4** showed similar findings. Therefore, synthesis of **5** was included in this work to prevent by-product formation by capping the free alkyne group.

Secondary structure analyses were performed with CD-measurements in NH_4HCO_3 buffer, showing random coil structures for C343-containing peptides. Fmoc-containing peptides formed ordered β-sheet structures but also unordered structures which could be further investigated by using other solvents or peptide concentrations. That formation of atypical β-sheet structures and π-π interactions after irradiation was only be observed for **5** could be a consequence of the side reaction occurring in samples of **1**. Reversibility of the thiol-disulfide redox-system and therefore the secondary structures could be demonstrated by CD- and LC-MS-measurements

of **7** and **9** incubated with different concentrations of the reducing agent DTT. It could be focus on developing methods to image reversibility in the future for example through TEM studies.

TEM-images of 100 µM samples show amorphous aggregates for **2**, **6** and **7** which is in line with CD-measurements. Irradiated samples of **1** also form aggregates and only rudimentary fibres, confirming the findings in CD-spectra. In contrast, analysis of **5** showed long twisted and untwisted fibres over the entire sample, indicating that the by-product plays a role in preventing **1** to self-assemble. From previous experiments of the Weil group, untwisted fibres can be assigned to Fmoc-ICA **8** and twisted structures to DiFmoc-ICA **9**. As a proof of concept experiment, coincubation of Fmoc-ICA **8** and C343-ICA **6** was carried out and showed strong self-assembly in 1:1 and 5:1 ratios with similar structures. Isopeptide coincubation tests could be performed in further experiments by using Iso(Fmoc-I)nvoc3CA-hexanoic acid **5** to reduce a disturbance caused by the by-product. Additionally, the alkyne group of **2** could be capped via click reaction to use this new model compound for further analysis.

In summary, the new photolabile pro-self-assembling peptide amphiphile **5** was synthesized, containing a group at which cell penetrating species could be attached. Successful deprotection after 30 s of irradiation and complete rearrangement via *S,N*-acyl shift could be shown through HPLC-analyses. Formation of ordered secondary structures was observed during CD- and TEM-measurements, showing two different types of fibres. In addition, reversibility of disulfide formation could be shown with DTT as a reducing agent. Considering these findings, **5** is suitable for further research regarding self-assembling behavior first outside and later inside living cells. Imaging could be achieved by coincubation with a C343-derivate as it was already shown in previous work of Pieszka.[41] In terms of fibrillation initiation, this system could be controlled precisely regarding timing and locational limitation. This could be a great advantage for cancer therapy research to reduce side effects.

Controllable assembly of synthetic nanomaterials that can be precisely deployed and tuned would be a major step forward when it comes to intracellular applications for medicine or in life science.

5 Material

5.1 Apparatus and equipment

Table 1: Apparatus and equipment.

Apparatus and equipment	**Appliance brand**
Analytical HPLC	Shimadzu with Atlantis T3 5 µm 4.6×100 mm column
Circular Dichroism	JASCO J-1500
Freeze Dryer	CHRIST Alpha 2-4 LSCbasic
HPLC	Shimadzu with Phenomenex Gemini 5 µm NX-C18 110 Å 150 × 30 mm column
LCMS	Shimadzu with Kinetex 2.6 µm EVO C18 100 Å LC 50x2.1 mm column
NMR	Bruker Avance II 400 MHz Bruker Avance III 700 MHz
Shaker	Eppendorf
SPPS	CEM Liberty Blue Automated Peptide Synthesizer
Tecan	Spark 20 M microplate reader
TEM	JEOL 1400
TEM Grids	Plano GmbH
Transparent flat bottom well-plate	Greiner Bio-One

5.2 Chemicals

Table 2: Chemicals.

Chemicals	Brand
6-Bromohexanoic acid	TCI
Acetonitrile	VWR
Boc-Ser-OH	Sigma-Aldrich
Copper-(II)-sulfate anhydrous	Fisher Scientific
Dimethylsulfoxid	Sigma-Aldrich
Dulbeco´s Phosphate Buffered Saline	Sigma-Aldrich
Coumarin343, pure, laser grade	Acros Organics
Fmoc-L-Ala-Wang-resin	Bachem
Fmoc-L-Cys(Trt)-Oh	Merck Novabiochem
Fmoc-L-Cys(MMT)-OH	Merck Novabiochem
Fmoc-L-Ile-OH	Merck Novabiochem
Fmoc-L-Ile(^{t}Bu)-OH chloride	TCI
Fmoc-L-Ser-OH	Merck Novabiochem
H-Ala-2-chlorotrityl-resin	Bachem
L-Ascorbic acid sodium salt, 99%	Acros Organics
N,N-Diisopropylethylamine	Sigma-Aldrich
N,N-Diisopropylcarbodiimid	VWR
N,N-Dimethylpyridin-4-amine	VWR
N,N-Dimethylformamide	VWR

Chemicals	Brand
Piperidine	Roth
Oxyma	CEM
Sodiumazide	Roth
Triisopropyl silane	Sigma-Aldrich
Trifluoroacetic acid	Roth
Tris(benzyltriazolylmethyl)amine	TCI
Uranyl acetate dihydrate	Merck

6 Experimental

The following chapter describes the methods used for synthesis, purification, and analysis that were performed to prepare this work. Reagents and solvents were purchased from commercial sources and were used without any further purification. Fmoc-ICA and DiFmoc-ICA were provided by Patrick Roth of the Max-Plank-Institute for Polymer Research. C343-ISA was provided by Sarah Chagri and nvoc-glycine was provided by Raphael Meyer of the Max-Plank-Institute for Polymer Research.

6.1 Synthesis

6.1.1 6-Azidohexanoic acid

6-Bromohexanoic acid (5 g, 0.026 mol, 1 equiv.) was dissolved in DMF and combined with sodium azide (5 g, 0.077 mol, 3 equiv.). The reaction mixture was heated to 85 °C under stirring for 16 h. After this, the reaction mixture was added to 100 mL of 0.1 M aqueous HCl. The product was extracted with DCM (4x 50 mL) and the organic layer washed with MilliQ water (1x 50 mL). After drying over sodium sulfate, DCM was removed under reduced pressure and the crude product was purified by column chromatography (1:1, CH/EA + FA, R_f=0.6) yielding 2.14 g (52.3%). The product (Figure 31) was analyzed by NMR-spectroscopy.

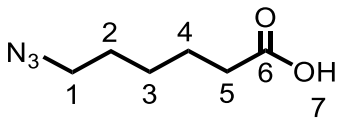

Figure 31: 6-Azidohexanoic acid.

1H-NMR: (400 MHz, DMSO-d_6) δ [ppm]= 12.02 (s, 1H, H_7), 3.32 (t, J = 6.8 Hz, 2H, H_1), 2.21 (t, J = 7.3 Hz, 2H, H_5), 1.61 – 1.43 (m, 4H, $H_{2,4}$), 1.40 – 1.26 (m, 2H, H_3).

6.1.2 C343-Ile

H-Ile-OtBu · HCl (335.6 mg, 1.5 mmol, 1 equiv.) and Coumarin343 (428 mg, 1.5 mmol, 1 equiv.) were dissolved in 15 mL dry DCM. The coupling reagents PyBOP (1.561 g, 3 mmol, 2 equiv.) and DIPEA (1.163 g, 9 mmol, 6 equiv.) were added and the reaction solution stirred at room temperature overnight. After that, solvents were removed under reduced pressure and the crude purified by flash column chromatography (2:1 CH/EA, RF=0.41). A solution of TFA and DCM

(20 mL, 1:1, 2 h) was used to cleave the ^{t}Bu protecting group. The solvents were removed under reduced pressure yielding 541.6 mg yellow-orange product (90.7%). The product (Figure 32) was analyzed by NMR-spectroscopy.

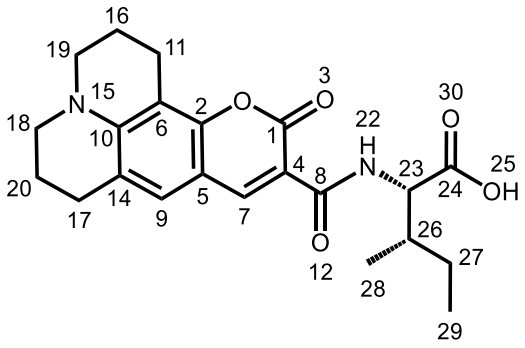

Figure 32: C343-Ile.

1H-NMR: (500 MHz, DMF-d_7) δ [ppm]= 9.25 (d, *J* = 8.4 Hz, 1H, H_{11}), 8.59 (s, 1H, H_{14}), 7.27 (s, 1H, H_5), 4.64 (dd, *J* = 4.7 Hz 8.5 Hz, 1H, H_3), 3.40 (p, *J* = 3.7 Hz, 4H, $H_{18,23}$), 2.93 (m, 2H, H_{20}), 2.77 (m, 2H, H_{21}), 1.97 (m, 4H, $H_{19,22}$), 1.58 (ddd, *J* = 5.0 Hz, 7.42 Hz, 12.8, 1H, H_4), 1.28 (p, *J* = 7.6 Hz, 7.4 Hz, 2H, H_7), 0.96 (m, 6H, $H_{5,8}$).

6.1.3 Merrifield solid-phase peptide synthesis

Peptides were synthesized using the Fmoc solid-phase peptide synthesis strategy (SPPS) by Merrifield, synthesizing the peptides from *C*- to *N*-terminus in the Liberty Blue Automated Microwave Peptide Synthesizer by CEM Corporation.

For the synthesis of isopeptides, a Wang-resin with an attached Fmoc-protected alanine was swollen in 5 mL DMF (RT; 45 min; 500 rpm) and filled into the SPPS-reaction vessel. Draining of the reaction vessel was followed by another short swelling process of 20 s. After that, the Fmoc group was removed by a deprotection step with 20% piperidine in DMF (v/v) and washed with DMF. Fmoc-protected cysteine or serine was coupled to the *N*-terminus with Oxyma and DIC as coupling reagents. After coupling, another Fmoc-deprotection step followed. Synthesis steps and reaction conditions at the SPPS-device are shown in Table 3.

After the completed coupling in the SPPS-device, the resin was transferred with DCM into a new reaction vessel. DCM was removed and the resin washed with dry DMF (3x 2 mL). For N-terminal protection, 1-(5-Methoxy-2-nitro-4-prop-2-ynyloxyphenyl)ethyl *N*-succinimidyl carbonate (nvoc3) (0.55 mmol, 1.1 equiv.) was dissolved in 5 mL dry DMF and added with

trimethylamine (1 mmol, 2 equiv.) to the resin and the mixture was shaken under argon atmosphere (RT, o.n., 80 rpm). The protection was followed by three washing steps with DCM (3x 2 mL) and DMF (3x 2 mL). Cysteine containing peptides were treated with a mixture of DCM/TIPS/TFA (6x 10 mL; 95%/5%/1%, 6x 10 min, 80 rpm) to cleave the MMT group off the side chain. After that, the resin was washed with DCM (3x 2 mL) and dry DMF (3x 2 mL) and the esterification was performed. Therefore, isoleucine (Fmoc or C343 protected) (1.2 equiv.), DMAP (1 equiv.) and DIC (0.001 equiv.) were solved in 5 mL dry DMF and added to the resin. The mixture was shaken under argon atmosphere (RT, o.n., 80 rpm) and the resin washed with DCM (3x 2 mL) and DMF (3x 2 mL). The synthesized isopeptides were cleaved from the resin and purified by HPLC. Every working step with nvoc3 was performed under exclusion of light.

C343-ICA was synthesized using a Chlorotrityl-resin with an attached unprotected alanine. Therefore, the first deprotection step, as mentioned above, wasn't needed. The described coupling, washing and deprotection cycle was performed with Fmoc-protected cysteine and isoleucine to produce the linear control peptide. The resin was transferred with DCM into a new reaction vessel. DCM was removed and the resin was washed with dry DMF (3x 2 mL). For N-terminal protection of the synthesized ICA, C343 (0.6 mmol, 1.2 equiv.) and PyBOP (1 mmol, 2 equiv.) were each dissolved in 2.5 mL dry DMF and added to the resin. DIPEA (2 mmol, 4 equiv.) was added and the mixture was shaken under argon atmosphere (RT, o.n., 80 rpm). C343-coupling was followed by washing steps with DMF (3x 2 mL) and DCM (3x 2 mL) before the peptide was cleaved from the resin and purified by HPLC. Every working step with C343 was performed under the exclusion of light. Synthesis scales of the different isopeptides and the control peptide are shown in Table 4.

Table 3: Synthesis steps at the SPPS-device.

Peptide synthesis step	**Program**
Deprotection	Fill with 20% piperidine in DMF (10 mL) Heat to 70 °C for 25 s Heat to 90 °C for 65 s Drain
Wash	Fill with DMF (7 mL) Drain for 7 s
Coupling	Fill with AA solution (0.5 mmol in DMF; 12 mL), DIC solution (1.0 M in DMF; 7 mL) and Oxyma solution (1.0 M in DMF; 5 mL) Heat to 70 °C for 30 s Heat to 90 °C for 120 s Drain

Table 4: Synthesis scale for the synthesized peptides.

Peptide	Scale [mmol]	Fmoc-Cys(MMT)-OH [mmol]	Fmoc-Cys(Trt)-OH [mmol]	Fmoc-Ser-OH [mmol]	Fmoc-Ile-OH [mmol]	C343-Ile-OH [mmol]
Iso(Fmoc-I)nvoc3CA	0.5	2.5	-	-	0.6	-
Iso(C343-I)nvoc3CA	0.5	2.5	-	-	-	0.6
Iso(Fmoc-I)nvoc3SA	0.1	-	-	0.5	0.12	-
Iso(C343-I)nvoc3SA	0.1	-	-	0.5	-	0.12
C343-ICA	0.5	-	2.5	-	0.6	-

6.1.4 Resin-cleavage

A mixture of TFA/TIPS/MilliQ water (10 mL, 95%/2.5%/2.5%) was added to the resin and shaken at room temperature for 2 h (80 rpm) for cleavage of the peptides from the resin and for cleavage of the side chain protecting groups. After washing with TFA, the solvents were removed under reduced pressure.

6.1.5 Purification through high performance liquid chromatography (HPLC)

The crude of the peptides was dissolved in ACN and MilliQ water (3:2, v/v) at concentrations up to 8 mg/mL and filtered through regenerated cellulose filters (0.20 µm) to remove particles. The solutions of the peptides were injected into a reversed phase HPLC using a setup by Shimadzu with a Phenomenex Gemini 5 µm NX-C18 110 Å 150 × 30 mm column. All measurements and purification steps were done using gradients of ACN and MilliQ water, acidified with 0.1% TFA, and a flowrate of 25 mL/min. Absorbance was recorded at 214, 254 and for the C343-peptides at an additional wavelength of 437 nm.

Purification of the linear control peptide C343-ICA was accomplished by using a gradient starting at 25% ACN. First, the gradient was linearly increased to 75% ACN in 13 min. The ACN concentration was increased to 100% in 2 min and held for 2 min before the gradient was again decreased to 25% in 3 min and held for 5 min. The collected fractions were combined and lyophilized (48 h) yielding 80 mg yellow-orange powder (27.9%). The product (Figure 33) was analyzed by NMR-spectroscopy and LC-MS.

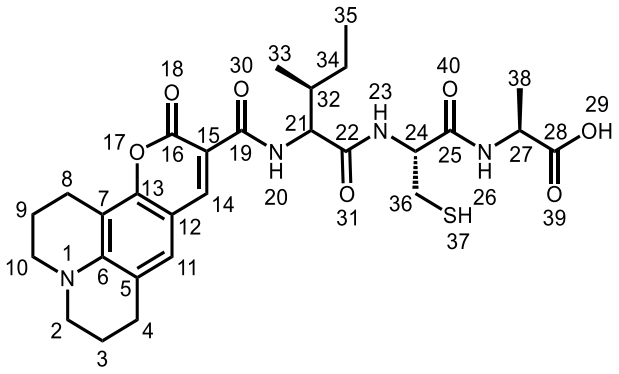

Figure 33: C343-ICA.

1H-NMR: (400 MHz, DMSO-d_6) δ [ppm]= 9.10 – 9.00 (m, 2H, $H_{11,14}$), 8.54 – 8.52 (m, 1H, H_{23}), 8.31 – 8.27 (m, 1H, H_{20}), 7.28 (s, 1H, H_{26}), 4.97 (s, 1H, H_{24}), 4.52 – 4.37 (m, 2H, $H_{21,36}$), 4.24 – 4.13 (m, 1H, H_{27}), 2.79 – 2.65 (m, 4H, $H_{2,10}$), 1.92 – 1.85 (m, 5H, $H_{4,8,32}$), 1.33 – 1.22 (m, 5H, $H_{34,38}$), 0.97 – 0.81 (m, 10H, $H_{3,9,33,35}$).

Iso(Fmoc-I)nvoc3CA was purified with a gradient starting at 0% ACN and a linear increase to 80% ACN in 32 min. ACN concentration was then increased to 100% in 2 min and held for 2min. After that, the gradient was decreased to 0% ACN in 2 min and held for 3 min. A following lyophilization of the collected fraction yielded 70 mg colorless powder (17.4%). The purified product was analyzed by NMR-spectroscopy (Figure 34) and LC-MS.

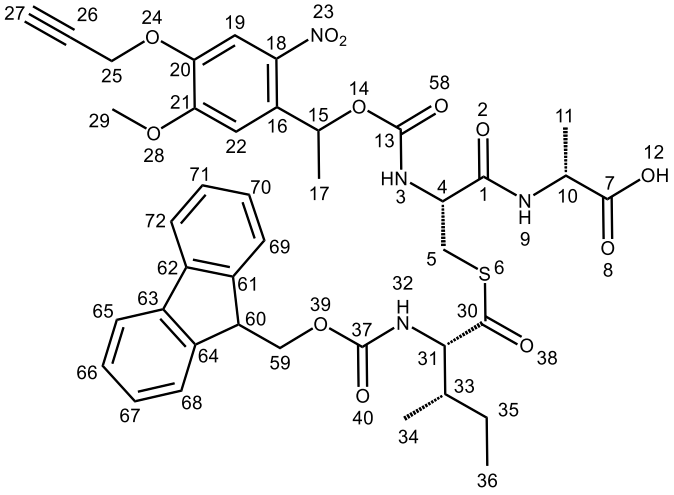

Figure 34: Iso(Fmoc-I)nvoc3CA.

1H-NMR: (400 MHz, DMSO-d_6) δ [ppm]= 8.38 – 7.93 (m, 1H, H_3), 7.93 – 7.82 (m, 2H, $H_{65,72}$), 7.79 – 7.69 (m, 4H, $H_{19,32,68,69}$), 7.46 – 7.25 (m, 5H, $H_{22,66,67,70,71}$), 7.18 (d, J = 14.4 Hz, 1H, H_9), 6.18 – 6.01 (m, 1H, H_{15}), 4.95 – 4.86 (m, 2H, H_{25}), 4.39 – 3.84 (m, 10H, $H_{4,5,10,29,31,59,60}$), 3.65 (s, 1H, H_{27}), 3.29 – 3.18 (m, 1H, H_{33}), 1.55 – 1.42 (m, 3H, H_{17}), 1.31 – 1.13 (m, 5H, $H_{11,35}$), 0.95 – 0.61 (m, 6H, $H_{34,36}$).

For the purification of Iso(C343-I)nvoc3CA, a starting concentration of 5% ACN was used and increased to 100% ACN in 30 min. After holding for 3 min, the gradient was decreased to 5% ACN in 2 min and held for another 5 min. The collected fractions were lyophilized and yielded 20 mg yellow-orange powder (5%). The product was analyzed by NMR-spectroscopy (Figure 35) and LC-MS.

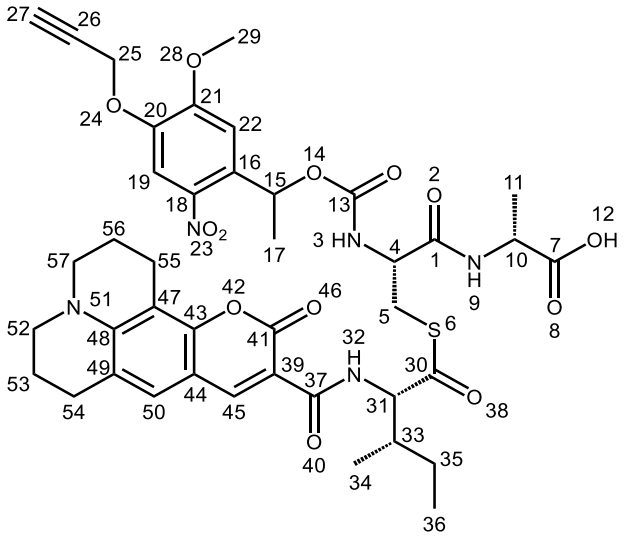

Figure 35: Iso(C343-I)nvoc3CA.

1H-NMR: (400 MHz, DMSO-d_6) δ [ppm]= 9.23 (d, 1H, H_{45}), 8.66 – 8.10 (m, 2H, $H_{3,50}$), 7.72 (s, 2H, $H_{19,32}$), 7.34 – 7.03 (m, 2H, $H_{9,22}$), 6.10 (s, 1H, H_{15}), 4.92 (s, 2H, H_{25}) 4.78 – 4.48 (m, 1H, H_4), 4.22 – 4.02 (m, 3H, $H_{5,10,31}$), 4.00 – 3.86 (m, 3H, H_{29}), 3.65 (s, 1H, H_{27}), 3.02 – 2.76 (m, 1H, H_{33}), 2.74 – 2.65 (m, 6H, $H_{52,54a,57,55a}$), 2.12 – 1.74 (m, 6H, $H_{54b,55b,53,56}$), 1.59 – 1.37 (m, 3H, H_{17}), 1.40 – 1.06 (m, 5H, $H_{11,35}$), 0.95 – 0.54 (m, 6H, $H_{34,36}$).

Iso(Fmoc-I)nvoc3SA and Iso(C343-I)nvoc3SA were purified with a gradient starting at 25% ACN that was linearly increased to 100% ACN in 20 min. The concentration was held for 5 min, then decreased to 25% in 5 min and again held for 5 min. After lyophilization (48 h), 10 mg colorless (12.7%) and 4 mg yellow-orange powder (4.8%) were obtained. Products were analyzed by NMR-spectroscopy (Figure 36 and Figure 37) and LC-MS.

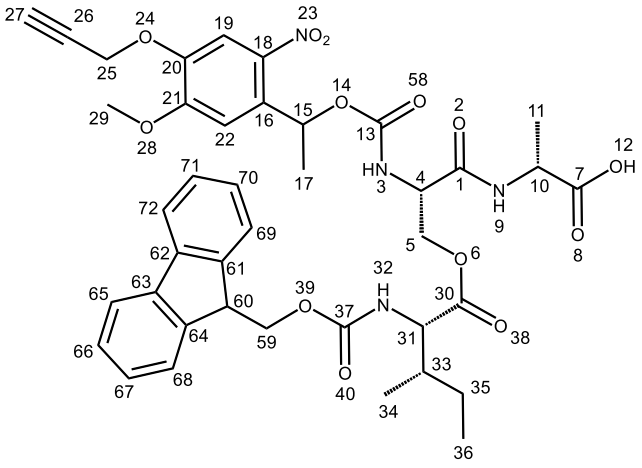

Figure 36: Iso(Fmoc-I)nvoc3SA.

1H-NMR: (400 MHz, DMSO-d_6) δ [ppm]= 8.36 (d, J = 39.8 Hz, 1H, H_3), 8.00 – 7.60 (m, 6H, $H_{19,32,65,68,69,72}$), 7.48 – 7.06 (m, 5H, $H_{22,66,67,70,71}$), 6.81 (s, 1H, H_9), 6.15 (m, 1H, H_{15}), 4.92 (s, 2H, H_{25}), 4.45 – 3.77 (m, 10H, $H_{4,5,10,29,31,59,60}$), 3.65 (s, 1H, H_{27}), 3.12 (m, 1H, H_{33}), 1.61 – 1.48 (m, 3H, $H_{17,}$), 1.26 – 1.22 (m, 5H, $H_{11,35}$), 0.90 – 0.63 (m, 6H, $H_{34,36}$).

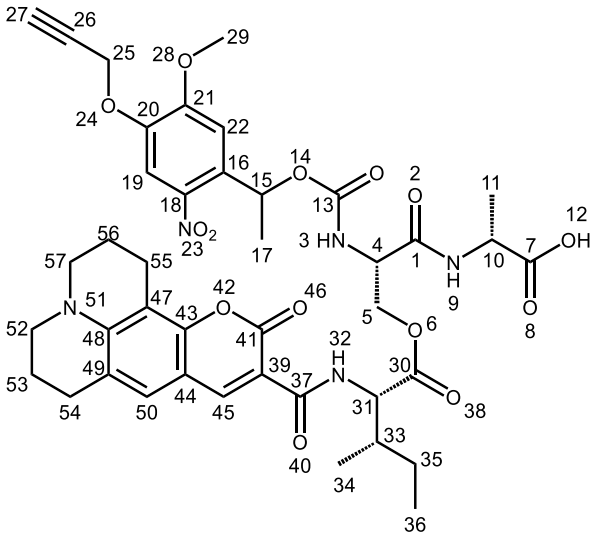

Figure 37: Iso(C343-I)nvoc3SA

1H-NMR: (700 MHz, DMSO-d_6) δ [ppm]= 9.20 – 8.93 (m, 1H, H_{45}), 8.61 – 8.24 (m, 2H, $H_{3,50}$), 7.95 (s, 1H, H_{32}), 7.86 – 7.68 (m, 1H, H_{19}), 7.35 – 7.12 (m, 2H, $H_{9,22}$), 6.30 – 6.06 (m, 1H, H_{15}), 4.93 (s, 2H, H_{25}), 4.69 – 4.37 (m, 1H, H_4), 4.39 – 4.09 (m, 4H, $H_{5,10,31}$), 3.93 (d, J = 16.8 Hz, 3H, H_{29}), 3.66 – 3.63 (m, 1H, H_{27}), 2.89 (m, 1H, H_{33}), 2.76 – 2.70 (m, 6H, $H_{52,54a,57,55a}$), 2.07 (m, 2H, $H_{54b,55b}$), 1.91 – 1.86 (m, 4H, $H_{53,56}$), 1.52 (d, J = 16.6 Hz, 3H, H_{17}), 1.39 – 1.12 (m, 5H, $H_{11,35}$), 1.05 – 0.60 (m, 6H, $H_{34,36}$).

6.1.6 Oxidation of C343-ICA

C343-ICA (6.7 mg, 0.006 mmol) was dissolved in 6.7 mL 20% DMSO in MeOH (v/v) and stirred at room temperature for 72 h. MeOH was removed under reduced pressure and 20 mL MilliQ water added to the mixture. After lyophilization, the crude product was dissolved in 2 mL DMF and filtered through regenerated cellulose filters (0.20 μm) before purification by reverse phase HPLC with the same parameters as described before. The used gradient started at 50% ACN and was increased up to 65% ACN in 10 min. An ACN concentration increase to 100% in 1 min followed and was held for 5 min. After that, the gradient was decreased to the starting concentration of 50% ACN and held again for 5 min. The collected fractions were combined and lyophilized (48 h) yielding 3 mg of yellow-orange powder (44.8%). Powder was analyzed by LC-MS (Figure 38).

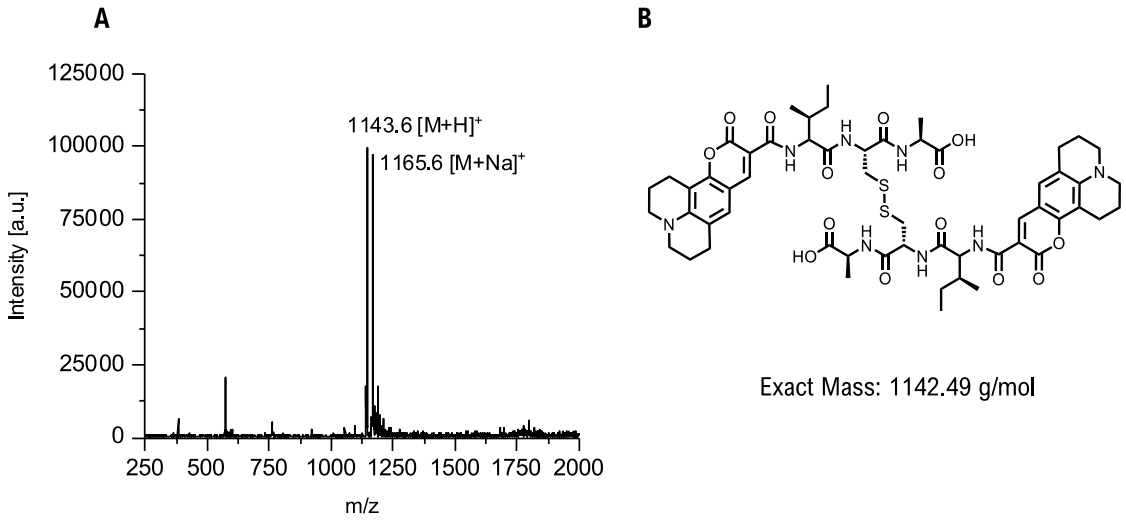

Figure 38: MS-spectrum (left) and molecular structure (right) of DiC343-ICA. Calculated: M = 1142.49 g/mol. Found: $[M+H]^+$ = 1143.6 g/mol, $[M+Na]^+$ = 1165.6 g/mol.

6.1.7 Copper-catalysed azide alkine cycloaddition (CuAAC) of Iso(Fmoc-I)nvoc3CA

Azidohexanoic acid (1.1 mg, 0.007 mmol, 1.2 equiv.) and Iso(Fmoc-I)nvoc3CA (4.6 mg, 0.006 mmol, 1 equiv.) were coupled by a copper-catalysed azide alkine cycloaddition (CuAAC) with TBTA (6.4 mg, 0.012 mmol, 2 equiv.), $CuSO_4$ (1.15 mg, 0.007 mmol, 1.2 equiv.) and sodium ascorbate (9.1 mg, 0.046 mmol, 8 equiv.) as reagents. First, azidohexanoic acid, the isopeptide and TBTA were dissolved in 1.6 mL DMSO in a small reaction vessel. $CuSO_4$ and sodium ascorbate were each dissolved in 0.3 mL MilliQ water and added successively to the mixture. After addition of the copper salt, it was stirred for 2 minutes before adding the sodium ascorbate solution. Afterwards, the reaction solution was stirred at room temperature overnight and under the exclusion of light. Solvents were removed under reduced pressure and the crude product purified by reverse phase HPLC with equal parameters as described before. A gradient starting at 0% ACN was linearly increased to 80% ACN in 32 min and then increased to 100% in 2 min. This concentration was held for 2min, subsequently decreased to 0% ACN in 2 min and held for another 3 min. Lyophilization of the combined fractions yielded 3 mg white powder (52.0%). Iso(Fmoc-I)nvoc3CA-hexanoic acid was characterized by LC-MS (Figure 39).

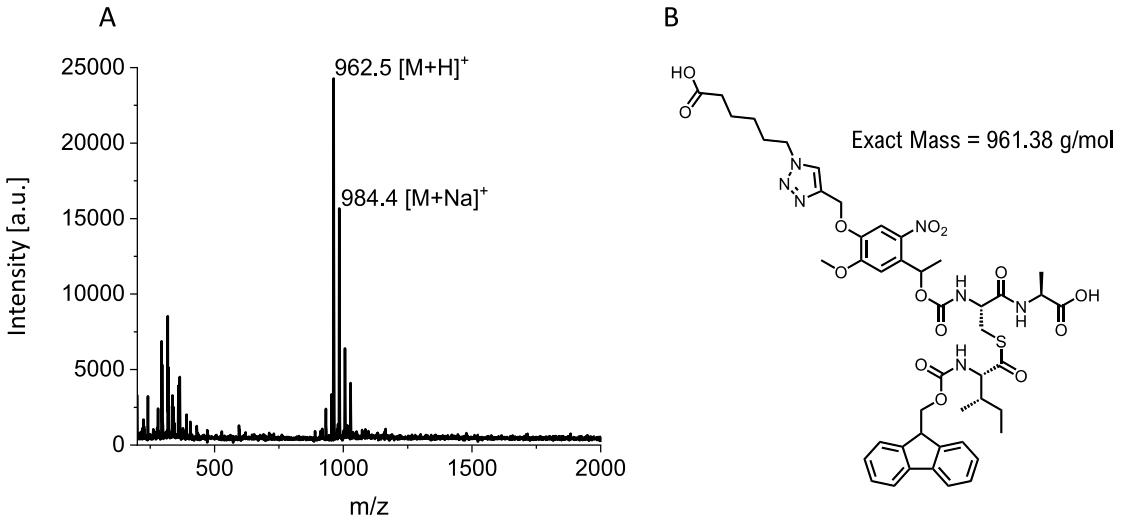

Figure 39: MS-spectrum (left) and molecular structure (right) of Iso(Fmoc-I)nvoc3CA-hexanoic acid. Calculated: M = 961.38 g/mol. Found: $[M+H]^+$ = 926.5 g/mol, $[M+Na]^+$ = 984.4 g/mol.

6.2 Characterization and analysis of synthesized peptides

For characterization and analysis of synthesized peptides and materials, the following methods and instruments were used.

6.2.1 COSY-^{1}H-NMR-spectroscopy

COSY-^{1}H-NMR-measurements were conducted to identify and characterize synthesized compounds. A solution of 3-7 mg peptide in DMSO-d_6 was measured at an AVANCE-400- , AVANCE-500 or an Avance-700-Spectrometer. The data was analyzed with the software "MestReNova" by Mastrelab. Chemical shift δ was indicated in part per million (ppm). Multiplets were abbreviated as s=singlet, d=doublet, t=triplet, q=quartet, m=multiplet.

6.2.2 LC-ESI-MS

Solutions of the synthesized peptides (50 µg/mL in MeOH) were injected into a LC-ESI-MS setup by Shimadzu using a Kinetex 2.6 µm EVO C18 100 Å LC 50 × 2.1 mm column. ACN and MilliQ water with 0.1% of formic acid were used as solvents. The gradient started at 5% ACN and the ACN concentration was linearly increased to 95% in 12 min. All data were processed in "Origin 2021b".

6.2.3 Peptide stability tests

Stability tests of all synthesized peptides were performed diluting 200 µM peptide solutions (MeOH) with equal amounts of NH_4HCO_3 buffer (5 mM). Samples were injected into an LC-ESI-MS setup by Shimadzu and measured after 0 min and 24 h. Incubation was realized in a shaker at 500 rpm and room temperature. Obtained data was edited in "Origin 2021b".

6.2.4 Photolysis rate of isopeptides

To determine the photolysis rate of synthesized isopeptides, a peptide solution (200 µM in MeOH) was mixed with an equal amount of NH_4HCO_3-buffer (pH=7.4, 5 mM). Samples of the solutions were irradiated at 365 nm for 0 s, 30 s, 60 s, 90 s, 120 s, and 600 s and injected into a HPLC. A reversed phase HPLC with a setup by Shimadzu and an Atlantis T3 5 µm 4.6×100 mm column with a flowrate of 1 mL/min was used. ACN and MilliQ water acidified with 0.1% TFA were used as solvents starting the gradient at 0% ACN. After that, ACN concentration was increased to 100% in 12 min and held for 3 min. The gradient was decreased linearly to 0% ACN in 2 min and held for another 3 min. Resulting data were analyzed with "Origin 2021b".

6.2.5 *S,N*-acyl and *O,N*-acyl shift-kinetics

Isopeptides were analyzed regarding their *S,N*-acyl or *O,N*-acyl shifts. Therefore, methanolic peptide solutions (200 µM) were diluted with an equal amount of NH_4HCO_3-buffer (pH=7.4; 5 mM). After irradiation for 30 s (365 nm), the samples were injected into a HPLC setup under the same conditions as described above. Starting at 0% ACN, ACN concentration was increased to 100% in 20 min and held for 3 min. The gradient was decreased linearly to 0% ACN in 2 min and held for another 4.5 min. Measurements were performed at 0 min, 30 min, 60 min, 90 min, 120 min, 240 min, 360 min, 24 h and 48 h after irradiation. Iso(Fmoc-I)nvoc3CA was analyzed via a shortened method (20 min) and date collected after 0 min, 20 min, 40 min, 60 min, 120 min, 240 min, 360 min and 24 h. Non-irradiated isopeptide and corresponding linear- and disulfide-peptides were injected as control. All data were processed by "Origin 2021b".

6.2.6 Structure analysis via Circular Dichroism (CD)

CD-measurements were used to analyze the secondary structure of synthesized peptides. Therefore, solutions with a concentration of 100 µM in MeOH were prepared and one sample of each analyzed isopeptide was irradiated at 365 nm for 30 s. MeOH was evaporated before residues were dissolved in 5 mM NH_4HCO_3-buffer (ph=7.4) and incubated for 24 h (RT; 500 rpm). All samples were measured from 180 nm to 300 nm with a data pitch of 0,2 nm, a bandwidth of 1,00 nm and a scanning speed of 20 nm/min at 20 °C. Spectra were measured via 3 times data accumulation and edited with “JACSO Spectra Manager II” and “Origin 2021b”.

6.2.7 Imaging of self-assembly through transmission electron microscopy (TEM)

DMSO-stock solutions (1 mM, 500 µM, 250 µM, 100 µM) of the synthesized peptides **1** and **3** were diluted 1:10 (v/v) with filtered PBS. Iso(Fmoc-I)nvoc3CA was solved in MeOH (100 µM) and one sample of each isopeptide was irradiated for 30 s at a wavelength of 365 nm. The solvent in MeOH containing samples was evaporated and replaced with filtered PBS yielding 100 µM solutions.

Coincubation tests were performed with 1:1 and 5:1 ratios of Fmoc-ICA and C343-ICA DMSO-stock solutions (1 mM) of the linear control peptides were diluted with filtered PBS yielding a concentration of 200 µM. Nvoc-glycine (5 mM) was added as an oxidizing agent and samples were irradiated at 365 nm for 30 s.

Coincubation of isopeptides was realized by mixing methanolic solutions of Iso(Fmoc-I)nvoc3CA and Iso(C343-I)nvoc3CA (200 µM) in a 1:1 or 5:1 ratio. Samples were irradiated at 365 nm for 30 s and MeOH was evaporated before resolving in filtered PBS.

All samples were incubated on a shaker at room temperature for 24 h (500 rpm). Copper grids, coated with a thin electron-transparent formvar-layer, were plasma etched with 20% oxygen plasma for 30 s. After that, 3 µL sample solution were placed on a copper grid and incubated for 5 min. The solution was removed carefully with a filter paper and the copper grids air dried. Copper grids were stained with 7 µL of aqueous 4% uranyl acetate solution and incubated for 2.5 min. Staining was stopped by washing copper grids three times with MilliQ water. Imaging of the air dried grids was accomplished in high vacuum at an acceleration voltage of 120 kV. Obtained images were edited with “Fiji ImageJ”.

6.2.8 Reduction of disulfides with DTT

Solutions of all ICA containing isopeptides and disulfides (200 µM in MeOH) were diluted with an equal amount of NH_4HCO_3 buffer (5 mM, pH=7.4). Different equivalents of DTT (0 equiv., 5 equiv., 10 equiv. and 100 equiv.) were added and isopeptides were irradiated for 30 s at 365 nm. Samples were incubated for 24 h (RT, 500 rpm) and analysed by LC-MS.

CD-measurements with ICA containing isopeptides and disulfides were performed by diluting 200 µM methanolic peptide solutions with DTT in MeOH (0 equiv., 5 equiv., 10 equiv. and 100 equiv.). Isopeptides were irradiated for 30 s at 365 nm and MeOH was evaporated of all samples. After resolving in NH_4HCO_3 buffer (5 mM, pH=7.4), the peptide solutions were incubated for 24 h (RT, 500 rpm) and measured between 180 nm to 300 nm.

6.2.9 Fluorescence spectroscopy

A Tecan SPARK 20M microplate reader was used to record emission intensities of irradiated C343-ICA-samples. Solutions of 100 µM C343-ICA in PBS were irradiated for 0 s, 30 s, 90 s, 120 s, and 600 s and measured in a transparent flat bottom well-plate. Emission was recorded between 400 and 500 nm and the data was processed in “Origin 2021b”.

Danksagung

Hiermit möchte ich mich herzlich bei Prof. Dr. Tanja Weil dafür bedanken, mir die Möglichkeit gegeben zu haben, meine Masterarbeit in ihrem Arbeitskreis anzufertigen. Des Weiteren möchte ich mich für die Bewertung und Korrektur dieser Arbeit bedanken.

Mein Dank gilt auch Prof. Dr. Andreas Walther für die Erstellung eines Zweitgutachtens dieser Arbeit.

Besonderen Dank möchte ich an meinen Gruppenleiter David Ng richten, der mir bei jeder Frage stets freundlich und unterstützend begegnet ist. Ich möchte mich ebenfalls für die gute Zusammenarbeit und das ausgesprochen angenehme Arbeitsklima unter seiner Leitung bedanken.

Ich möchte mich ebenfalls bei allen Mitarbeitern des Instituts bedanken, die an der Messung meiner Proben beteiligt waren. Besonderer Dank gilt dabei Dr. Zhixuan Zhou für die Messungen meiner LC-MS Proben. Raphael Meyer und Sarah Chagri möchte ich für die Bereitstellung von Materialien danken.

Mein größter Dank gilt meinem Betreuer Patrick Roth, der mir alles geduldig erklärt und gezeigt hat, sodass ich mich sehr schnell gut zurechtgefunden habe. Während der gesamten Zeit konnte ich bei Rückfragen oder anderen Problemen immer zu ihm kommen und mit einer ausführlichen Antwort und Unterstützung rechnen. Zusätzlich möchte ich mich für die Aufnahme der TEM-Bilder und die umfassende Korrektur meiner Arbeit bedanken.

Ich möchte mich ebenfalls für die gute Zusammenarbeit und das freundliche Arbeitsklima bei allen Mitgliedern der Arbeitsgruppe bedanken, die stets ein offenes Ohr hatten und auch gerne über fachliche Fragen diskutierten. Die spaßigen Mittagspausen mit Patrick, Raphael, Konrad, Julian, Jana und Nelly erzeugten immer gute Laune.

Ich bedanke mich herzlichst bei meiner Familie und meinen Freunden, die mir während der Erstellung dieser Arbeit zur Seite standen und mich unterstützt haben. Besonders möchte ich mich meinen „co-working“ Partnerinnen bei Alicia Bopp und Laura Wüst bedanken.

7 Appendix

Supporting information, images and spectra studied in this work are listed in this chapter.

7.1 List of Abbreviations

AA	amino acid
ACN	acetonitrile
C343	coumarin343
CD	circular dichroism
DCM	dichloromethane
DIC	diisopropylcarbodiimide
DMAP	4-(dimethylamino)-pyridine
DMF	*N,N*-dimethylformamide
DMSO	dimethylsulfoxide
Fmoc	fluorenylmethyloxycarbonyl
HPLC	high performance liquid chromatography
ICA	isoleucine-cysteine-alanine
ISA	isoleucine-serine-alanine
Ile	isoleucine
LC-MS	liquid chromatoghraphy–mass spectrometry
MMT	Monomethoxytrityl
NHS	*N*-hydroxysuccinimide
NMR	nuclear magnetic resonance
Nvoc3	1-(5-Methoxy-2-nitro-4-prop-2-ynyloxyphenyl)ethyl *N*-succinimidyl carbonate
Oxyma	ethyl-cyanohydroxyiminoacetate
PBS	phosphate-buffered saline
PG	protection group
PyBOP	benzotriazol-1-yloxytripyr-rolidinophosphonium hexafluorophosphate
R_T	Retention Time
SPPS	solid-phase peptide synthesis
TEM	transmission electron microscopy
TFA	trifluoroacetic acid
TIPS	triisopropyl silane
UV	ultra violet

7.2 Supplementary Data

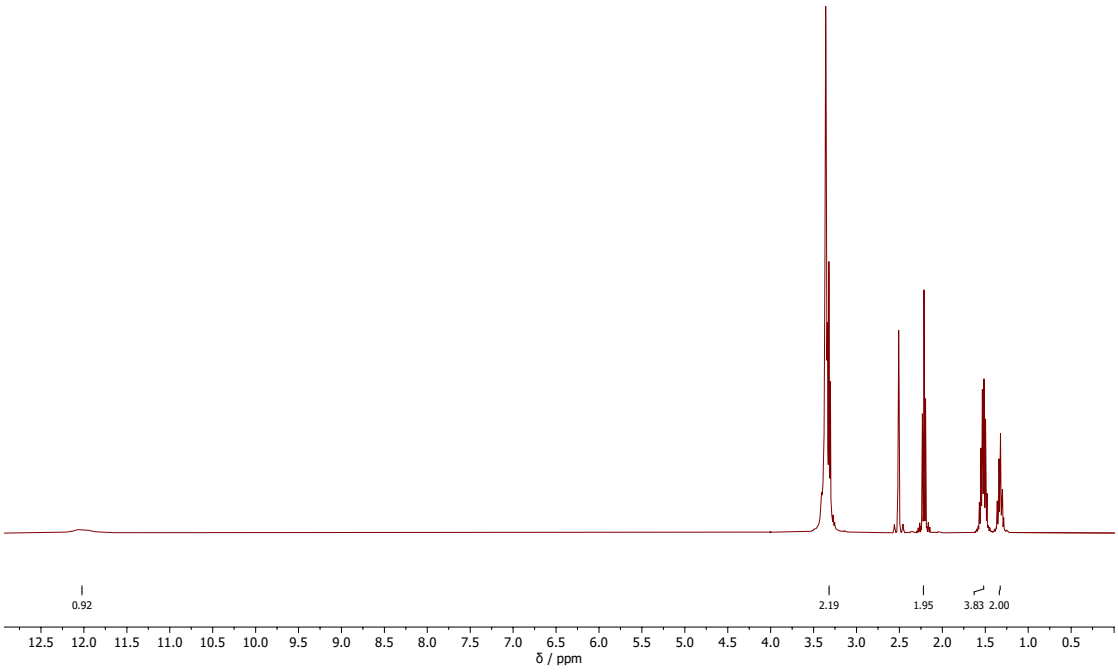

Figure 40: 1H-NMR of 6-azidohexanoic acid.

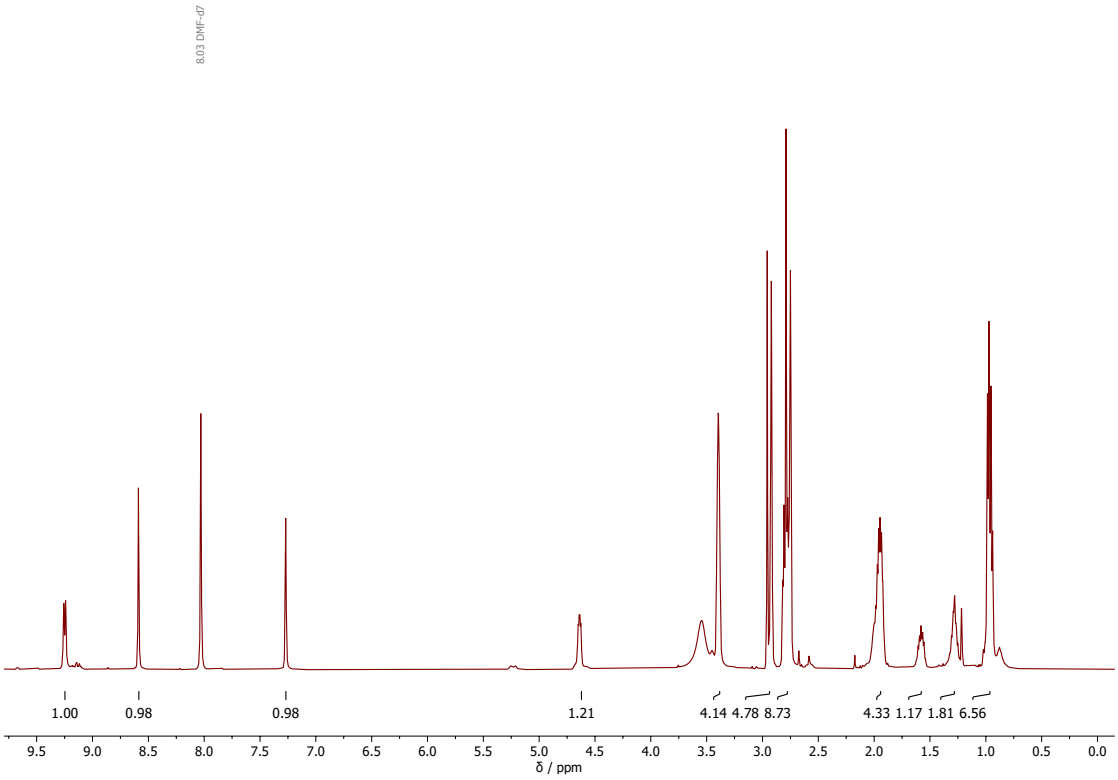

Figure 41: 1H-NMR of C343-Ile.

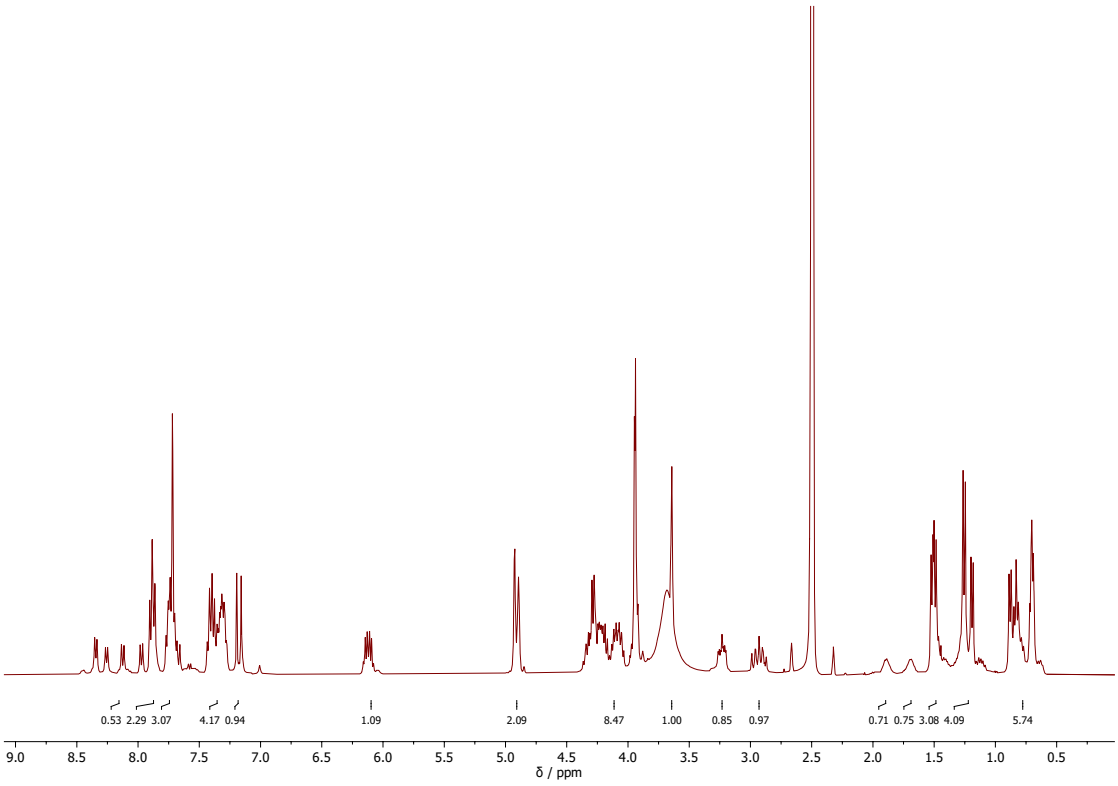

Figure 42: 1H-NMR of Iso(Fmoc-l)nvoc3CA **1**.

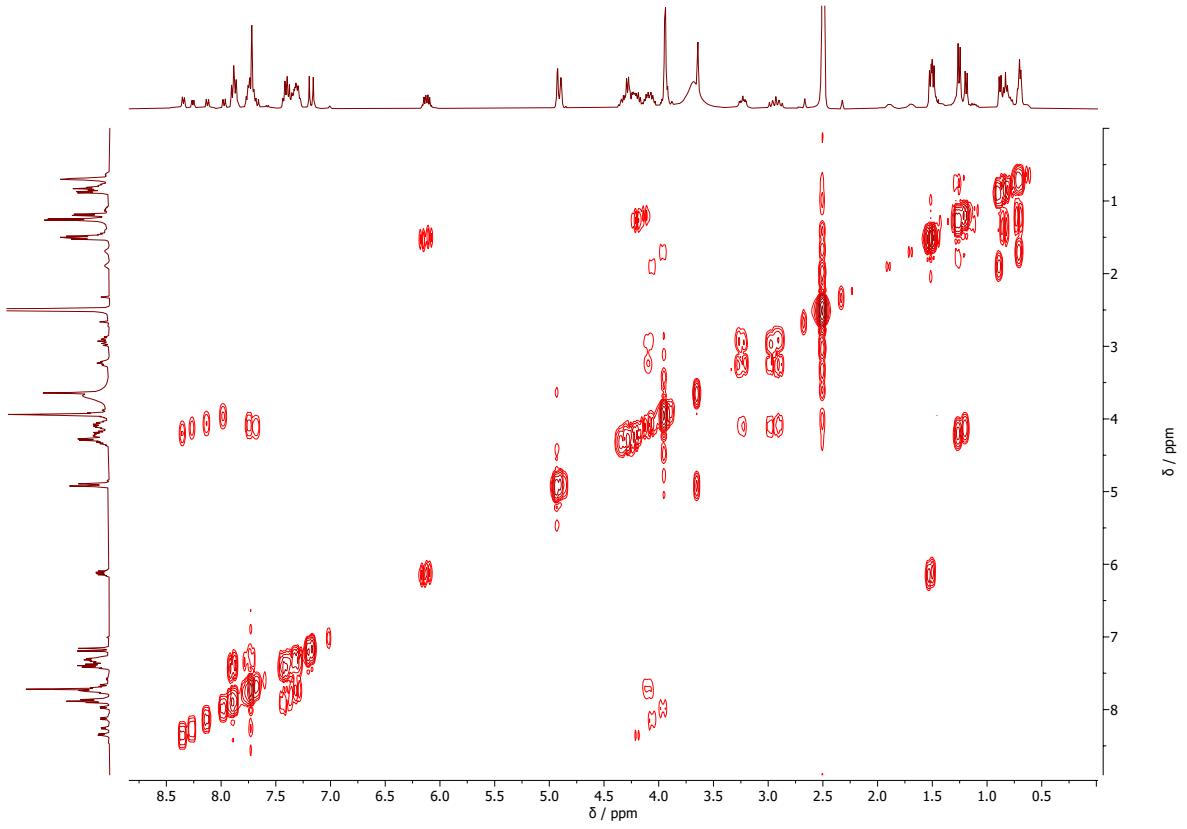

Figure 43: COSY-NMR of Iso(Fmoc-l)nvoc3CA **1**.

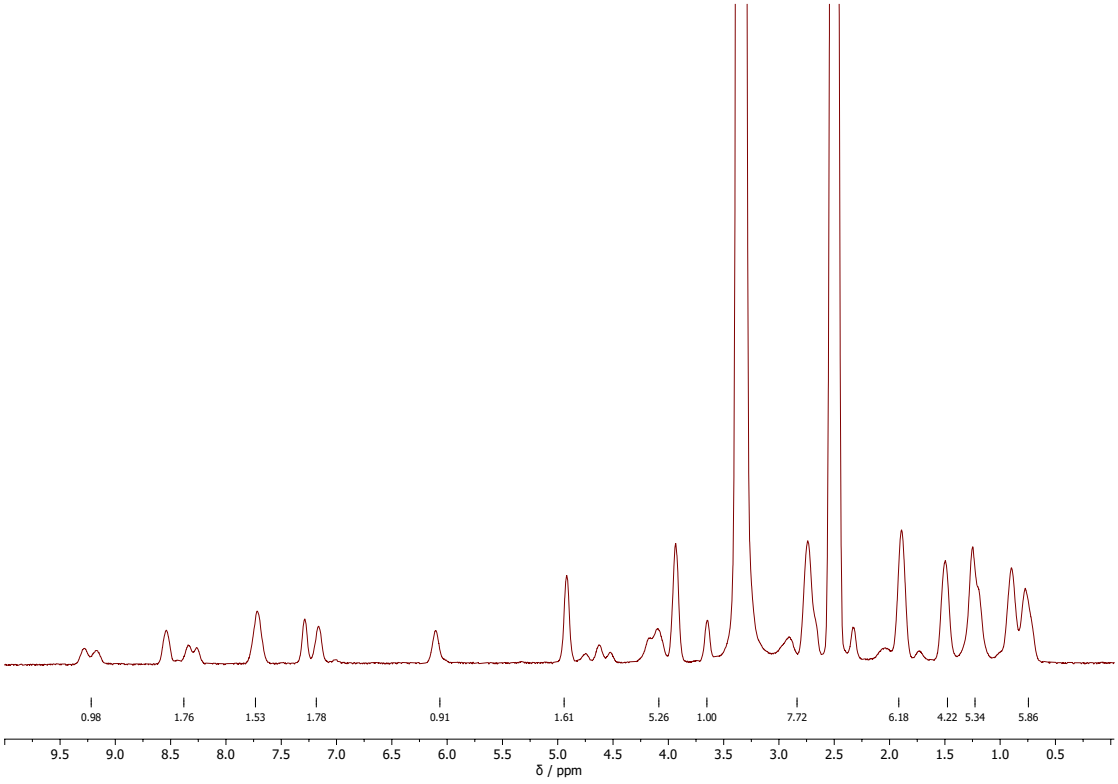

Figure 44: 1H-NMR of Iso(C343-I)nvoc3CA **2**.

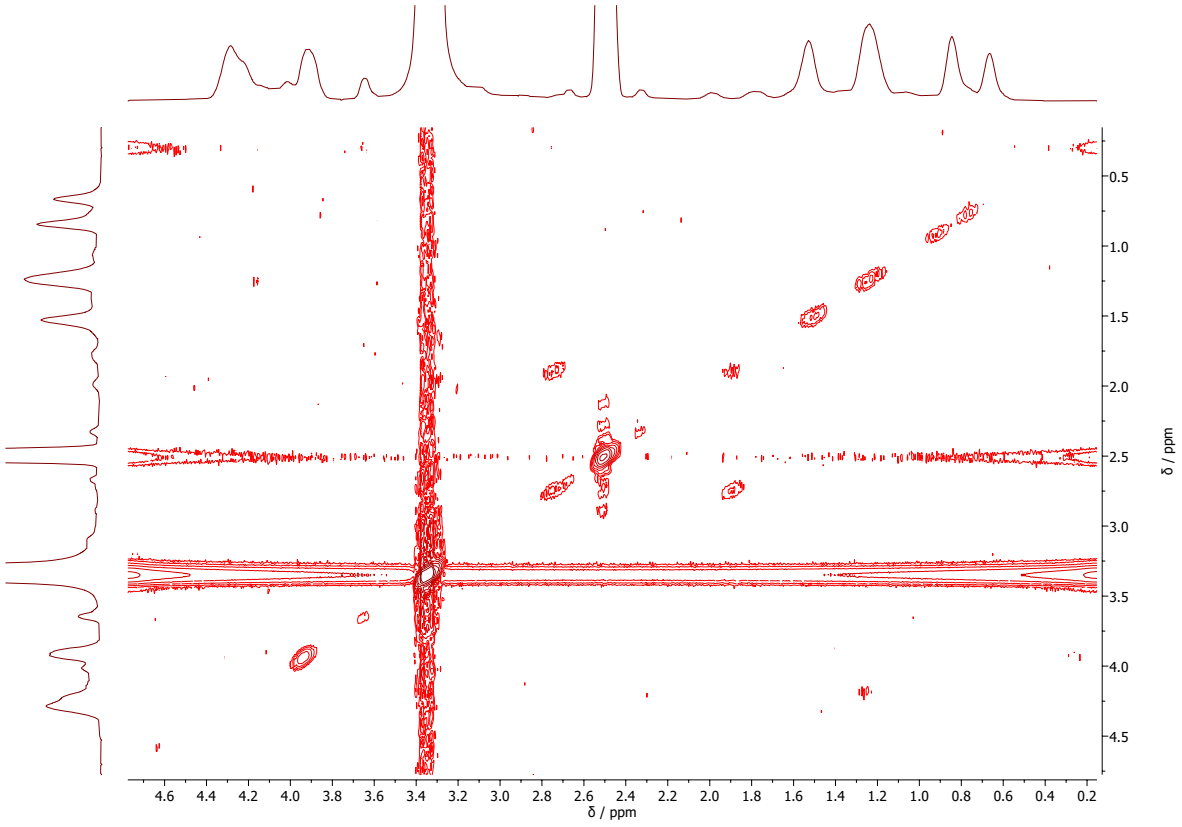

Figure 45: COSY-NMR of Iso(C343-I)nvoc3CA **2**.

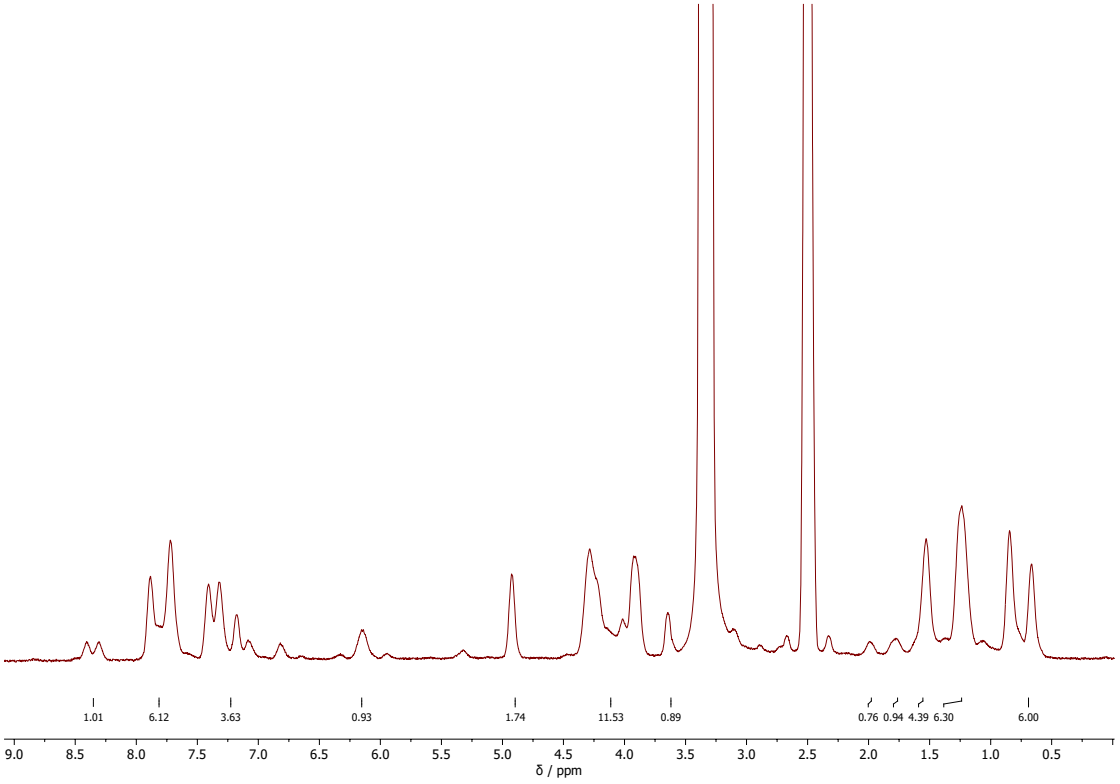

Figure 46: 1H-NMR of Iso(Fmoc-I)nvoc3SA **3**.

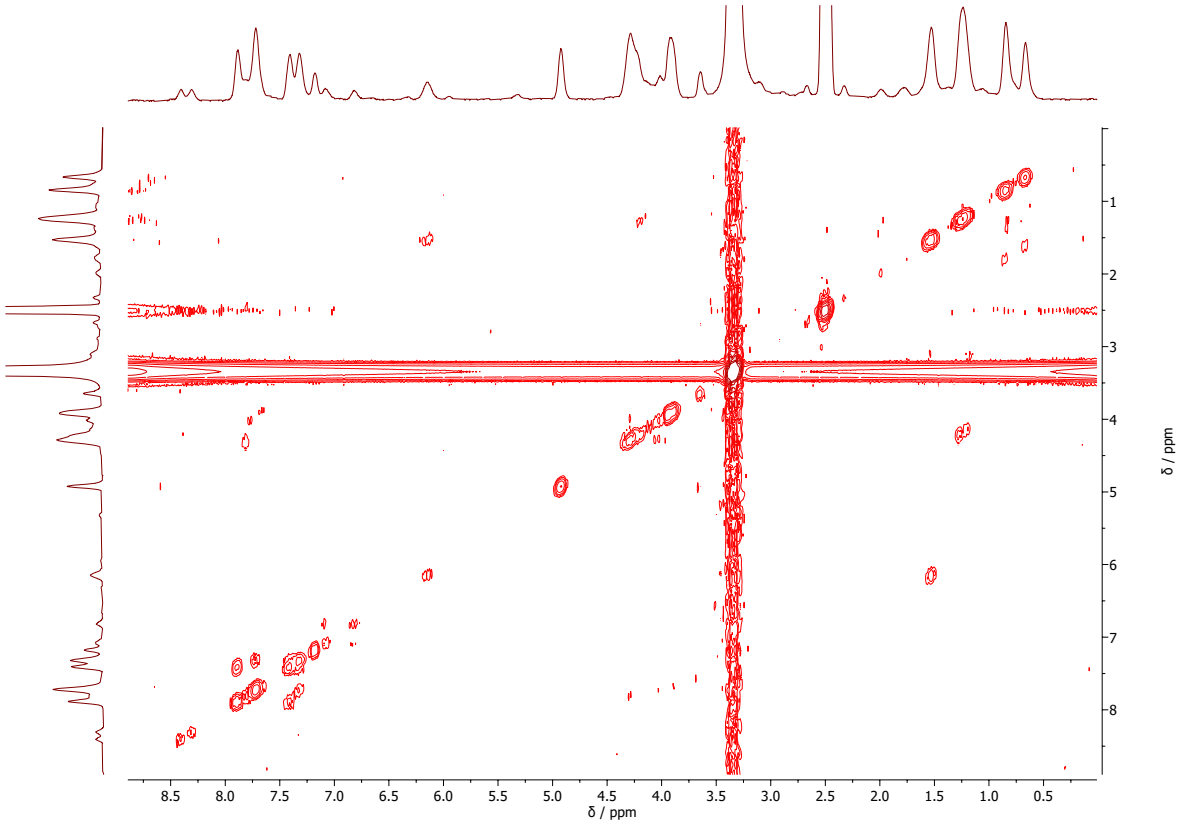

Figure 47: COSY-NMR of Iso(Fmoc-I)nvoc3SA **3**.

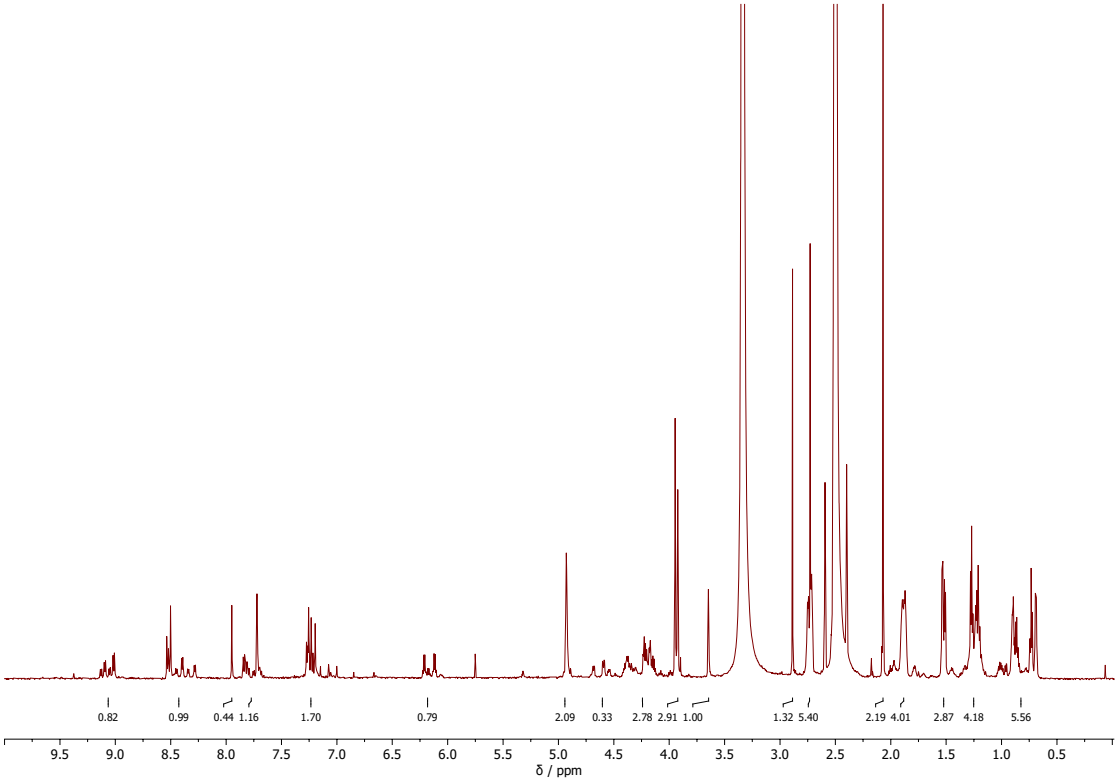

Figure 48: 1H-NMR of Iso(C343-I)nvoc3SA **4**.

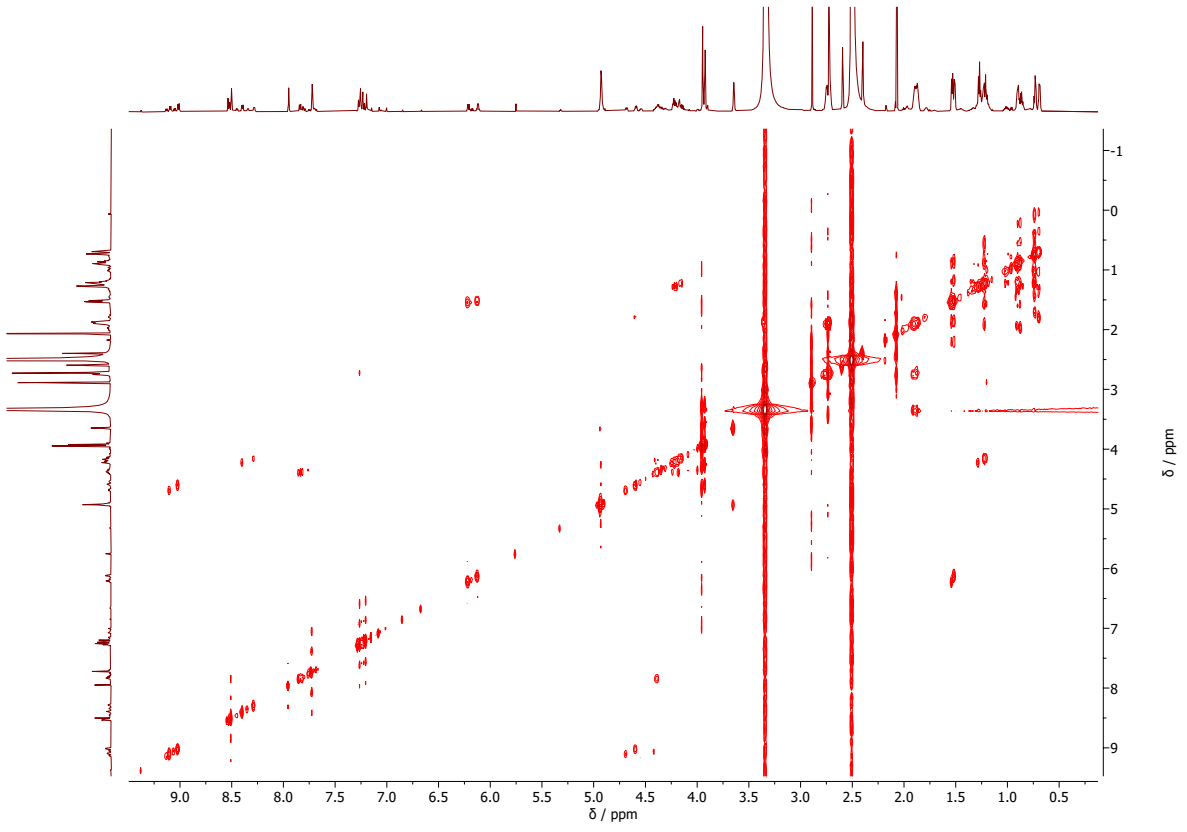

Figure 49: COSY-NMR of Iso(C343-I)nvoc3SA **4**.

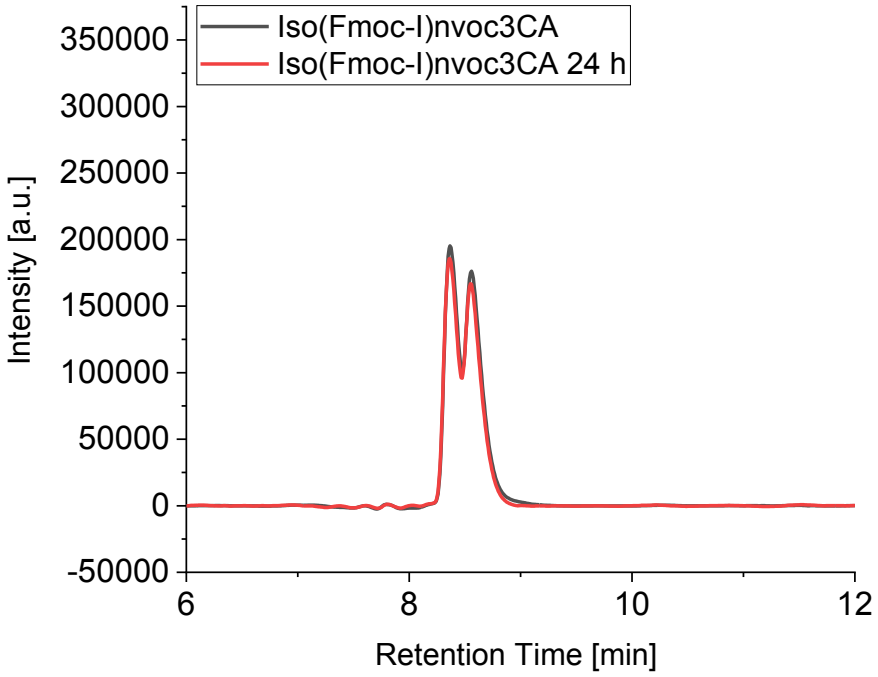

Figure 50: LC-chromatograms of Iso(Fmoc-I)nvoc3CA (100 µM) after 0 min and 24 h incubation in MeOH/ NH_4HCO_3 buffer (1:1; 5 mM, pH=7.4).

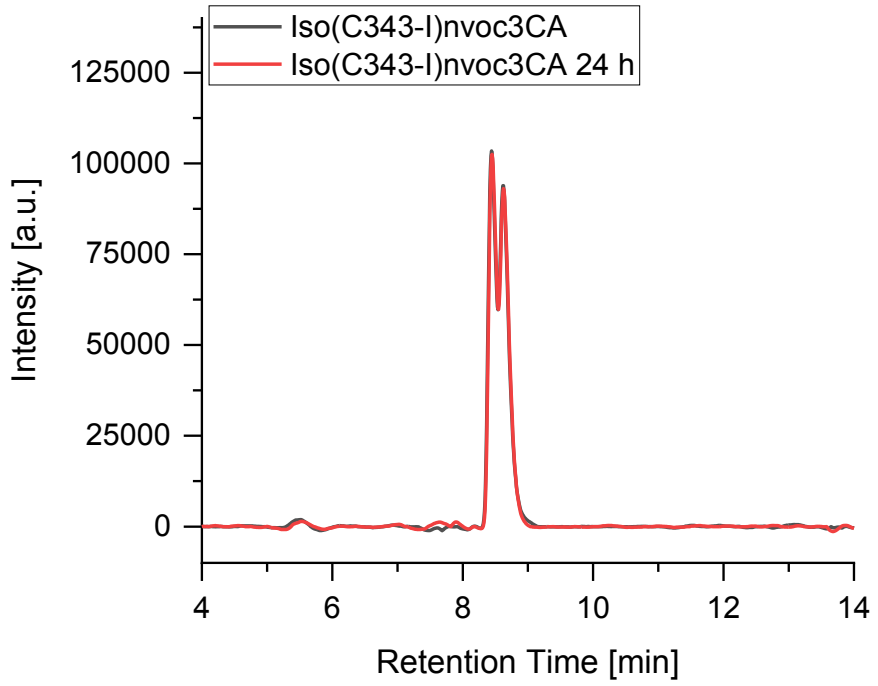

Figure 51: LC-chromatograms of Iso(C343-I)nvoc3CA (100 µM) after 0 min and 24 h incubation in MeOH/ NH_4HCO_3 buffer (1:1; 5 mM, pH=7.4).

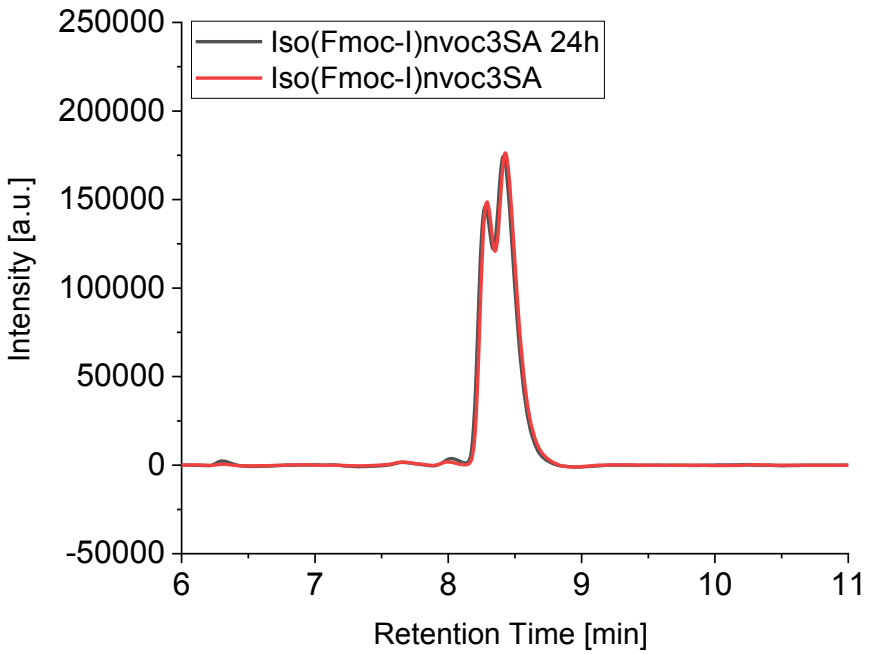

Figure 52: LC-chromatograms of Iso(Fmoc-I)nvoc3SA (100 µM) after 0 min and 24 h incubation in MeOH/ NH_4HCO_3 buffer (1:1; 5 mM, pH=7.4).

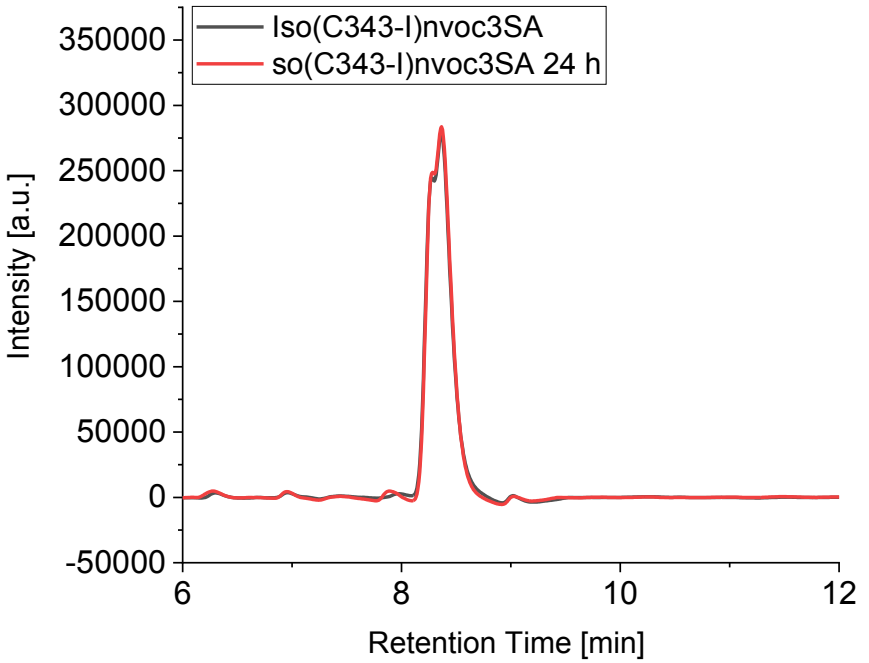

Figure 53: LC-chromatograms of Iso(Fmoc-I)nvoc3CA (100 µM) after 0 min and 24 h incubation in MeOH/ NH_4HCO_3 buffer (1:1; 5 mM, pH=7.4).

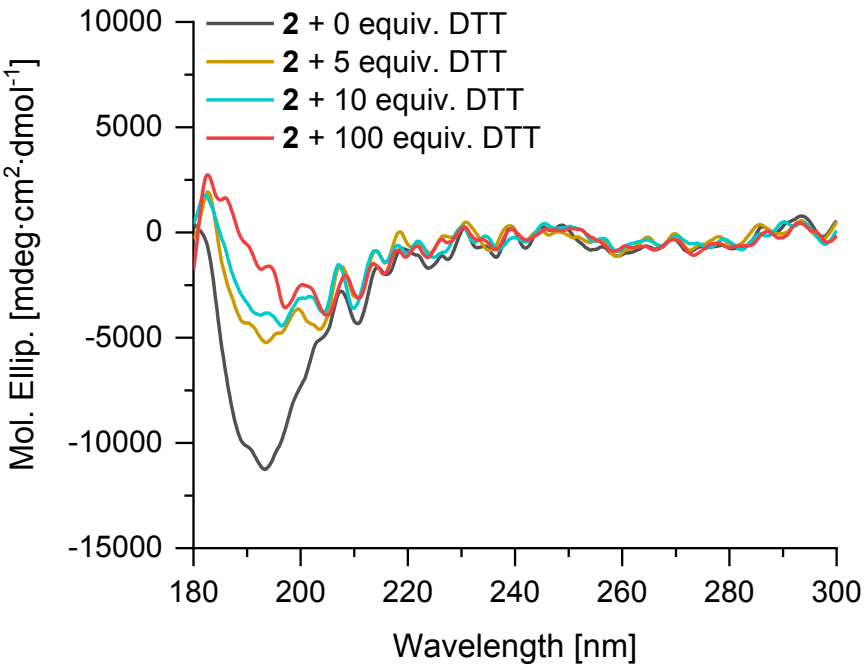

Figure 54: CD-spectra of irradiated Iso(C343-I)nvoc3CA containing 0, 5, 10 or 100 equiv. of DTT.

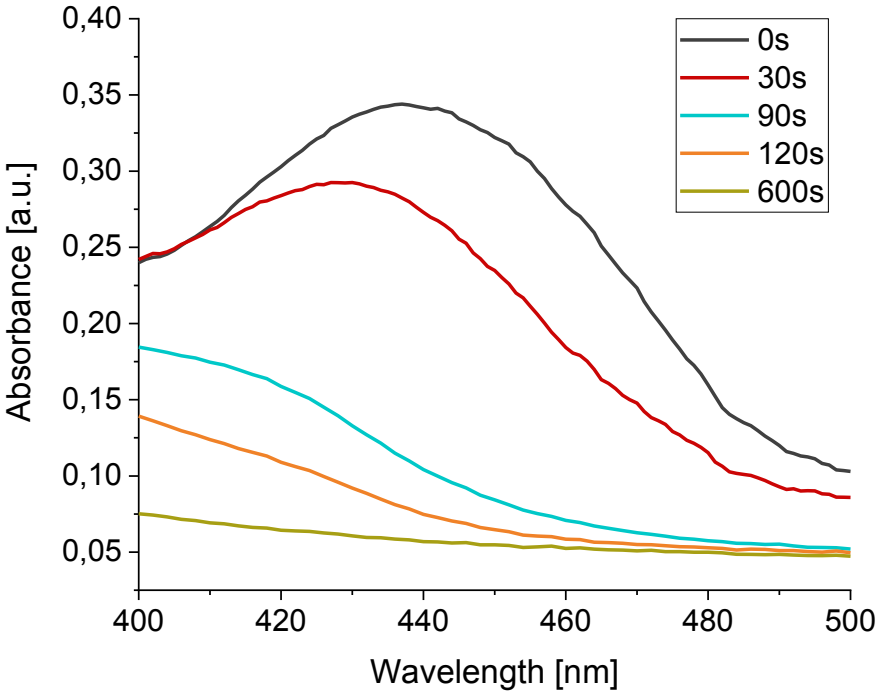

Figure 55: Absorbance of C343-ICA after different irradiation times.

7.3 Literature

(1) Berg, J. M.; Tymoczko, J. L.; Gatto, G. J.; Stryer, L. *Stryer Biochemie*; Springer Berlin Heidelberg: Berlin, Heidelberg, 2018. https://doi.org/10.1007/978-3-662-54620-8.

(2) *Intensivkurs Biochemie*, 1. Aufl.; Dettmer, U., Ed.; Vorklinik; Elsevier, Urban & Fischer: München Jena, 2005.

(3) Smith, L. J.; Fiebig, K. M.; Schwalbe, H.; Dobson, C. M. The Concept of a Random Coil: Residual Structure in Peptides and Denatured Proteins. *Folding and Design* **1996**, *1* (5), R95–R106. https://doi.org/10.1016/S1359-0278(96)00046-6.

(4) Mason, J. M.; Arndt, K. M. Coiled Coil Domains: Stability, Specificity, and Biological Implications. *ChemBioChem* **2004**, *5* (2), 170–176. https://doi.org/10.1002/cbic.200300781.

(5) Testa, O. D.; Moutevelis, E.; Woolfson, D. N. CC+: A Relational Database of Coiled-Coil Structures. *Nucleic Acids Research* **2009**, *37* (suppl_1), D315–D322. https://doi.org/10.1093/nar/gkn675.

(6) Sarma, A. D.; Oehrle, N. W.; Emerich, D. W. Plant Protein Isolation and Stabilization for Enhanced Resolution of Two-Dimensional Polyacrylamide Gel Electrophoresis. *Analytical Biochemistry* **2008**, *379* (2), 192–195. https://doi.org/10.1016/j.ab.2008.04.047.

(7) Cherkaoui, S.; Bettinger, T.; Hauwel, M.; Navetat, S.; Allémann, E.; Schneider, M. Tracking of Antibody Reduction Fragments by Capillary Gel Electrophoresis during the Coupling to Microparticles Surface. *Journal of Pharmaceutical and Biomedical Analysis* **2010**, *53* (2), 172–178. https://doi.org/10.1016/j.jpba.2010.01.039.

(8) Kimmerlin, T.; Seebach, D. '100 Years of Peptide Synthesis': Ligation Methods for Peptide and Protein Synthesis with Applications to β-Peptide Assemblies*. *The Journal of Peptide Research* **2005**, *65* (2), 229–260. https://doi.org/10.1111/j.1399-3011.2005.00214.x.

(9) Fischer, E.; Fourneau, E. Über einige Derivate des Glykocolls. In *Untersuchungen über Aminosäuren, Polypeptide und Proteïne (1899–1906)*; Fischer, E., Ed.; Springer: Berlin, Heidelberg, 1906; pp 279–289. https://doi.org/10.1007/978-3-642-99499-9_21.

(10) Sifferd, R. H.; du Vigneaud, V. A NEW SYNTHESIS OF CARNOSINE, WITH SOME OBSERVATIONS ON THE SPLITTING OF THE BENZYL GROUP FROM CARBOBENZOXY DERIVATIVES AND FROM BENZYLTHIO ETHERS. *Journal of Biological Chemistry* **1935**, *108* (3), 753–761. https://doi.org/10.1016/S0021-9258(18)75265-4.

(11) Harington, C. R.; Mead, T. H. Synthesis of Glutathione. *Biochem J* **1935**, *29* (7), 1602–1611.

(12) McKay, F. C.; Albertson, N. F. New Amine-Masking Groups for Peptide Synthesis. *J. Am. Chem. Soc.* **1957**, *79* (17), 4686–4690. https://doi.org/10.1021/ja01574a029.

(13) Merrifield, R. B. **Solid Phase Peptide Synthesis. I. The Synthesis of a Tetrapeptide**. *J. Am. Chem. Soc.* **1963**, *85* (14), 2149–2154. https://doi.org/10.1021/ja00897a025.

(14) Behrendt, R.; White, P.; Offer, J. Advances in Fmoc Solid-Phase Peptide Synthesis. *Journal of Peptide Science* **2016**, *22* (1), 4–27. https://doi.org/10.1002/psc.2836.

(15) Amblard, M.; Fehrentz, J.-A.; Martinez, J.; Subra, G. Methods and Protocols of Modern Solid Phase Peptide Synthesis. *MOLECULAR BIOTECHNOLOGY* **2006**, *33*, 16.

(16) Fields, G. B. Introduction to Peptide Synthesis. *Current Protocols in Protein Science* **2001**, *26* (1), 18.1.1-18.1.9. https://doi.org/10.1002/0471140864.ps1801s26.

(17) Mendes, A. C.; Baran, E. T.; Reis, R. L.; Azevedo, H. S. Self-Assembly in Nature: Using the Principles of Nature to Create Complex Nanobiomaterials. *WIREs Nanomedicine and Nanobiotechnology* **2013**, *5* (6), 582–612. https://doi.org/10.1002/wnan.1238.

(18) Kegel, W. K.; van der Schoot, P. Competing Hydrophobic and Screened-Coulomb Interactions in Hepatitis B Virus Capsid Assembly. *Biophysical Journal* **2004**, *86* (6), 3905–3913. https://doi.org/10.1529/biophysj.104.040055.

(19) Alberts, B.; Johnson, A.; Lewis, J.; Raff, M.; Roberts, K.; Walter, P. The Self-Assembly and Dynamic Structure of Cytoskeletal Filaments. *Molecular Biology of the Cell. 4th edition* **2002**.

(20) Grzelczak, M.; Vermant, J.; Furst, E. M.; Liz-Marzán, L. M. Directed Self-Assembly of Nanoparticles. *ACS Nano* **2010**, *4* (7), 3591–3605. https://doi.org/10.1021/nn100869j.

(21) Acar, H.; Srivastava, S.; Chung, E. J.; Schnorenberg, M. R.; Barrett, J. C.; LaBelle, J. L.; Tirrell, M. Self-Assembling Peptide-Based Building Blocks in Medical Applications. *Advanced Drug Delivery Reviews* **2017**, *110–111*, 65–79. https://doi.org/10.1016/j.addr.2016.08.006.

(22) Lee, S.; Trinh, T. H. T.; Yoo, M.; Shin, J.; Lee, H.; Kim, J.; Hwang, E.; Lim, Y.; Ryou, C. Self-Assembling Peptides and Their Application in the Treatment of Diseases. *International Journal of Molecular Sciences* **2019**, *20* (23), 5850. https://doi.org/10.3390/ijms20235850.

(23) Kumada, Y.; Hammond, N. A.; Zhang, S. Functionalized Scaffolds of Shorter Self-Assembling Peptides Containing MMP-2 Cleavable Motif Promote Fibroblast Proliferation and Significantly Accelerate 3-D Cell Migration Independent of Scaffold Stiffness. *Soft Matter* **2010**, *6* (20), 5073–5079. https://doi.org/10.1039/C0SM00333F.

(24) Matson, J. B.; Stupp, S. I. Drug Release from Hydrazone-Containing Peptide Amphiphiles. *Chem. Commun.* **2011**, *47* (28), 7962–7964. https://doi.org/10.1039/C1CC12570B.

(25) Gelain, F.; Bottai, D.; Vescovi, A.; Zhang, S. Designer Self-Assembling Peptide Nanofiber Scaffolds for Adult Mouse Neural Stem Cell 3-Dimensional Cultures. *PLOS ONE* **2006**, *1* (1), e119. https://doi.org/10.1371/journal.pone.0000119.

(26) Vlieghe, P.; Lisowski, V.; Martinez, J.; Khrestchatisky, M. Synthetic Therapeutic Peptides: Science and Market. *Drug Discovery Today* **2010**, *15* (1), 40–56. https://doi.org/10.1016/j.drudis.2009.10.009.

(27) Beesley, J. L.; Woolfson, D. N. The de Novo Design of α-Helical Peptides for Supramolecular Self-Assembly. *Current Opinion in Biotechnology* **2019**, *58*, 175–182. https://doi.org/10.1016/j.copbio.2019.03.017.

(28) Woolfson, D. N. The Design of Coiled-Coil Structures and Assemblies. In *Advances in Protein Chemistry*; Fibrous Proteins: Coiled-Coils, Collagen and Elastomers; Academic Press, 2005; Vol. 70, pp 79–112. https://doi.org/10.1016/S0065-3233(05)70004-8.

(29) Fleming, S.; Ulijn, R. V. Design of Nanostructures Based on Aromatic Peptide Amphiphiles. *Chem. Soc. Rev.* **2014**, *43* (23), 8150–8177. https://doi.org/10.1039/C4CS00247D.

(30) Rad-Malekshahi, M.; Lempsink, L.; Amidi, M.; Hennink, W. E.; Mastrobattista, E. Biomedical Applications of Self-Assembling Peptides. *Bioconjugate Chem.* **2016**, *27* (1), 3–18. https://doi.org/10.1021/acs.bioconjchem.5b00487.

(31) van Herpt, J. T.; Stuart, M. C. A.; Browne, W. R.; Feringa, B. L. A Dithienylethene-Based Rewritable Hydrogelator. *Chemistry – A European Journal* **2014**, *20* (11), 3077–3083. https://doi.org/10.1002/chem.201304064.

(32) Lin, Y.; Qiao, Y.; Tang, P.; Li, Z.; Huang, J. Controllable Self-Assembled Laminated Nanoribbons from Dipeptide - Amphiphile Bearing Azobenzene Moiety. *Soft Matter* **2011**, *7* (6), 2762–2769. https://doi.org/10.1039/C0SM01050B.

(33) Pelton, J. T.; McLean, L. R. Spectroscopic Methods for Analysis of Protein Secondary Structure. *Analytical Biochemistry* **2000**, *277* (2), 167–176. https://doi.org/10.1006/abio.1999.4320.

(34) Eisenhaber, F.; Persson, B.; Argos, P. Protein Structure Prediction: Recognition of Primary, Secondary, and Tertiary Structural Features from Amino Acid Sequence. *Critical Reviews in Biochemistry and Molecular Biology* **1995**, *30* (1), 1–94. https://doi.org/10.3109/10409239509085139.

(35) Fu, H.; Grimsley, G. R.; Razvi, A.; Scholtz, J. M.; Pace, C. N. Increasing Protein Stability by Improving Beta-Turns. *Proteins: Structure, Function, and Bioinformatics* **2009**, *77* (3), 491–498. https://doi.org/10.1002/prot.22509.

(36) J. Mart, R.; D. Osborne, R.; M. Stevens, M.; V. Ulijn, R. Peptide-Based Stimuli-Responsive Biomaterials. *Soft Matter* **2006**, *2* (10), 822–835. https://doi.org/10.1039/B607706D.

(37) Sheehan, F.; Sementa, D.; Jain, A.; Kumar, M.; Tayarani-Najjaran, M.; Kroiss, D.; Ulijn, R. V. Peptide-Based Supramolecular Systems Chemistry. *Chem. Rev.* **2021**, *121* (22), 13869–13914. https://doi.org/10.1021/acs.chemrev.1c00089.

(38) Zhang, D.; Qi, G.-B.; Zhao, Y.-X.; Qiao, S.-L.; Yang, C.; Wang, H. In Situ Formation of Nanofibers from Purpurin18-Peptide Conjugates and the Assembly Induced Retention Effect in Tumor Sites. *Advanced Materials* **2015**, *27* (40), 6125–6130. https://doi.org/10.1002/adma.201502598.

(39) Ye, D.; Shuhendler, A. J.; Cui, L.; Tong, L.; Tee, S. S.; Tikhomirov, G.; Felsher, D. W.; Rao, J. Bioorthogonal Cyclization-Mediated in Situ Self-Assembly of Small-Molecule Probes for Imaging Caspase Activity in Vivo. *Nature Chem* **2014**, *6* (6), 519–526. https://doi.org/10.1038/nchem.1920.

(40) Liang, G.; Ren, H.; Rao, J. A Biocompatible Condensation Reaction for Controlled Assembly of Nanostructures in Living Cells. *Nature Chem* **2010**, *2* (1), 54–60. https://doi.org/10.1038/nchem.480.

(41) Pieszka, M.; Han, S.; Volkmann, C.; Graf, R.; Lieberwirth, I.; Landfester, K.; Ng, D. Y. W.; Weil, T. Controlled Supramolecular Assembly Inside Living Cells by Sequential Multistaged Chemical Reactions. *J. Am. Chem. Soc.* **2020**, *142* (37), 15780–15789. https://doi.org/10.1021/jacs.0c05261.

(42) Ng, D. Y. W.; Vill, R.; Wu, Y.; Koynov, K.; Tokura, Y.; Liu, W.; Sihler, S.; Kreyes, A.; Ritz, S.; Barth, H.; Ziener, U.; Weil, T. Directing Intracellular Supramolecular Assembly with N-Heteroaromatic Quaterthiophene Analogues. *Nat Commun* **2017**, *8* (1), 1850. https://doi.org/10.1038/s41467-017-02020-2.

(43) Zhou, Z.; Maxeiner, K.; Moscariello, P.; Xiang, S.; Wu, Y.; Ren, Y.; Whitfield, C. J.; Xu, L.; Kaltbeitzel, A.; Han, S.; Mücke, D.; Qi, H.; Wagner, M.; Kaiser, U.; Landfester, K.; Lieberwirth, I.; Ng, D. Y. W.; Weil, T. In Situ Assembly of Platinum(II)-Metallopeptide Nanostructures Disrupts Energy Homeostasis and Cellular Metabolism. *J. Am. Chem. Soc.* **2022**, *144* (27), 12219–12228. https://doi.org/10.1021/jacs.2c03215.

(44) Chagri, S.; Ng, D. Y. W.; Weil, T. Designing Bioresponsive Nanomaterials for Intracellular Self-Assembly. *Nat Rev Chem* **2022**, *6* (5), 320–338. https://doi.org/10.1038/s41570-022-00373-x.

(45) Schelhaas, M.; Waldmann, H. Protecting Group Strategies in Organic Synthesis. *Angewandte Chemie International Edition in English* **1996**, *35* (18), 2056–2083. https://doi.org/10.1002/anie.199620561.

(46) Isidro-Llobet, A.; Álvarez, M.; Albericio, F. Amino Acid-Protecting Groups. *Chem. Rev.* **2009**, *109* (6), 2455–2504. https://doi.org/10.1021/cr800323s.

(47) Atherton, E.; Fox, H.; Harkiss, D.; Logan, C. J.; Sheppard, R. C.; Williams, B. J. A Mild Procedure for Solid Phase Peptide Synthesis: Use of Fluorenylmethoxycarbonylamino-Acids. *J. Chem. Soc., Chem. Commun.* **1978**, No. 13, 537–539. https://doi.org/10.1039/C39780000537.

(48) Carpino, L. A.; Shroff, H.; Triolo, S. A.; Mansour, E.-S. M. E.; Wenschuh, H.; Albericio, F. The 2,2,4,6,7-Pentamethyldihydrobenzofuran-5-Sulfonyl Group (Pbf) as Arginine Side Chain Protectant. *Tetrahedron Letters* **1993**, *34* (49), 7829–7832. https://doi.org/10.1016/S0040-4039(00)61487-9.

(49) Akabori, S.; Sakakibara, S.; Shimonishi, Y.; Nobuhara, Y. A New Method for the Protection of the Sulfhydryl Group during Peptide Synthesis. *BCSJ* **1964**, *37* (3), 433–434. https://doi.org/10.1246/bcsj.37.433.

(50) Chagri, S.; Ng, D. Y. W.; Weil, T. Designing Bioresponsive Nanomaterials for Intracellular Self-Assembly. *Nat Rev Chem* **2022**, *6* (5), 320–338. https://doi.org/10.1038/s41570-022-00373-x.

(51) Yu, H.; Li, J.; Wu, D.; Qiu, Z.; Zhang, Y. Chemistry and Biological Applications of Photo-Labile Organic Molecules. *Chemical Society Reviews* **2010**, *39* (2), 464–473. https://doi.org/10.1039/B901255A.

(52) Paola Pelliccioli, A.; Wirz, J. Photoremovable Protecting Groups: Reaction Mechanisms and Applications. *Photochemical & Photobiological Sciences* **2002**, *1* (7), 441–458. https://doi.org/10.1039/B200777K.

(53) Norrish, R. G. W.; Bamford, C. H. Photodecomposition of Aldehydes and Ketones. *Nature* **1936**, *138* (3502), 1016–1016. https://doi.org/10.1038/1381016a0.

(54) G. Bochet, C. Photolabile Protecting Groups and Linkers. *Journal of the Chemical Society, Perkin Transactions 1* **2002**, *0* (2), 125–142. https://doi.org/10.1039/B009522M.

(55) Kaczmarek, L. A. Synthesis of a Depsipeptide with Photolabile Protective Group and Fluorescence Label. 79.

(56) Nandivada, H.; Jiang, X.; Lahann, J. Click Chemistry: Versatility and Control in the Hands of Materials Scientists. *Advanced Materials* **2007**, *19* (17), 2197–2208. https://doi.org/10.1002/adma.200602739.

(57) Devaraj, N. K.; Finn, M. G. Introduction: Click Chemistry. *Chem. Rev.* **2021**, *121* (12), 6697–6698. https://doi.org/10.1021/acs.chemrev.1c00469.

(58) *The Nobel Prize in Chemistry 2022*. NobelPrize.org. https://www.nobelprize.org/prizes/chemistry/2022/press-release/ (accessed 2022-10-26).

(59) Kolb, H. C.; Finn, M. G.; Sharpless, K. B. Click Chemistry: Diverse Chemical Function from a Few Good Reactions. *Angewandte Chemie International Edition* **2001**, *40* (11), 2004–2021. https://doi.org/10.1002/1521-3773(20010601)40:11<2004::AID-ANIE2004>3.0.CO;2-5.

(60) Chang, P. V.; Prescher, J. A.; Sletten, E. M.; Baskin, J. M.; Miller, I. A.; Agard, N. J.; Lo, A.; Bertozzi, C. R. Copper-Free Click Chemistry in Living Animals. *Proceedings of the National Academy of Sciences* **2010**, *107* (5), 1821–1826. https://doi.org/10.1073/pnas.0911116107.

(61) Agalave, S. G.; Maujan, S. R.; Pore, V. S. Click Chemistry: 1,2,3-Triazoles as Pharmacophores. *Chemistry – An Asian Journal* **2011**, *6* (10), 2696–2718. https://doi.org/10.1002/asia.201100432.

(62) Dondoni, A. Triazole: The Keystone in Glycosylated Molecular Architectures Constructed by a Click Reaction. *Chemistry – An Asian Journal* **2007**, *2* (6), 700–708.

https://doi.org/10.1002/asia.200700015.

(63) Deiters, A.; Cropp, T. A.; Mukherji, M.; Chin, J. W.; Anderson, J. C.; Schultz, P. G. Adding Amino Acids with Novel Reactivity to the Genetic Code of Saccharomyces Cerevisiae. *J. Am. Chem. Soc.* **2003**, *125* (39), 11782–11783. https://doi.org/10.1021/ja0370037.

(64) Wang, Q.; Chan, T. R.; Hilgraf, R.; Fokin, V. V.; Sharpless, K. B.; Finn, M. G. Bioconjugation by Copper(I)-Catalyzed Azide-Alkyne [3 + 2] Cycloaddition. *J. Am. Chem. Soc.* **2003**, *125* (11), 3192–3193. https://doi.org/10.1021/ja021381e.

(65) Link, A. J.; Vink, M. K. S.; Tirrell, D. A. Presentation and Detection of Azide Functionality in Bacterial Cell Surface Proteins. *J. Am. Chem. Soc.* **2004**, *126* (34), 10598–10602. https://doi.org/10.1021/ja047629c.

(66) Hou, J.; Liu, X.; Shen, J.; Zhao, G.; Wang, P. G. The Impact of Click Chemistry in Medicinal Chemistry. *Expert Opinion on Drug Discovery* **2012**, *7* (6), 489–501. https://doi.org/10.1517/17460441.2012.682725.

(67) H. El-Sagheer, A.; Brown, T. Click Chemistry with DNA. *Chemical Society Reviews* **2010**, *39* (4), 1388–1405. https://doi.org/10.1039/B901971P.

(68) Franke, R.; Doll, C.; Eichler, J. Peptide Ligation through Click Chemistry for the Generation of Assembled and Scaffolded Peptides. *Tetrahedron Letters* **2005**, *46* (26), 4479–4482. https://doi.org/10.1016/j.tetlet.2005.04.107.

(69) Sun, X.-L.; Stabler, C. L.; Cazalis, C. S.; Chaikof, E. L. Carbohydrate and Protein Immobilization onto Solid Surfaces by Sequential Diels−Alder and Azide−Alkyne Cycloadditions. *Bioconjugate Chem.* **2006**, *17* (1), 52–57. https://doi.org/10.1021/bc0502311.

(70) Seebach, D.; Overhand, M.; Kühnle, F. N. M.; Martinoni, B.; Oberer, L.; Hommel, U.; Widmer, H. β-Peptides: Synthesis by Arndt-Eistert Homologation with Concomitant Peptide Coupling. Structure Determination by NMR and CD Spectroscopy and by X-Ray Crystallography. Helical Secondary Structure of a β-Hexapeptide in Solution and Its Stability towards Pepsin. *Helvetica Chimica Acta* **1996**, *79* (4), 913–941. https://doi.org/10.1002/hlca.19960790402.

(71) Schreier, W. J.; Kubon, J.; Regner, N.; Haiser, K.; Schrader, T. E.; Zinth, W.; Clivio, P.; Gilch, P. Thymine Dimerization in DNA Model Systems: Cyclobutane Photolesion Is Predominantly Formed via the Singlet Channel. *J. Am. Chem. Soc.* **2009**, *131* (14), 5038–5039. https://doi.org/10.1021/ja900436t.

(72) Zottig, X.; Al-Halifa, S.; Babych, M.; Quittot, N.; Archambault, D.; Bourgault, S. Guiding the Morphology of Amyloid Assemblies by Electrostatic Capping: From Polymorphic Twisted Fibrils to Uniform Nanorods. *Small* **2019**, *15* (33), 1901806. https://doi.org/10.1002/smll.201901806.